Title
Automated Assessment of Safety-Critical Dynamics in Multi-modal Transportation Systems

Authors
Medury, Aditya
Yu, Mengqiao
Bourdais, Cedric
et al.

Publication Date
2016-05-20

Peer reviewed

AUTOMATED ASSESSMENT OF SAFETY-CRITICAL DYNAMICS IN MULTI-MODAL TRANSPORTATION SYSTEMS

FINAL TECHNICAL REPORT
(DRAFT)

PREPARED BY THE

UC BERKELEY SAFE TRANSPORTATION RESEARCH AND EDUCATION CENTER

MAY 20, 2016

ADITYA MEDURY

MENGQIAO YU

CEDRIC BOURDAIS

OFFER GREMBEK

ACKNOWLEDGEMENTS

The authors would like to thank Sensys Networks, Inc., the City of Danville and the California Department of Transportation for their support of this project. We especially acknowledge the technical support and access to data from Sensys Networks, and in particular, Ajith Muralidharan, Christopher Flores, Pravin Varaiya, and Rene Sanchez. We also appreciate the inputs from Nicolas Saunier regarding *Traffic Intelligence*. We also appreciate the contributions of Ying Ni, Sudatta Mohanty and Meihua Luo who have been involved during various stages of this effort.

This study was supported by the University of California Center on Economic Competitiveness in Transportation (UCCONNECT) Faculty Grant Program.

EXECUTIVE SUMMARY

With the advent of emerging technologies, urban intersections are being increasingly equipped with various types of video-based and in-pavement sensing systems to facilitate round-the-clock monitoring and optimization of multi-modal flows. In comparison, the assessment of the safety performance of these facilities continues to be largely based on either crash history or citizen grievances. Herein lies an opportunity to apply advanced sensing platforms to proactively monitor safety-critical events of multi-modal road users.

This work presents a traffic safety monitoring framework which showcases the capabilities of utilizing in-pavement sensors to provide a detailed, automated assessment of mobility and safety-related performance measures for multi-modal traffic at signalized intersections. This effort supplements the crash data-based retrospective studies by routinely monitoring the safety-critical behavior of multimodal traffic. Herein, the term safety-critical refers to any action or interaction that can adversely impact a road user's safety, including jaywalking, red-light running, and drivers not yielding to pedestrians. Unlike in-person surveys and video analysis techniques which are limited in their scope to short term study periods, in-pavement sensors facilitate round-the-clock, non-intrusive data collection over continuous periods of time. Consequently, the development of suitable automated algorithms to analyze this data can generate a report of safety-critical multi-modal dynamics. Such an output can be used by agencies to proactively identify, and address, hazardous locations before a crash occurs.

In order to analyze mode-specific and multi-modal safety-critical dynamics, it is necessary to infer the various motorized and non-motorized movements taking place across the intersection. In this regard, a trajectory-based mode classification algorithm is presented which distinguishes the sensor events on the crosswalk as events triggered by motorized and non-motorized modes. Thereafter, the inferred trajectories are used to analyze mode-specific safety-critical concerns, such as non-motorized movement on the crosswalk against a pedestrian signal, as well as driver red light violations. In addition, driver yielding behavior in the presence of non-motorized activity is investigated. Additional trajectory and mode classification algorithms are also presented. Finally, some preliminary comparisons between in-pavement and video-based automated algorithms are also made.

The accuracy of the trajectory-based classification when differentiating between non-motorized and motorized events on the crosswalk is 94.5% and 89.2% within the training and test data respectively. In comparison, the accuracy of a sensor-specific binary logit classifier on the same datasets shows an accuracy of 99.6% and 96.9% respectively. The analysis of driver yielding behavior when turning right during a pedestrian green reveals two types of yielding: : (i) drivers who wait behind the crosswalk while allowing pedestrians to cross; and (ii) drivers who yield, but aggressively encroach into the intersection. Such type of behavior is typically difficult to capture, and quantify, in traditional observational studies. The insights gained from this behavior can have important implications for other intersections as well (both signalized and non-signalized), where aggressive yielding behavior may be more common in reality (but not as well documented).

In summary, this study demonstrates the feasibility of using a sensor-based classification framework to automatically monitor safety-critical interactions at signalized intersections over extended periods of time.

Key Components

The report is divided into the following eleven chapters that describe the overall project and its findings:

Chapter 1 – Introduction provides an overview of prior studies from the literature that have evaluated traffic safety at intersections.

Chapter 2 – Data Sources describes the study intersection with details about the sensors, their installation and the types of data obtained from them.

Chapter 3 – Data Processing describes the steps taken to process the data into the form that is required for the subsequent data analysis. In particular, this chapter outlines the development of a intuitive data visualization tool which integrates the data received from the different types of sensors.

Chapter 4 – Trajectory-based Classification of Modes details the algorithms designed to infer the different movements of motor vehicles and non-motorized modes.

Chapter 5 – Extracting Variables for Right Turn Safety Analysis presents the algorithm developed to detect yielding decisions of right turning vehicles in the presence of non-motorize modes on the crosswalk.

Chapter 6 – Assessment of Right Turn-related Safety provides results regarding the right turn-on-green yielding rates and surrogate safety measures for yielding/non-yielding, as well as additional quantitative analysis to identify factors to explain the yielding/non-yielding behavior.

Chapter 7 – Analysis of Mode-specific Safety Critical Behavior uses the trajectory-based algorithm to identify instances of jaywalking and red light running.

Chapter 8- Sensor-based Classification of Motorized/Non-motorized Modes discusses an alternative classification approach to distinguishing sensor events triggered by motorized and non-motorized modes.

Chapter 9- Alternative Algorithms for Inferring Non-motorized Trajectories provides some additional discussion on frameworks to infer trajectories of non-motorized modes along crosswalks

Chapter 10- Additional Algorithms for Inferring Non-motorized Trajectories provides some discussion on additional frameworks developed to infer trajectories of non-motorized modes along crosswalks

Chapter 11- Conclusion summarizes the results, contributions and shortcomings of this work along with a discussion of scope for future research

1 Introduction

Recent mobility trends in the context of California, as well as the United States, reveal that travel is becoming increasing multi-modal in nature. The results of the 2010-12 California Household Travel Survey (CHTS) (California Department of Transportation, 2013) indicate that while driving is still the most dominant mode of choice (75%), its mode share has decreased by 10% since 2000. In comparison, walking (17%), transit (4.5%) and biking (1.5%) have doubled their, albeit small, but increasingly significant mode share. Similarly, the results of the 2009 National Household Travel Survey indicate an average American made 17 more walk trips in 2009 than in 2001, covering nine additional miles (Pucher et al., 2011).

Given this emergence of multi-modal travel, it is of immense concern that the corresponding improvements made to traffic safety have not been commensurate across all modes. Figure 1 shows the recent trends in traffic fatalities for the state of California for cars/light trucks and pedestrians/bicyclists. Herein, it can be seen that while traffic fatalities have reduced for cars and light trucks by about 40% between 2006 and 2011, the change in the number of pedestrians and bike fatalities has been much less drastic and non-monotonic.

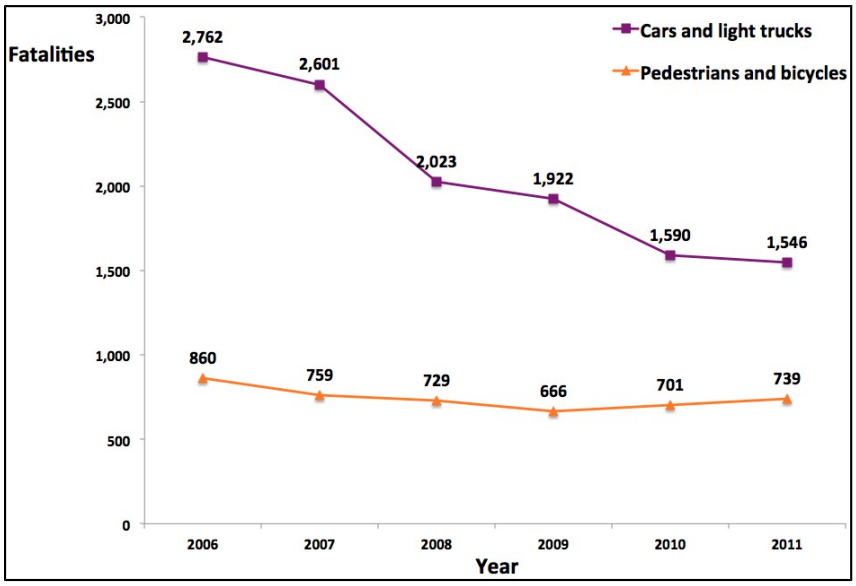

Figure 1.1 Trends in traffic fatalities in California from 2006 to 2011

Source: Statewide Integrated Traffic Records System (SWITRS) database

From an administrative standpoint, while there has been an effort made by agencies to improve safety for all travelers, recent performance assessments indicate that there is a need for a more concerted implementation. For instance, in 2011, the Bay Area Metropolitan Transportation Commission (MTC) and the Association of Bay Area Governments (ABAG) adopted a performance target of reducing the number of injuries and fatalities from all collisions across all modes by 50% below 2005 levels by 2040 (Metropolitan Transportation Commission, 2013). However, the same report acknowledges that given the investments planned for this period, the projected decline in the number of injuries and fatalities is likely to fall short of the adopted target. In the case of Caltrans, the 2014 State Smart Transportation Initiative (SSTI) review (California Department of Transportation, 2014) of the state agency's efforts suggests that Caltrans should generally rethink its approach to facilities in metro areas by putting

pedestrian, bicyclist and livability concerns before auto-mobility. The report also calls for incorporating the performances measures suggested by Caltrans in its 2010 Smart Mobility Report (which includes multi-modal travel mobility, reliability and safety) into its programs and activities.

While there has been considerable research done to systematically quantify the safety performance of transportation facilities based on crash history, there is little work on routinely measuring the safety-critical behavior of road-users as surrogate measures of traffic safety. In addition to monitoring the crash frequencies, transportation agencies should also be able to evaluate the performance of their facilities on safety-critical behavior, such as yielding. This is especially crucial in multi-modal environments where the dynamics are not well captured by existing performance measures. In addition, as the emphasis on heavier instrumentation of intersections through video cameras and other in-pavement sensors increases, there is an opportunity to generate comprehensive performance evaluations of multi-modal safety and mobility at these locations to proactively identify, and address, hazardous locations even before a crash occurs.

A unique opportunity in this regard is provided by the data made available through the Safety and Mobility System (SAMS) developed by Sensys Networks, Inc., which is an intersection detection platform that was primarily developed for traffic signal operation and round-the-clock vehicular mobility and safety performance monitoring (Muralidharan et al., 2014). SAMS provides a time synchronized database of road-user activity in the traffic lanes and crosswalks, as well as the precise details of the signal phasing at an intersection. The availability of such detailed data provides a unique opportunity to propose/validate new safety performance measures that can provide a detailed view of multi-modal intersections.

The next section provides an overview of the different types of multi-modal traffic safety studies that have been undertaken in the literature.

1.1 Literature Review

Given the increase in the emphasis on multi-modal mobility and the associated safety concerns, there is a need to efficiently account for them in the various transportation operations and safety frameworks. In this regard, one of the major challenges associated with efficiently designing and planning for a multi-modal environment is a limited understanding of safety-critical behavior of road-users based on existing data streams that are available to researchers and agencies. Traditionally, the most common form of data collected to assess multi-modal traffic are aggregated volume counts, which help us appreciate the mode share at a particular location, such as an intersection or a mid-block crossing. Another form of data which helps us understand the burden of injury of the different modes is the total number of collisions to have taken place over a long period of time. Together, the elements of traffic volume and collisions help ascribe the element of risk to various modes at a given location.

However, the associated shortcomings of direct measures, such as crash frequency and crash risk, include a small sample size of crashes and the lack of details associated with such data to help understand the innate crash causing mechanism (Tarko et al., 2009). In order to address this issue, researchers have introduced surrogate measures of safety, which utilize traffic conflict techniques to identify near-misses between different modes. Some examples of surrogate measures include time-to-collision, post-encroachment time, and gap time, that quantify the spatial and temporal proximity of different modes (Gettman and Head, 2003, Laureshyn et al., 2010). Traffic conflict techniques benefit from a larger sample size that allows for a more significant representation of the various inter-modal safety-critical interactions taking place at a location.

However, there are two major limitations of both forms of studies. Firstly, these studies typically involve recording videos and then manually processing them to identify different behaviors and conflicts, which requires tremendous human effort. Secondly, as a result of the significant processing time for videos,

these studies are typically conducted over shorter periods of time (two to four hours) at each location. Such short periods of observation can limit the insights that can be obtained.

Consequently, in order to minimize the human involvement in quantifying safety-critical behavior, the use of computer vision techniques to automate traffic safety monitoring has become an emerging research area in recent times. Two major research efforts in this regard have been the development of an automated road safety analysis system (Saunier and Sayed, 2007), which in turn laid the foundations for the development of an open source software system called *Traffic Intelligence* (Jackson et al., 2013, St-Aubin et al., 2013). In addition, Caltrans has begun exploring video-based data collection for collecting count data for different modes, including bicycles and pedestrians (California Department of Transportation, 2012). In this context, the open source project is an exciting prospect for it provides opportunities to build on an existing code base and suitably modify it to cater to each project's need. For a comprehensive review of computer vision techniques for the analysis of urban traffic, please refer to (Buch et al., 2011).

Finally, researchers have investigated different aspects of mode-specific and multi-modal interactions as part of traffic safety-related studies. For pedestrian-related activity, researchers have investigated pedestrian crossing behavior as a function of signal phasing using observational studies (Jason and Liotta, 1982; Tiwari et al, 2007; King et al, 2009), automated video analysis (Yu et al., 2011, Brosseau et al., 2013), as well as survey-based responses (Yagli, 2000). For safety-related concerns pertaining to motor vehicles, red light violations have been investigated using crash data (Retting et al., 1999; Bonneson et al., 2001), sensor events (Grembek et al., 2007, Zhang et al., 2009) as well as video-based analysis (Elmitiny et al., 2009). Finally, studies associated with multi-modal safety concerns have looked into pedestrian-vehicle conflicts using crash data (Leden, 2002, Mohamed et al., 2013), in-person observational studies (Abdulsattar et al, 1996), video-based data collection (Milazzo et al., 1998; Hubbard et al., 2009; Ling et al., 2014), as well as automated video analyses (Ismail et al., 2009, Alhajyseen et al., 2013).

Based on the review of traffic safety literature, it has been observed that most observational studies tend to be limited in scope as the data collection process is tailored to study a specific type of interaction. In the case of automated video analysis, researchers have developed algorithms which are multi-purpose in nature. However, a significant shortcoming of video-based analysis is that while it can be standardized and replicated across multiple locations, collecting and analyzing video data over extended periods of time can be challenging. On the other hand, the use of in-pavement sensors for traffic safety investigations has been largely focused on safety-related concerns of motor vehicles only. Consequently, using in-pavement sensors to study multi-modal traffic safety at signalized intersections represents a unique opportunity for traffic safety.

1.2 Problem Statement

The proposed research effort is aimed at developing a detailed, automated assessment of several mobility and safety-related performance measures for multi-modal traffic at signalized intersections. Such an effort supplements the crash data-based retrospective studies by routinely monitoring the safety-critical behavior of multimodal traffic. Herein, the term *safety-critical* refers to any action or interaction that can adversely impact a road user's safety, such as jaywalking, red-light running, drivers not yielding to pedestrians, etc. Unlike in-person surveys and video analysis techniques which are limited in their scope to short term study periods, in-pavement sensors facilitate round-the-clock, non-intrusive data collection over long periods of time. Consequently, the development of suitable automated algorithms to analyze this data can generate a comprehensive understanding of safety-critical multi-modal dynamics. In particular, such an automated algorithm can evaluate multi-modal traffic at different levels of safety-related concerns:

1. Mode-specific counts (which is an important attribute in safety studies, also referred to as *exposure*);
2. Mode-specific safety-critical behavior:
    i. Vehicular traffic: red-light violations;
    ii. Non-motorized traffic: using the crosswalk without pedestrian signal actuation;
3. Multi-modal safety-critical interactions:
    i. Yielding rate of drivers to pedestrians;
    ii. Calculation of surrogate measures of safety such as post-encroachment time.

In addition to using in-pavement sensors, video recordings taken from the study location will be used to train and test the accuracy of the algorithms. The video recordings shall also be used to explore automated video analysis techniques to contrast its approach against in-pavement sensors.

The next chapter discusses the different types of sensor data available from the study intersection in Danville.

2 Data Sources

This chapter provides details about the study intersection in Danville, the sensor types, their layout, as well as the types of data obtained from them.

2.1 Study Intersection

The study intersection locates at Diablo Road and Green Valley Road, Danville, CA, shown in Figure 2.1.

Figure 2.1 Location of study intersection (Source: Google Maps)

This intersection is instrumented with the Safety and Mobility System (SAMS) developed by Sensys Networks, Inc., which is an intersection detection platform that was developed for traffic signal operation and round-the-clock vehicular mobility and safety performance monitoring (Muralidharan et al., 2014). SAMS provides a time-synchronized database of activity in the vehicular lanes and crosswalks, as well as the precise details of the signal phasing at an intersection. The system configuration of the sensing architecture includes: 1) the vehicle detection system; 2) signal control system, 3) crosswalk detection system, and 4) video recording system.

2.2 Vehicular Lane Detection System

The vehicular lane detection system includes stop bar and departure lane detectors, called magnetometer sensors, or magsensors. Each vehicle passing the magsensors generates a detected and an undetected event. There were 31 magsensors installed at the study intersection as per the layout shown in Figure 2.2. Unfortunately nine magsensors stopped functioning, and were thus not available for the entire duration of the study. The events triggered at the magsensors are assumed to be triggered by motor vehicles as per their design specifications.

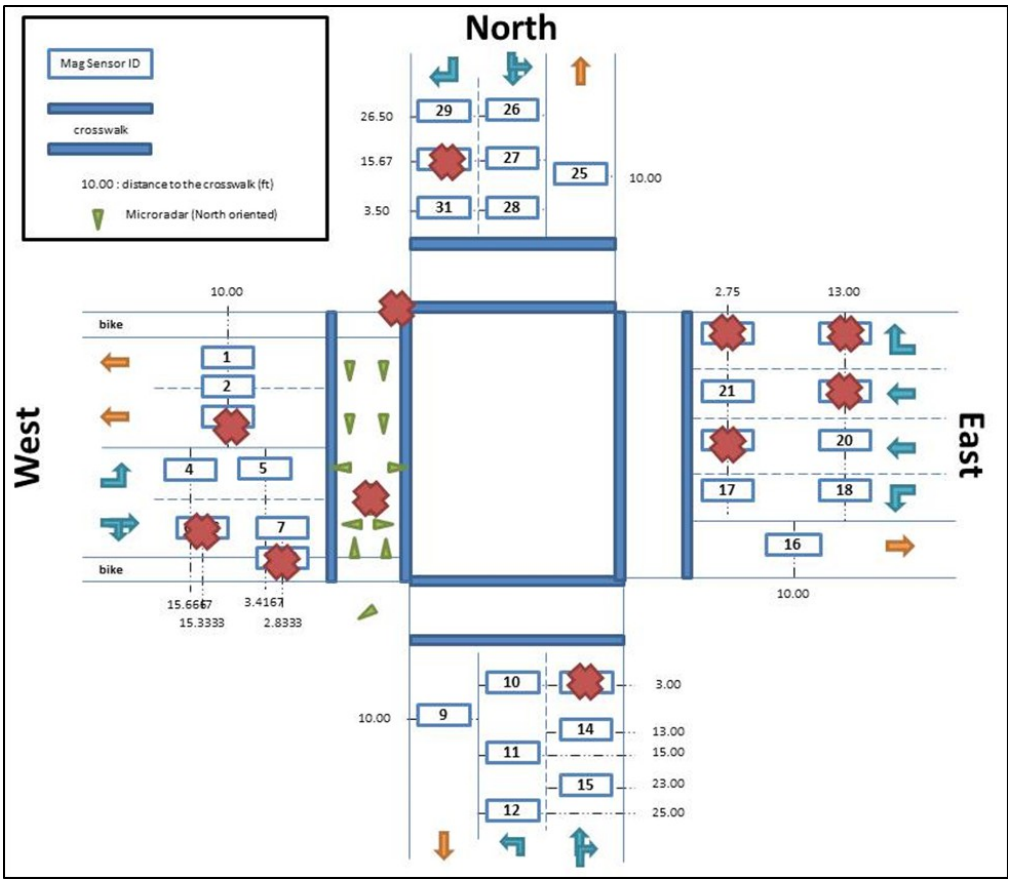

Figure 2.2 Layout of magsensors

2.3 Signal Control System

The signal control system records the signal event data. The EDI card in controller cabinet broadcasts signal phase and then Sensys AP translates this data and sends them to the server. The timing plan is shown in Figure 2.3; there are 8 partially overlapped vehicular and pedestrian-activated phases. The cycle length and each phase time vary upon time.

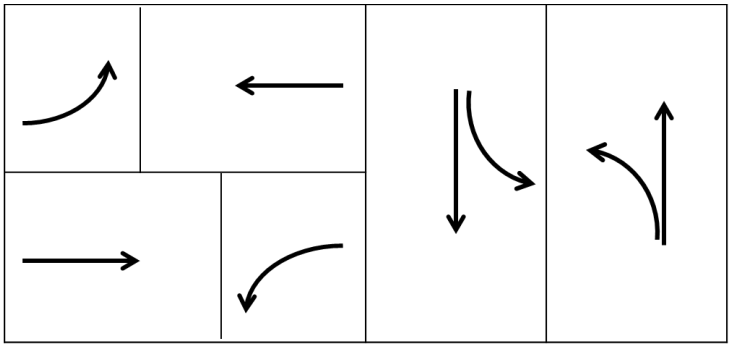

Figure 2.3 Timing plan of study intersection

2.4 Crosswalk Detection System

2.4.1 Sensys Microradar Sensor

Microradar sensors have a programmable detection range between 4’ (1.2 m) and 10’ (3 m). The width of a detection zone is approximately 90 degrees and the default range is 6’ (2 m). Microradar sensors are installed very close to the roadway surface and these in-ground sensors can transmit high frequency RF pulses and measure reflections. Figure 2.4 shows how a microradar sensor works to detect objects within its detection zone.

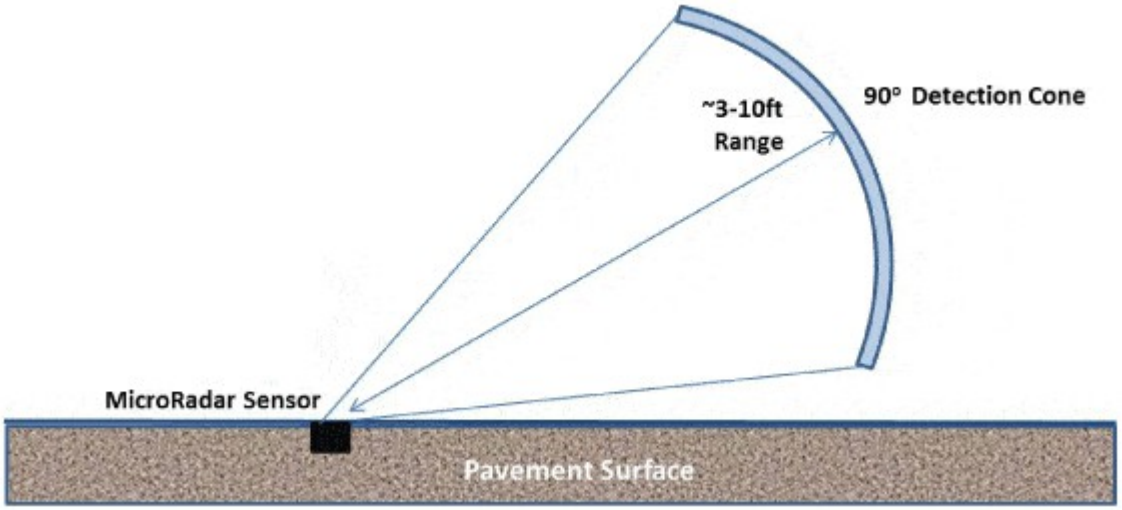

Figure 2.4 Detection process of a microradar sensor (Source: Sensys Networks, Inc.)

Both stationary and moving objects can be detected within the detection zone. Figure 2.5 shows a simplified example of how these sensors are activated as a pedestrian (red), bicycle (red), and automobile (black) pass by.

Figure 2.5 Examples of Microradar Activations (Source: Muralidharan et al. (2014))

In the microradar sensor, a detection line is initially set up as a base line, shown as the red dash line in Figure 2.6. A signal has to go above this line for detecting an object. In Figure 2.6a (right), the pedestrian is approaching the detection zone of the nearest sensor while in Figure 2.6b (right), the pedestrian is passing it. It can be observed that the blue and grey line is above the base line in Figure 2.6b (left).

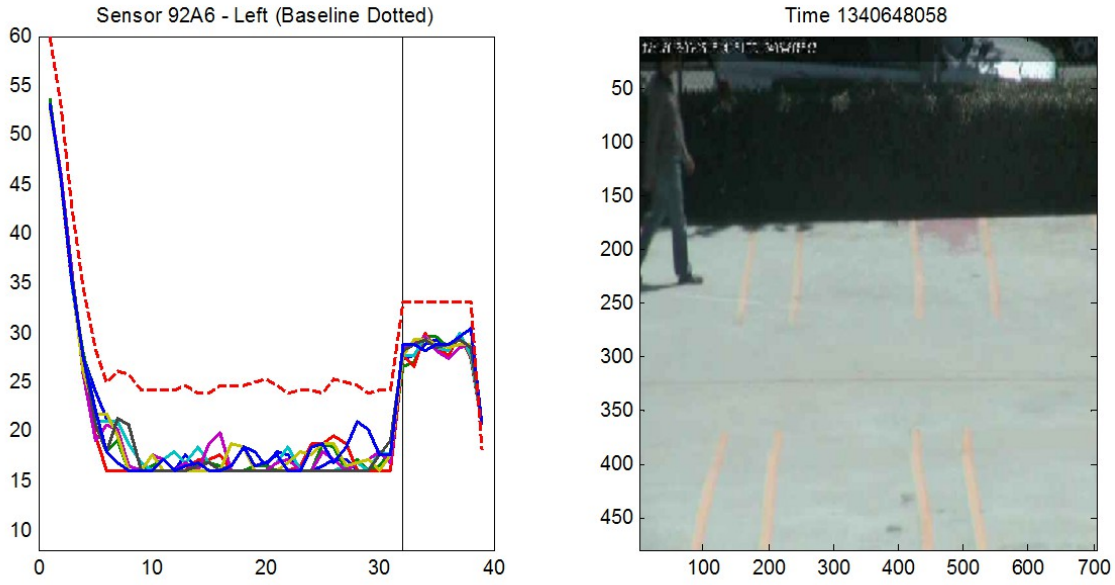

Figure 2.6a Mechanism of detection (Source: Muralidharan et al. (2014))

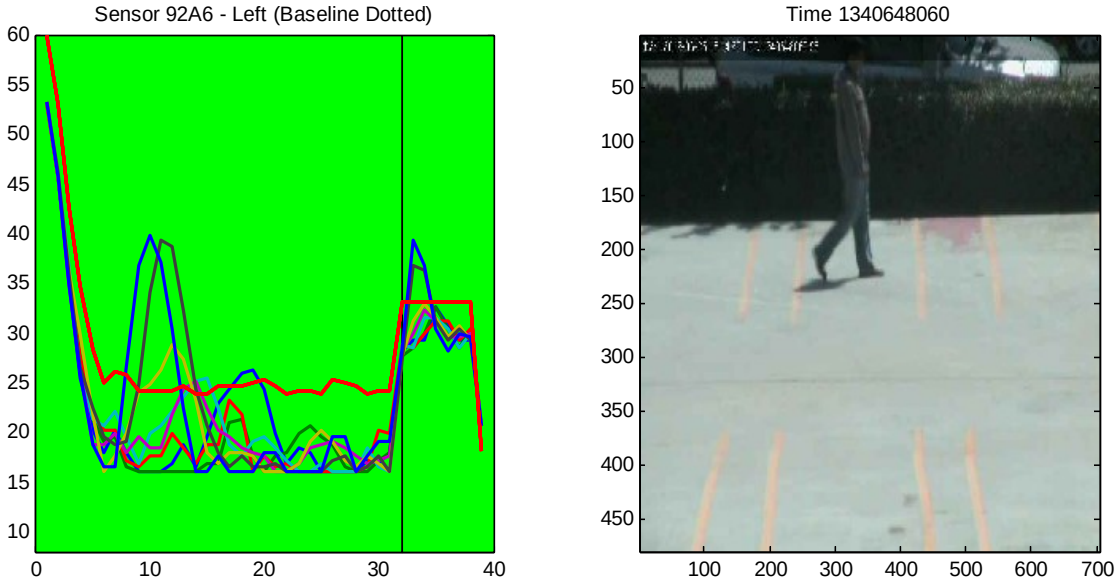

Figure 2.6b Mechanism of detection for a microradar (Source: Muralidharan et al. (2014))

2.4.2 Layout and Installation

In this project, only one of the crosswalks, shown in Figure 2.7, is instrumented with 13 microradar sensors with the intention of the detection zones covering most of the crosswalk area as well as the adjoining waiting areas. The layout of these sensors is presented in Figure 2.8. Once again, the sensors crossed out in red stopped functioning through the course of the study.

Figure 2.7 Location of study crosswalk (Source: Muralidharan et al. (2014))

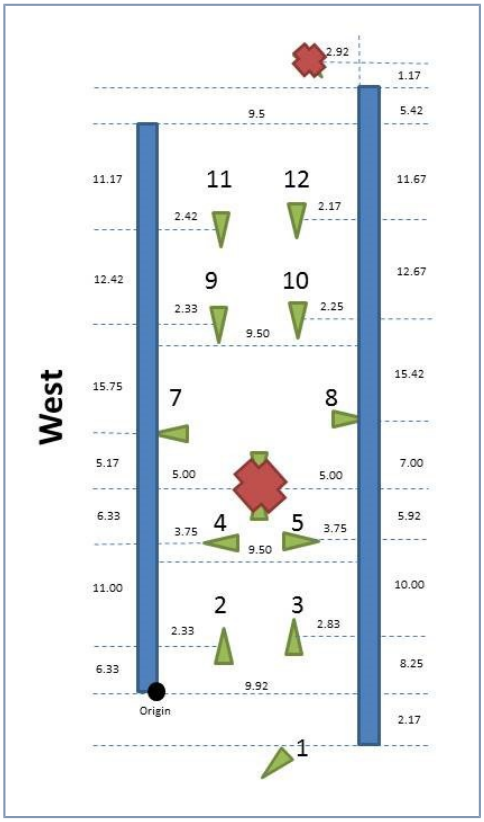

Figure 2.8 Layout of microradar sensors

2.5 Camera Detection System

A video camera is installed at the southern edge of the crosswalk facing the crosswalk, as shown in Figure 2.9. Video recordings can be scheduled to be triggered at specific time intervals, and stored within the camera with remote downloading capability.

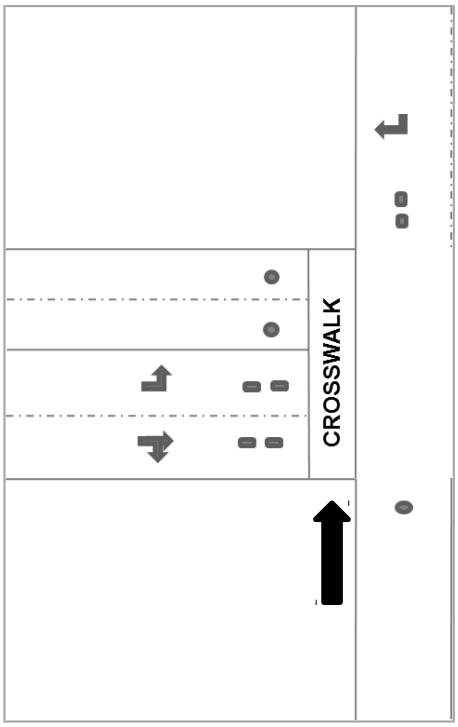

Figure 2.9 Location of the camera

In addition to using the video data to establish a ground truth for events taking place on the crosswalk, the videos can also be utilized to track the trajectories of vehicles/pedestrians/bicycles using automated video analysis techniques, which will be discussed further in Chapter 10.

2.6 Cost Estimates

The cost incurred to equip a signalized intersection with the type of sensors described above depends on the size of the intersection. In terms of a general estimate, to equip the stop-bar and departure lanes with magsensors for signal actuation and other mobility-related performance measures would be around $15,000-$20,000. The additional cost of instrumenting all crosswalks with microradars to detect and evaluate the safety of non-motorized modes would be between $8,000 and $12,000. Finally, the average service life of a magsensor and microradar is 10 years and 8 years respectively.

3 Data Processing

In this chapter, the raw data received from the sensor system at the Danville intersection are processed to extract individual events and their associated attributes. These events are calculated for each sensor type (microradars, magsensors, and signal phase), and aggregated by each day.

3.1 Description of Raw Data

3.1.1 Microradar Data

The raw microradar data provides a constant stream of status updates for all sensors. These status updates are given in a set of three messages that can be represented as follows:

<id> <timestamp> <bulk>

<id.0> <timestamp> <status> [DIR1]

<id.1> <timestamp> <status>

where

id *is the sensor ID, hex value*

id.0 *is sub-channel 0 of the sensor,*

[DIR1] is a flag indicating a reverse moving object

id.1 *is sub-channel 1 of the sensor,*

timestamp *is the UTC timestamp of the event*

bulk *is the token value indicating the signal strength of the microradar, (baseline: 128)*

status *is an integer indicating sub-channel status*

0 – detection off

1 – detection on

3 – watchdog detection on (if an event is active for an extended period of time)

4 – watchdog detection off (if a sensor is inactive for an extended period of time)

Based on the above mentioned template, the important status updates of sub-channels 0 and 1 are summarized as follows:

- (0,0): The sensor detection is off
- (4,4): The sensor detection has been off for an extended period of time, but sensor is relaying the message that it is still functional
- (3,3): The sensor detection is on, but due to no change in the active status of the sensor, the sensor is relaying the message that it is still functional
- (1,0): The sensor is detecting an object within its detection zone
- (1,1): The sensor is detecting an object within its detection zone, and the object size/reflection strength is high

The difference between sub-channel status (1,0) and (1,1) is unqualified, and requires validation using video data. However, based on discussions with Sensys, it appears that (1,1) is likely to be triggered for bigger object sizes.

Finally, to illustrate a single microradar event, consider the sequence of status updates for Sensor ID 96dd as shown in Table 3.1:

Table 3.1 Example of a microradar event

Update	Messages	Time since last update	Sensor Status
1	96dd 1390611599.563 128 96dd.0 1390611606.438 4 96dd.1 1390611606.438 4	-	De-activated
2	96dd 1390611606.438 138 96dd.0 1390611606.438 1 96dd.1 1390611606.438 0	16.875 seconds	Activated
3	96dd 1390611606.563 142 96dd.0 1390611606.563 1 96dd.1 1390611606.563 1	0.125 seconds	Active
4	96dd 1390611606.813 138 96dd.0 1390611606.813 1 96dd.1 1390611606.813 0	0.25 seconds	Active
5	96dd 1390611607.563 128 96dd.0 1390611607.563 0 96dd.1 1390611607.563 0	0.75 seconds	De-activated

The sequence of updates shown in Table 3.1 is interpreted as follows:

- *Update 1*: The sub-channel status (4,4) indicates that the sensor has been inactive for some time. In addition, it can be observed that the bulk value corresponds to 128 which is the baseline for when the sensor is inactive.
- *Update 2*: A new event has been triggered as indicated by the transition of the sub-channel status from (4,4) to (1,0). The bulk value also increased 138 (>128).
- *Update 3*: The sensor is still active, but the sub-channel status changed from (1,0) to (1,1)—perhaps indicative of a change in the size of the object that is reflecting the microradar signal. The corresponding bulk value is 142, which is also higher than the previous bulk update.
- *Update 4*: The sub-channel status returned to (1,0) but the sensor is still activated.
- *Update 5*: The sensor is de-activated as the sub-channel changes to (0,0) and the bulk value returns to 128.

The raw data containing a chronological sequence of sensor updates is provided by Sensys in a .csv file. This file is read through a MATLAB code which develops a database structure for all events associated with the microradar sensors for a given day (as defined by Pacific Standard Time). For each microradar event associated with a sensor, the following attributes are generated:

1. Activation time

2. De-activation time
3. Event duration
4. Average bulk value (average of the different bulk values observed during an event)
5. Time-averaged bulk value (time-weighted average of the different bulk values observed during an event)
6. Maximum bulk value
7. Whether the sub-channel status was (1,1) during an event
8. The duration for which the sub-channel status was (1,1)

That rationale for generating the various supplementary attributes is to assess, with the help of video data, as to whether there are any attributes, or combination of attributes, which can help differentiate the different modes from each other.

3.1.2 Magsensor Data

Unlike the microradar data, the raw magsensor data do not contain any additional details beyond activation and de-activation time for each sensor. Consequently, its status updates follow a more simplied template:

<id> <timestamp> <status>

where

id	*is the sensor ID, hex value*
timestamp	*is the UTC timestamp of the event*
status	*is an integer indicating magsensor status*
	0 – detection off
	1 – detection on

Subsequently, the raw magsensor data are converted into a structured database for each calendar day containing, the following attributes for each sensor event:

1. Activation time
2. De-activation time
3. Event duration

As indicated earlier, the magsensors are designed to be triggered by motor vehicles. Hence, it is assumed for the sake of simplicity that all magsensor events are associated with motor vehicles.

3.1.3 Signal Phase Data

The raw data corresponding to the signal phasing provides an update for every change in the signal. There are 8 vehicular phases, some of which may partially overlap which each other. In addition, there are four pedestrian phases for the pedestrian-activated signals installed on each crosswalk. Consequently, for each signal phase update, the active phase state is characterized by a timestamp and the following values:

- 0: Red
- 1:Yellow (relevant for vehicular phases only)
- 2: Green

Additional information regarding the number of rings, cycle number, etc., is also included in the raw data, but was not utilized for the purposes of this study.

The raw data were subsequently re-organized as a data structure containing the activation and de-activation times (in PST) for each vehicular and pedestrian phase.

3.1.4 Video Data

In addition to the sensor data, the camera could be triggered remotely to record and store videos, which could later be downloaded. However, unlike the sensor data which could be collected for multiple days, the video data collection is more memory intensive. Consequently, the video recordings were scheduled for morning and evening peak hours which were chosen to coincide with higher pedestrian activity—typically associated with the neighboring elementary school's hours. The web interface used to access the camera is shown in Figure 3.1.

As Figure 3.1 shows, the crosswalk of interest cannot be completely viewed. Consequently, the camera orientation was adjusted to maximize the crosswalk coverage while providing some visibility of the right turning lane on the northern approach of the intersection. The optimized orientation of the camera also ensures that all the microradars installed within the crosswalk are also visible.

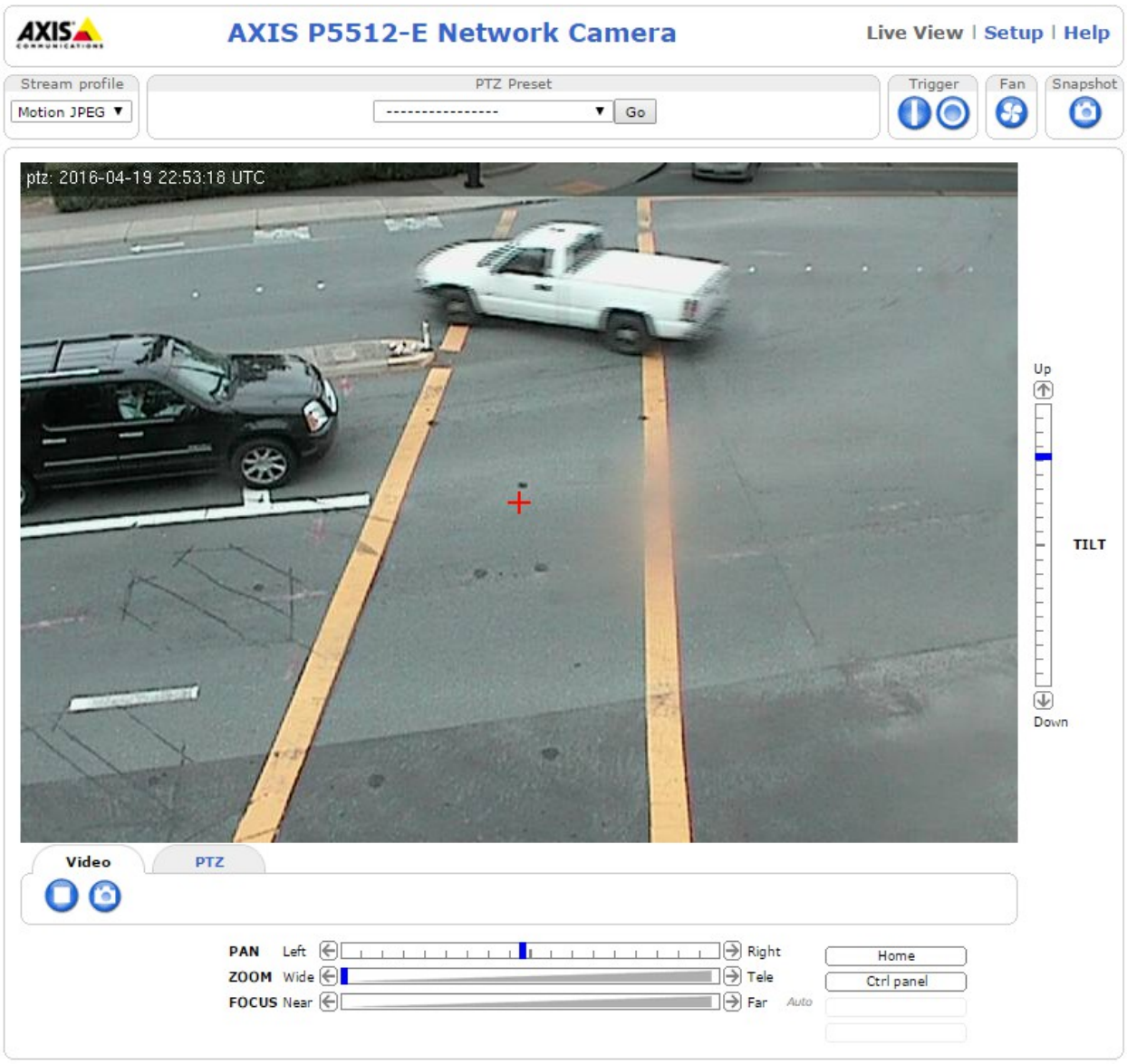

Figure 3.1 Web interface to access the camera remotely

3.2 Data Visualization Tool

While the processed sensor and video data can provide some useful insights when analyzed in isolation, the real benefits of the study arrive from combining all the data elements. In order to realize such an integrated data processing framework, an interactive data visualizing tool was developed as part of the effort which packaged the information obtained from the microradars, magsensors, signal phase system, and videos (when available), in an intuitive way. The key features that were desired from this tool included:

- Taking advantage of the time synchronization of the various data streams to depict a visual representation of the various activations/de-activations in a manner that could mimic modes moving from one part of the intersection to another
- Integrate the videos with the sensor data
- Provide an interactive interface to access and visualize data from different dates and times
- Label microradar events and use as ground-truth for algorithm validation and testing

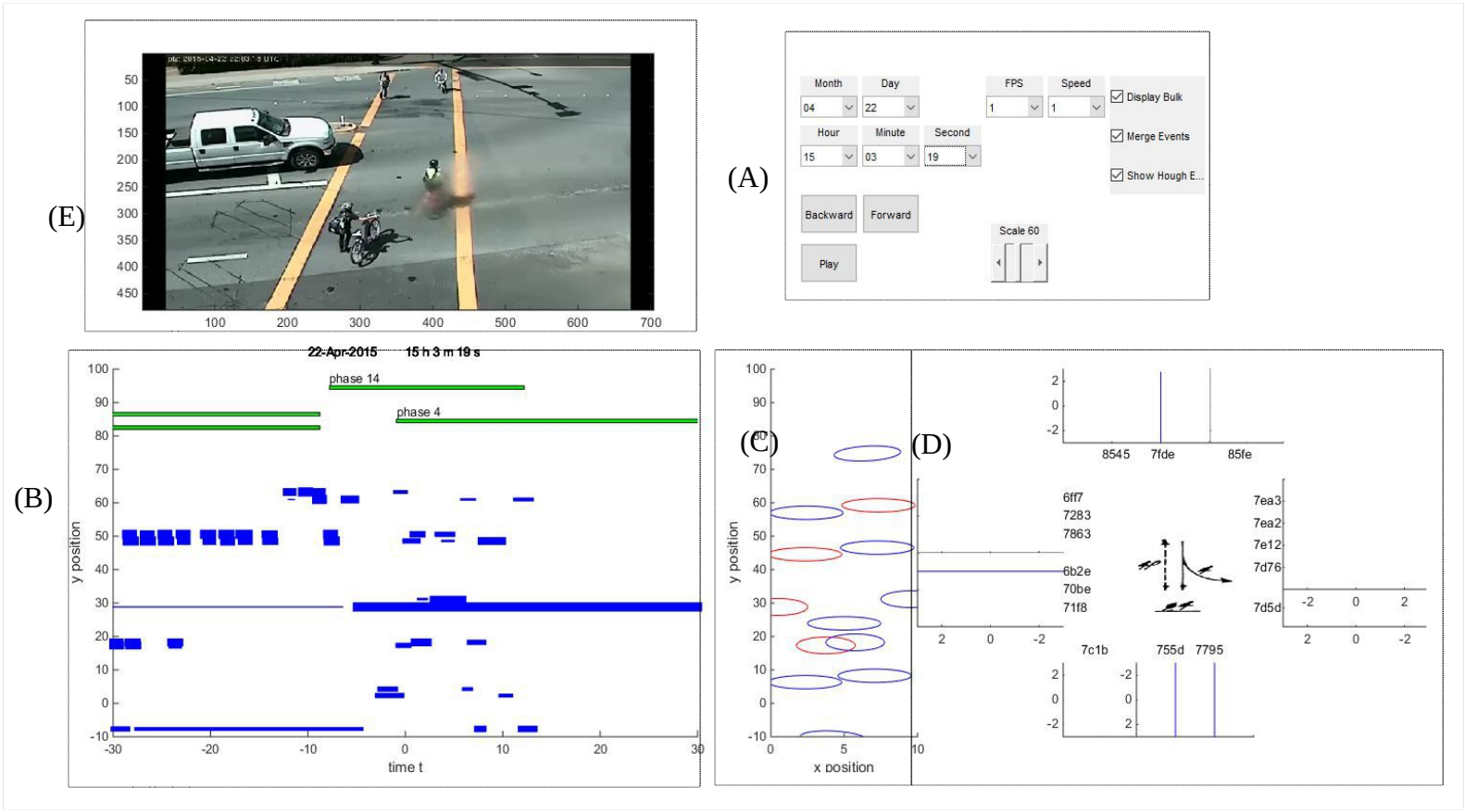

Figure 3.2 Data visualization tool

Figure 3.2 shows the data visualizing tool, which has the following five components:

A. This module allows for different dates and times to be selected for viewing, either as a movie, or by manually moving the frames backwards or forwards. The frames per second are selected as a function of the 8 hz frequency of the microradars (either 1, 2, 4, or 8 frames per second).

B. This module provides a time-space diagram of the microradar activation/deactivations. The y-axis represents the location of the sensors along the crosswalk. The x-axis represents time, with 0 representing the current time, and positive and negative values representing future and past time respectively. The blue bars represent the duration of a sensor event. The thickness of the bars is proportional to the average bulk value (an option that is available in module A). The green bars on top show the durations of different phases. When the play option is selected, the time-space diagram moves from right to left, and sensor states of the future get initiated over time.
C. This module provides a visual representation of which sensors are currently active (shown in red). The lighting up of sensors matches the bars in module B which overlap with time 0.
D. This module includes time-space diagrams of the different magsensors that are located closest to the intersection. The orientation of these time-space diagrams is chosen so that past-to-future event transitions are aligned with the movements of the vehicles. For instance, events for sensors 8545 and 7c1b move from top to bottom, while events for sensors 7c1b and 85fe on the move from bottom to top.
E. This module displays the video frames associated with the current timestamp, if available.

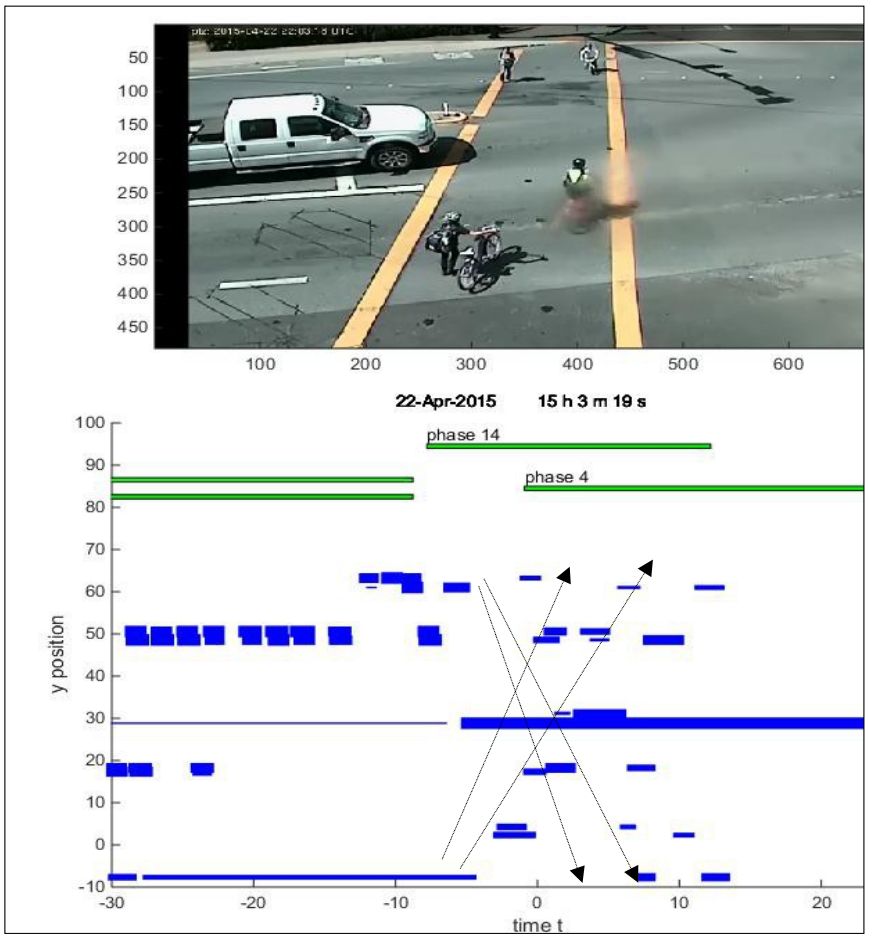

Figure 3.3 Separation of trajectories as visible from the time-space diagram

In the particular instant that is being captured by Figure 3.2, the video frame shows a combination of pedestrians and cyclists riding/walking their cycle at different parts of the crosswalk. A closer view of the time-space diagram can visually reveal the presence of four trajectories separating out over time, as

indicated by the arrows in Figure 3.3. Phase 14 corresponds to the lead pedestrian phase for this crosswalk, while phase 4 corresponds to the vehicular phase for north-to-south-and-west movements. The presence of a vehicle stopping in front of the stop bar location is getting captured by a long microradar event in the time-space diagram as displayed around y=30.

3.2.1 Labeling microradar events

The consolidation of the video and sensor data also enables us to label the microradar events as pedestrians, cyclists, motor vehicles, etc., based on the evidence presented by the video recordings. Consequently, a drop-down menu was also added to this interface which facilitated manual labeling of the sensor events as one among the following options:

Not labeled

1. 1 pedestrian (NS)
2. 1 pedestrian (SN)
3. 2 pedestrians (NS)
4. 2 pedestrians (SN)
5. 3+ pedestrians (NS)
6. 3+ pedestrians (SN)
7. Cycle (walk) (NS)
8. Cycle (walk (SN)
9. Cycle (ride) (NS)
10. Cycle (ride) (SN)
11. Passenger vehicle (Straight)
12. Passenger vehicle (Left)
13. Passenger vehicle (Right)
14. Passenger vehicle (Stopped)
15. Truck/trailer (Straight)
16. Truck/trailer (Left)
17. Truck/trailer (Right)
18. Truck/trailer (Stopped)
19. Bus (Straight)
20. Bus (Left)
21. Bus (Right)
22. Bus (Stopped)
23. Others

Figure 3.4 Labeling active microradar events

These labels are manually coded for each microradar event that is activated during the time periods for which the video recordings are also collected.

With the help of the labeled microradar data, the development and testing of classification algorithms to differentiate between events triggered by motorized and non-motorized modes can be undertaken, which is the focus of the next chapter.

4 Trajectory-based Classification of Modes

An in-pavement sensing platform facilitates non-intrusive data collection over long periods of time by summarizing the traffic movements at the intersection as a sequence of sensor detections. However, in order to re-create the activity of the different modes from the individual sensor events, it is important to develop a methodology to (a) infer which modes are triggering the sensors, and (b) track the movements of those modes through the intersection. In particular, the microradars on the crosswalk can be triggered by motorized vehicles moving in to/out of the vehicular lanes, or by non-motorized modes using the crosswalk. The ability to distinguish modes is also a necessary first step to count modes, as well as identify mode-specific and multi-modal safety-critical events.

In this chapter, the sensor and video data are used to develop and test algorithms which classify the microradar events along the crosswalk as motorized and non-motorized modes. More specifically, a trajectory-based classification method is proposed which combines the microradar and magsensor data to track the progression of sensor activations/de-activations across the intersection over time. The available video recordings are used to label the matching microradar events, and the labeled events are used to both calibrate as well as test the algorithms.

Figures 4.1 and 4.2 represent a simplified numbering scheme for the microradars and magsensors used in the algorithms. The sensors that have been crossed out in the figures stopped functioning during the course of this study, and were thus excluded from the algorithmic development.

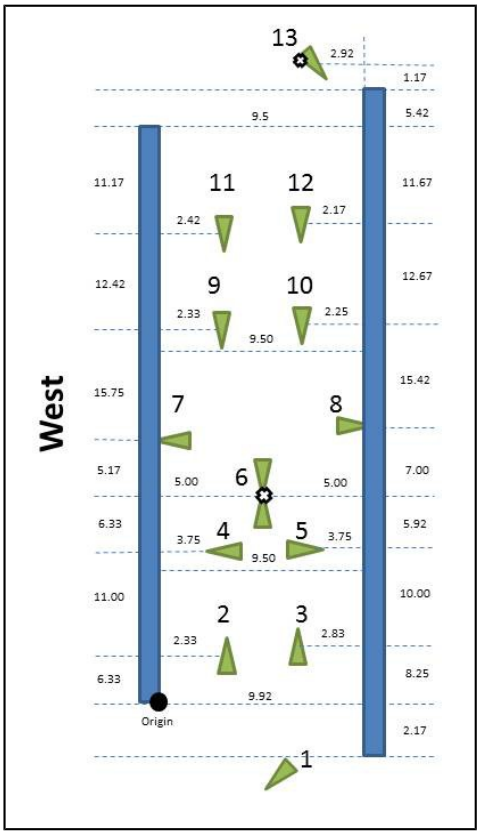

Figure 4.1 Simplified microradar referencing scheme

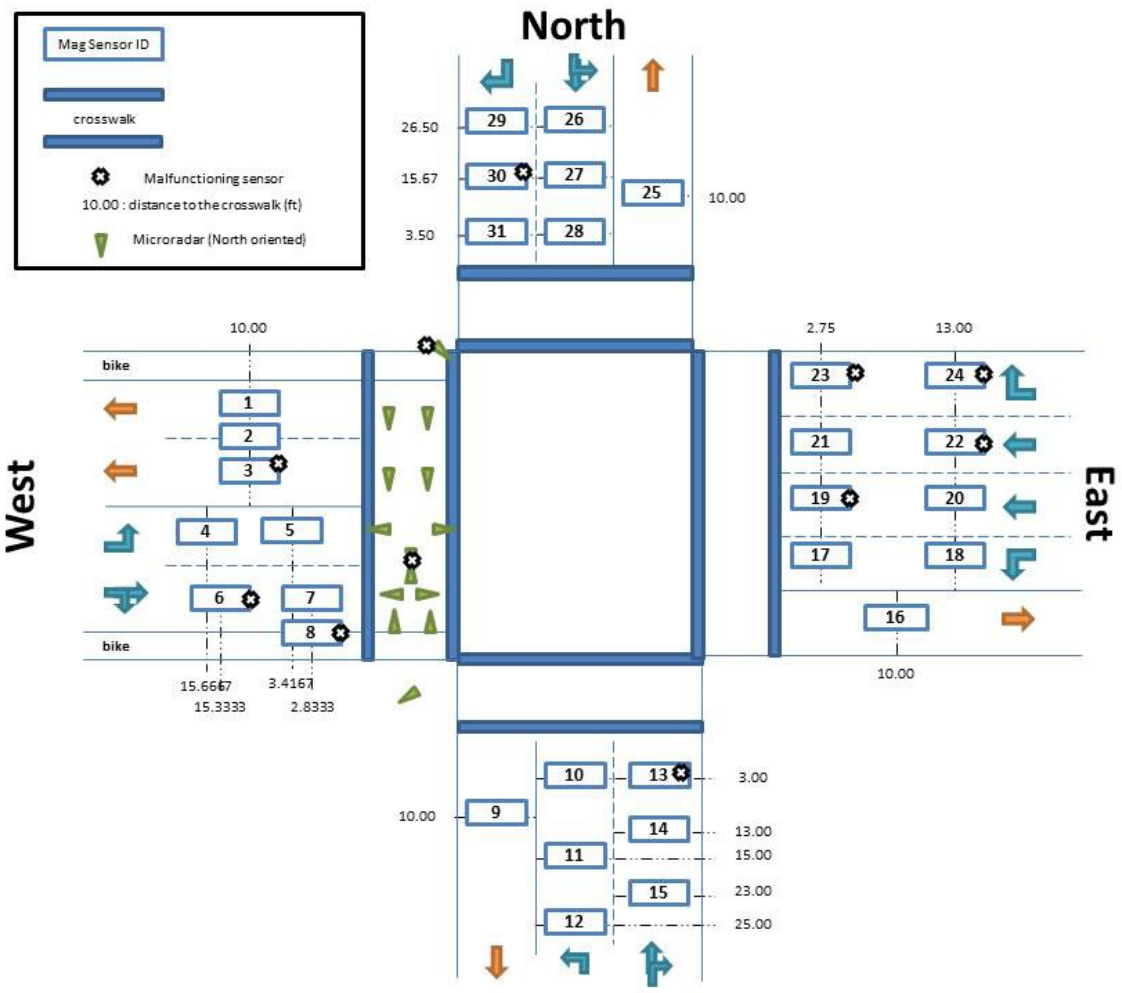

Figure 4.2 Simplified magsensor referencing scheme

A trajectory can be defined a sequence of sensor events that can be associated with a mode moving from one part of the intersection to another. Using the notations provided in Figures 4.1 and 4.2, some potential examples of different trajectories are as follows:

- Right movement (North to West): Magsensor 31 → Microradar 12 → Microradar 11 → Magsensor 2
- Straight movement (West to East): Magsensor 7 → Microradar 4 → Microradar 5 → Magsensor 16
- Crosswalk (North to South): Microradar 11 → Microradar 9 → Microradar 8 → Microradar 3

The examples shown above are illustrative of how a trajectory-based classifier seeks to extract different movements. However, some of the potential challenges associated with tracking objects across sensors can be as follows:

- The path of a moving object may lie outside the detection zone of some sensors (e.g., walking outside of the crosswalk), which results in the complete trajectory not getting captured.
- Some sensors along the path of a trajectory may have stopped working (e.g., for a straight movement from east to west, sensors 19 and 3 stopped working during the course of the study)
- There may be multiple objects moving around the intersection simultaneously (e.g., pedestrians walking in opposite directions, cars yielding to pedestrians, etc.)

The proposed trajectory-based algorithm seeks to overcome these issues by incorporating information such as the time separation between successive sensor events, the bulk value and channel statuses of the microradar events, overlapping sensor events, etc.

4.1 Movements

Since the emphasis of the study is on multi-modal behavior, the algorithm development largely focuses on the leading pedestrian phase associated with the crosswalk (phase 14), which also overlaps with the north-to-south and north-to-east green time. Consequently, the movements which are considered for trajectory-based classification are as follows:

- Right (N W)
- Right (W S)
- Straight (E W)
- Straight (W E)
- Crosswalk (N S)
- Crosswalk (S N)

It is acknowledged that the left turn algorithms have not been developed as part of the effort. However, since the analysis focuses on the pedestrian phase, their omissions do not significantly impact the study. In addition, the approach used to develop the trajectory-based classifiers is similarly applicable for the left turn movements.

4.2 Data

In order to develop the algorithms, the microradar, magsensor and signal phase data were obtained from Sensys Networks for the following days:

- April 22-24, 2015
- October 12-16, 2015

Videos were also recorded for the following time periods:

- 3:02 PM to 4:02 PM, April 22, 2015
- 8:19 AM to 9:19 AM, April 22, 2015
- 7:30 AM to 8:30 AM, October 12-16, 2015
- 2:30 PM to 3:30 PM, October 13-16, 2015

The microradar events overlapping with the video recordings were labeled using the data visualization tool, and were used to both calibrate the algorithms as well as test the accuracy of their results.

4.3 Data Preparation for Trajectory-Based Classification

4.3.1 Sorting Microradar and Magsensor Events Chronologically

Prior to identifying trajectories for the different movements, the microradar and magsensor events are sorted chronologically. Herein, there exist two sorting options to choose from: the sensors's activation time, or its de-activation time. In the proposed approach, the de-activation time is chosen as the sorting criterion since there can sometimes be long delays between a vehicle arriving at and departing from a sensor location, especially at stop bar locations.

A summary of the steps taken to prepare the data for trajectory-based classification is as follows:

- Input: Start and end date for the analysis
  i. Find the start and end times of all the pedestrian phases (phase 14) during the study period
  ii. Find all microradar events taking place 15 seconds before and after each phase 14

- The 15 second buffer is added to capture the events taking place before and after the pedestrian phases

iii. Find all magsensor events taking place 25 seconds before and after each phase 14
- The additional 10 second buffer helps capture any additional magsensor events that may be a part of a trajectory.

iv. Sort all the identified sensor events by their de-activation time,

v. Store supplementary data associated with each sensor event, such as:
- Activation time, event duration,
- Time-averaged and non-time averaged bulk value (for microradars),
- Maximum bulk value (for microradars),
- Presence of channel status (1,1) (for microradars),

vi. Initialize the classifier decision to zero for all right turn, straight, and crosswalk movements (zero corresponds to an unclassified sensor event).

Once the data are sorted, the events are processed in batch to classify each type of trajectory in the following order:

i. Right (N W)
ii. Right (W S)
iii. Straight (E W)
iv. Straight (W E)
v. Crosswalk (N S and S N)

The order of the trajectory classification is selected based on the extent of information involved for each movement. However, the sensitivity of the accuracy of the classifier to this ordering scheme can also be tested in the future.

4.3.2 Identifying All Right (N W) Movements

Figure 4.3 highlights the sensors that can be potentially triggered by a vehicle turning right from the north side of the intersection. Some of the sensors associated with this movement may not be available for trajectory classification, since they stopped responding during the course of the study.

The trajectory associated with any right (N W) turning vehicle can be divided into three stages:

1. Stop bar lane detection (Magsensors 31, 30, 29)
2. Crosswalk detection (Microradars 11, 12, 9)
3. Exit lane detection (Magsensors 1, 2, 3)

In each of the above-mentioned stages, it is essential to detect the presence of at least one sensor event. While the associated sensors can be part of other types of movements as well, the objective is to identify a set of conditions which can maximize the likelihood of capturing right turn trajectories within the unclassified sensor events.

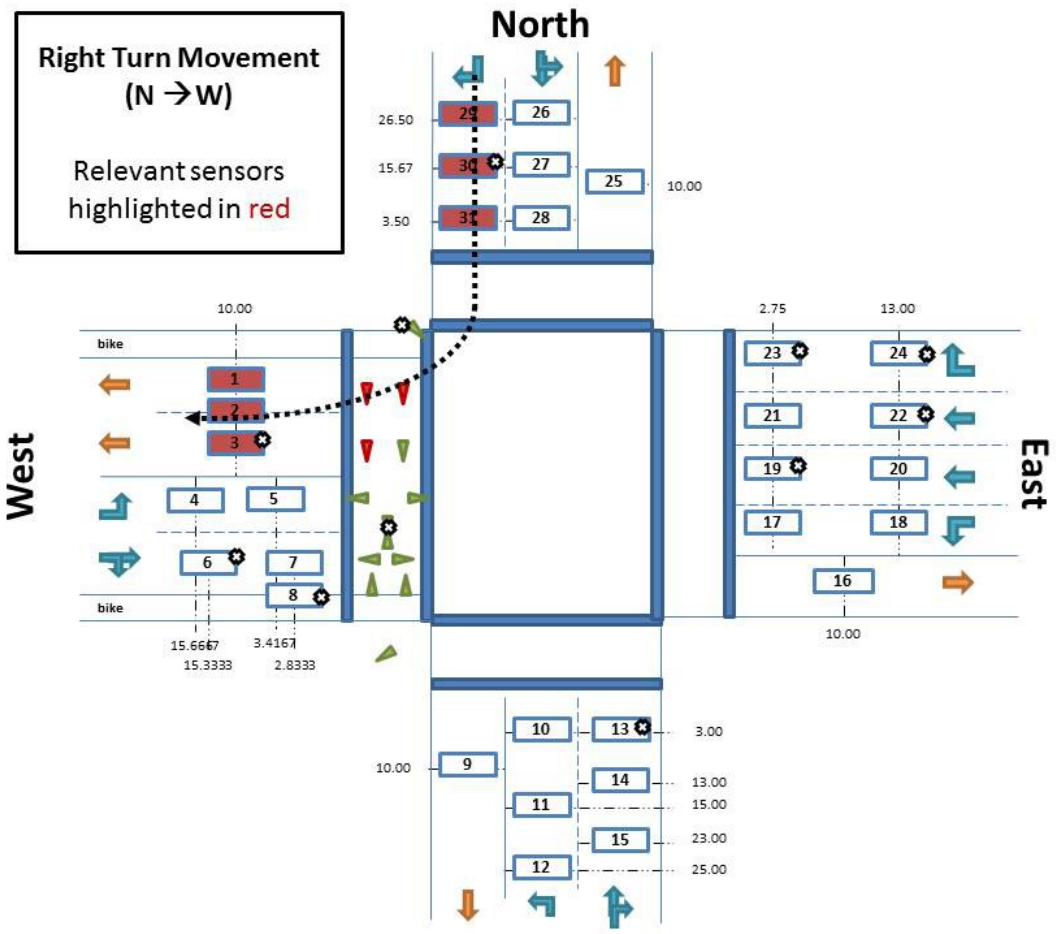

Figure 4.3 Scenario highlighting the sensors which may get activated by a right turn (N□W)

Another consideration for trajectory classification is to identify the logical sequence in which to identify the events associated with the trajectory. While trajectories can be inferred from identifying the relevant unclassified sensors events in a chronological order, one of the challenges with right turning vehicles is the presence of pedestrians/cyclists crossing at the crosswalk prior to the vehicle movement. Consequently, it is possible to misclassify a non-motorized event as part of a right-turn trajectory.

To overcome this issue, trajectories can be identified in a reverse chronological order, beginning with the exit lane sensors. An analysis of the labeled data from April 22 and 24 reveals that the time difference between microradar detections labeled as right turns (9, 11, 12) and the subsequent exit lane magsensors tends to be smaller than the time difference between the same crosswalk events and the previous stop bar lane events, as shown in Figure 4.4. The large time variation for the first half of the right turn trajectory can attribute to a wider range of speeds as vehicles approach the crosswalk, as opposed to when they leave the crosswalk.

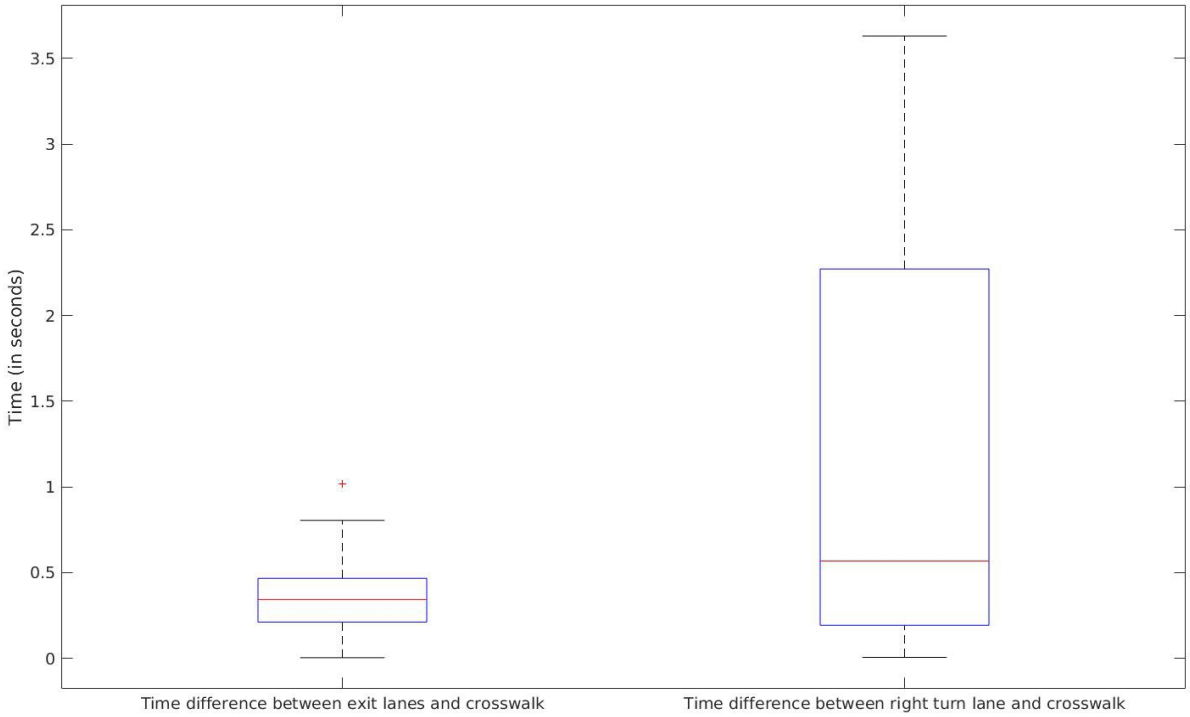

Figure 4.4 Box plot of time differences between right turn microradar events labeled on the crosswalk and the associated magsensor events in the vehicular lanes

The relevant sensors identified in the exit lanes (as well as the crosswalk) are not likely to be simultaneously triggered by a right turning vehicle. Instead, a subset of them may get triggered based on the vehicle's trajectory and size, and their selection is conditioned upon there being a time overlap in their detections. In the case of the crosswalk sensors, based on the microradar events labeled in the training data, microradar 11 is observed to be a regular occurrence in right turn trajectories. Thus, the identification of microradar 11 is made a requirement for a successful trajectory identification.

Using the reasoning described above, the details of the proposed algorithm for right (N□W) movements can be summarized as follows:

- Input: Dataset of microradars and magsensor events triggered around the pedestrian phases, and sorted by their de-activation times
  1. Starting from the end of the dataset, and classifying trajectories in a reverse chronological order:
     a. Exit lane detection: Find the first available unclassified magsensor 1, 2 or 3 *(end of the trajectory)*
        i. Identify any overlapping magsensor events for sensors 1, 2 or 3 with the trajectory-initiating magsensor.
     b. Crosswalk detection: Find the first available unclassified microradar events associated with sensors 11, 12 or 9
        i. Select the sensor 11 event and any or both of sensor 12 or 9 events, if at least one of them overlaps with sensor 11. (The other sensor should either overlap with sensor 11 or the third sensor.)

c. Stop bar lane detection: Once the exit lane and crosswalk activations have been identified, find the first available unclassified magsensor event associated with sensor 31. *(start of the trajectory)*
    i. Once the relevant magsensor 31 event has been identified, search for the first available unclassified event for magsensor 30 (if available), followed by magsensor 29. *(Optional for trajectory identification)*
d. Resume the classifier from the next available unclassified exit lane magsensor

- Additional constraints on the trajectory:
    - A completed trajectory should not take more than 6 seconds from the time the stop bar sensor 31 is de-activated.
        - Such a time constraint is included to prevent events separated far in time from being included as part of the same trajectory.
    - *Exit lane considerations*: If multiple unclassified events are observed for any of the exit lane magsensors prior to the identification of an unclassified crosswalk event, the trajectory is not feasible.
        - The likelihood of detecting two exit lane events corresponding to the same magsensor prior to detecting a crosswalk event is low.
    - *Physical considerations based on distance separation*: The time difference between exit lane and crosswalk de-activation should be at least 0.3 seconds.
    - *Crosswalk consideration*: If multiple events associated with microradar 9 are observed prior to the stop bar de-activation, the trajectory is not feasible.
    - *Stop bar lane consideration*: The time difference between sensors 31, 30 and 29 should not be more than 2 seconds.

The rule-based constraints described above have been added to capture the time taken by the vehicles to move between the various sensors, as well as recognize event sequences which are unlikely to be representative of a right turning vehicle's trajectory. The specific values chosen for these constraints were manually calibrated with the help of the training data.

4.3.3 Identifying All Right (W S) Movements

Similar to the right (N W) movement, Figure 4.5 highlights the sensors that can be potentially triggered by a vehicle turning right when approaching from the west side of the intersection. The trajectory described in Figure 4.5 traverses the following types of detectors:

1. Stop bar lane detection (Magsensors 8)
2. Crosswalk detection (Microradars 2, 3)
3. Exit lane detection (Magsensors 9)

Unlike the right (N W) movement, the magsensor closest to the stop bar lane for the right (W S) movement stopped functioning during the course of the study. Consequently, the trajectory algorithm is developed to infer the right turn movements using only the crosswalk and exit lane sensors.

Given the absence of stop bar sensor, it is assumed that during a W S movement, both the relevant microadars (2 and 3) get triggered by the vehicles. This assumption is consistent with the labeled observations in the training data.

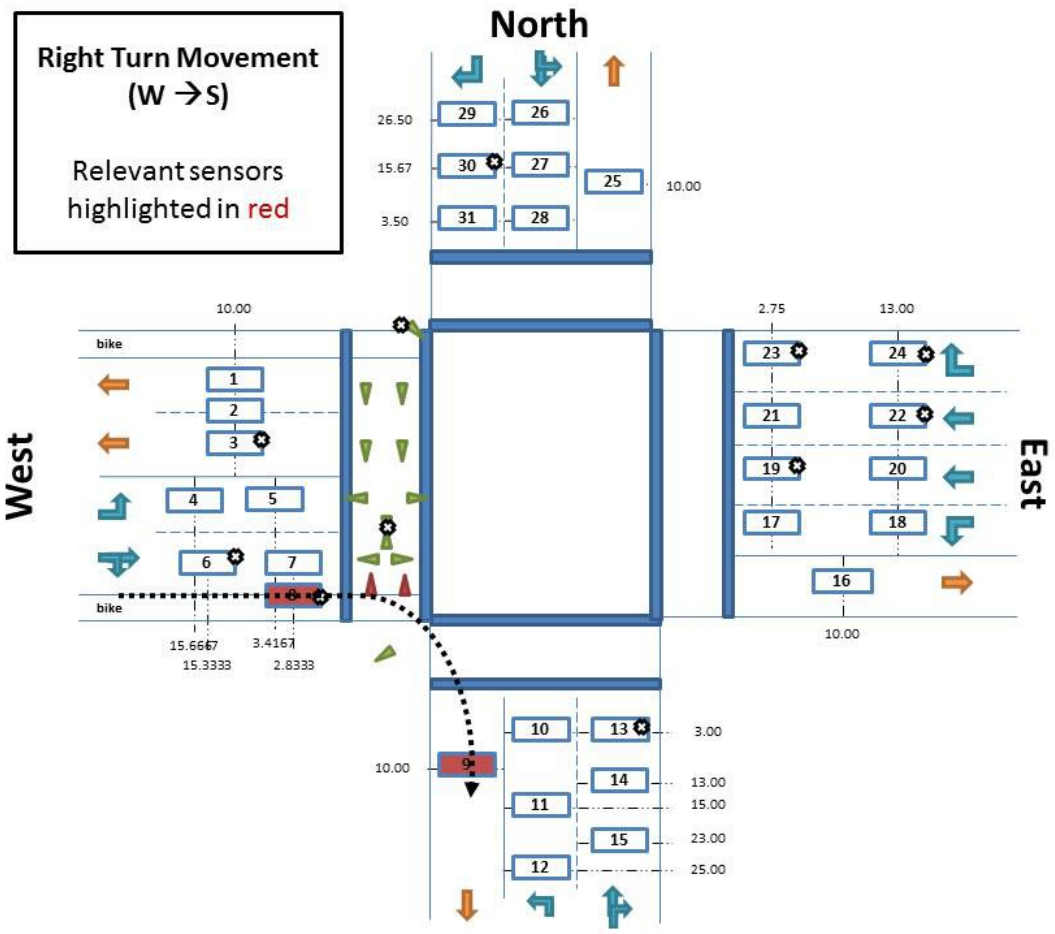

Figure 4.5 Scenario highlighting the sensors which may get activated by a right turn (W S)

Given that the trajectory classification is reliant only on two of the three stages of the vehicle movement, the trajectory is initiated using the crosswalk sensors, and terminated at the exit lane sensor. The inference takes place in chronological order and the steps associated with the proposed algorithm are summarized below:

- Input: Dataset of microradars and magsensors sorted by their de-activation times
  1. Starting from the end of the dataset, progressing upwards:
     a. Crosswalk detection: Find the first available unclassified microradar events associated with microradar sensor 2 *(start of the trajectory)*
        i. Identify any microradar sensor 3 event which overlaps with the previously identified sensor 2 event.
     b. Exit lane detection: Once both crosswalk detections have been identified, find the first available unclassified magsensor event associated with sensor 9. *(end of the trajectory)*
     c. Resume the classifier from the next available unclassified crosswalk microradar 2.
- Additional constraints on the trajectory:
  - A completed trajectory should not take more than 3 seconds from the time microradar 2 is de-activated.
  - *Physical consideration based on distance separation*: The time difference between exit lane and crosswalk de-activation should be at least 1 second.

4.3.4 Identifying All Straight (E→W) Movements

Figure 4.6 highlights the sensors that can be potentially triggered by a straight moving vehicle from east to west. The trajectory described in Figure 4.6 traverses the following types of detectors:

4. Stop bar lane detection (Magsensors 19, 20, 21, 22)
5. Crosswalk detection (Microradars 9, 10, 11, 12)
6. Exit lane detection (Magsensors 1, 2, 3)

Similar to the right (W→S) movement, the relevant magsensors in the exit lanes and stop bar lanes are not reliable. Consequently, searching for complete trajectories is this case can be difficult. To supplement the missing information, the approach taken for this particular movement classifier incorporates additional microradar event information, such as the subchannel status, bulk value, etc.

Even though the lack of complete trajectories restricts the classification approach, since the straight (E→W) classification follows the right (N→W) classification, some of the microradar events associated with sensors 9, 11, and 12 already get classified. Consequently, assuming that the right (N→W) algorithm classifies all the underlying right turn trajectories, information specific to microradars can help differentiate the non-motorized events from the remaining events triggered by motor vehicles, i.e. the E→W movements.

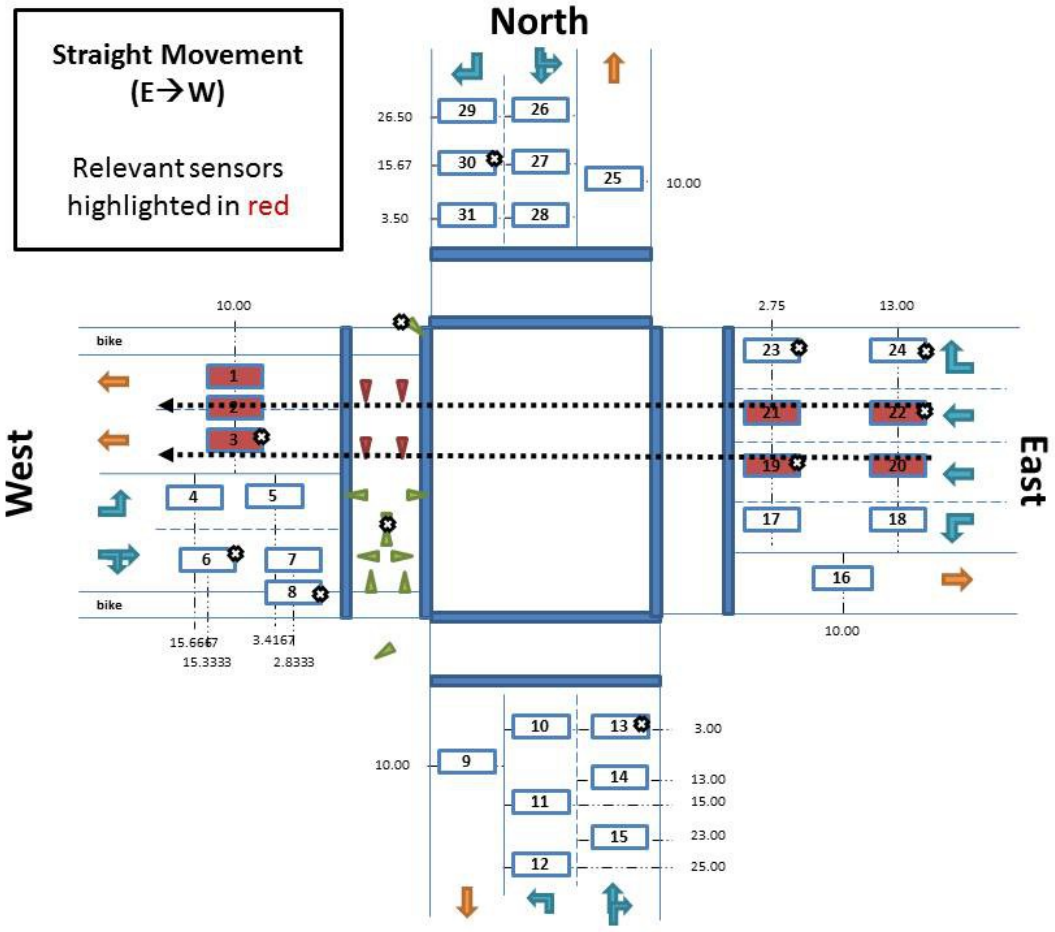

Figure 4.6 Scenario highlighting the sensors which may get activated by a straight movement (E→W)

The algorithm for straight movements (E→W) is summarized below:

- Input: Dataset of microradars and magsensors sorted by their de-activation times
  1. Starting from the beginning of the dataset, progressing chronologically:

a. Crosswalk detection: Find the first available unclassified microradar event associated with sensors 9, 10, 11, or 12 *(start of the trajectory)*
    i. Find any overlapping microradar events with the first microradar event given the following sensor pairing: (9, 10), (11,12).
b. Exit lane detection: Once the crosswalk sensor pairs have been identified, find the first available unclassified magsensor event associated with magsensor 1, 2 or 3.
c. End of the trajectory:
    i. If an exit lane magsensor (1,2 or 3) has been identified, and if the entire trajectory takes less than 2 seconds from the first microradar de-activation, consider the trajectory eligible for classification.
    ii. If an exit lane sensor could not be identified, apply the following constraints for the crosswalk sensor pair to be considered eligible for classification:
        1. The time difference between the de-activations of the individual microradar events is less than 0.25 seconds.
        2. One of the following criteria should have been satisfied:
            a. The microradars overlap in their detection times by at least 80% (with respect to the microradar detected last)
            b. At least one of microradar events observes a maximum bulk value of 140 or more
            c. At least one of the microradar events observes a sub-channel status of (1,1).
d. Resume the classifier from the next available unclassified microradar.

As is described above, if an eligible exit lane magsensor cannot be identified (to account the scenario that magsensor 3 is inactive), the crosswalk sensor pair is scrutinized further by imposing constraints of significant overlap between their respective event durations, or alternatively finding presence of sensor-specific indicators that might be likely to be associated with motor vehicles. Once again, the specific values chosen for the rule-based constraints are calibrated using the training data.

4.3.5 Identifying All Straight (W□E) Movements

Figure 4.7 highlights the sensors that can be potentially triggered by a straight moving vehicle from west to east. The trajectory described in Figure 4.6 traverses the following types of detectors:

7. Stop bar lane detection (Magsensor 7)
8. Crosswalk detection (Microradars 4, 5)
9. Exit lane detection (Magsensor 16)

Unlike the straight (E□W) classifier, the sensors associated with this trajectory are fully functional. Consequently, the classification algorithm shall seek to find events for each stage of the trajectory.

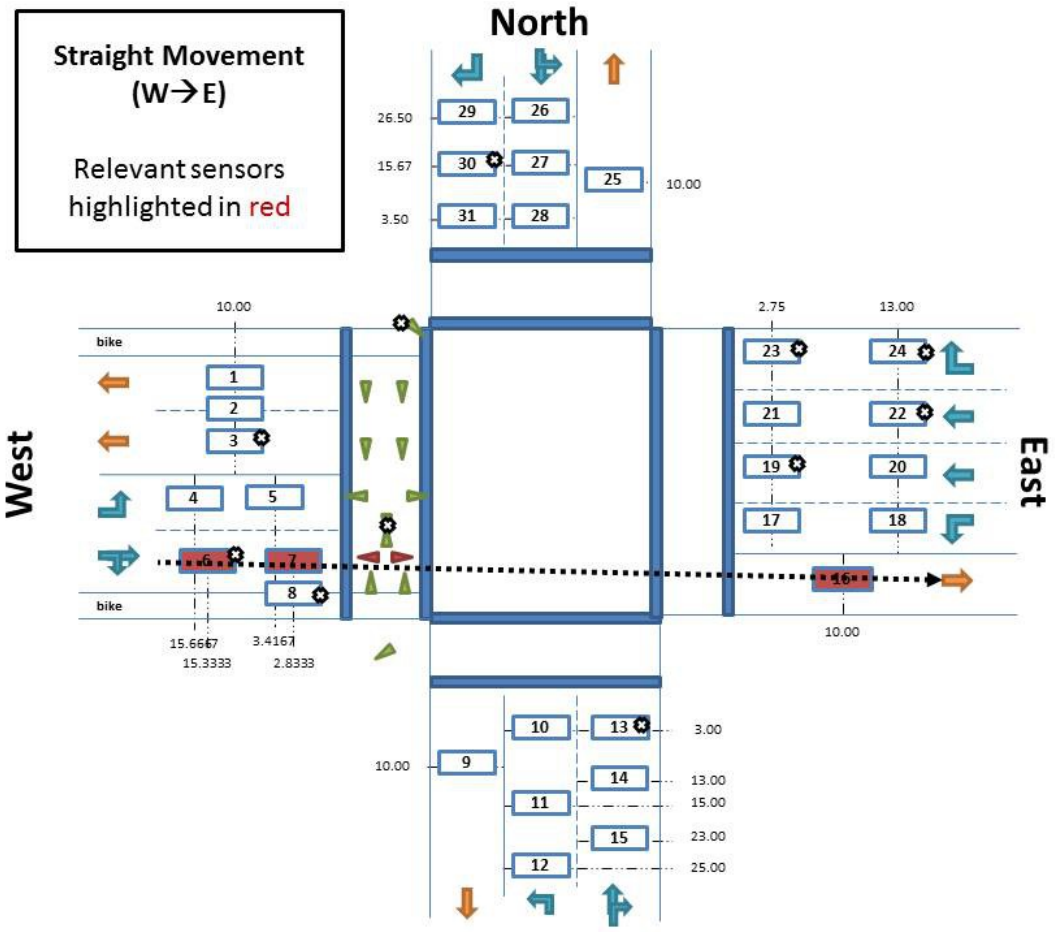

Figure 4.7 Scenario highlighting the sensors which may get activated by a straight movement (W→E)

The algorithm for classifying straight (W→E) movements is summarized below:

- Input: Dataset of microradars and magsensors sorted by their de-activation times
  1. Starting from the beginning of the dataset, progressing chronologically:
     a. Stop bar lane detection: Find the first available unclassified event associated with magsensor 7 *(start of the trajectory)*
     b. Crosswalk detection: Find the first available unclassified event associated with microradar 5:
        i. Find any microradar 4 event that overlaps with the selected microradar 5 event. (optional)
     c. Exit lane detection: Once the crosswalk sensors have been identified, find the first available unclassified magsensor event associated with magsensor 16. *(end of the trajectory)*
     d. Additional constraints:
        i. The time difference between the de-activations of magsensors 7 and 16 should not be more than 4 seconds.
        ii. The time difference between the first crosswalk de-activation and magsensor 16 should not be more than 3 seconds.
     e. Resume the classifier from the next available unclassified stop bar magsensor.

Once the right and straight movement classifiers have been sequentially implemented, the remaining unclassified events are evaluated for detecting crosswalk movements.

4.3.6 Identifying All Crosswalk Movements (N□S, S□N)

In order to infer trajectories on the crosswalk, it is important to recognize that during a pedestrian phase, people are likely to travel in opposite directions and initiate their crossings at different times and with different speeds. Consequently, the crosswalk trajectory estimation must accommodate these differences.

The proposed approach uses a simplified crosswalk representation by pairing sensors that are located in close proximity to each other and assigning them a common location value, as shown in Figure 4.8. Using the simplified Y-axis notation, trajectories are assigned a direction based on the location of the first unclassified microradar that is observed during the analysis. For instance, if the first unclassified microradar lies in the top half of the crosswalk, it is assumed that the road user is traveling from north to south, or else vice-versa. Thereafter, the identification of subsequent sensors is determined by comparing the time taken between successive sensor detections with a wide range of crossing speeds. Hence, the proposed methodology allows for speed variation between successive sensor detections as long as the total duration of the trajectory is within some reasonable bounds.

In addition, the estimated trajectory is confirmed only when it observes sensor detections at least three distinct y-axis locations. For instance, if a N□S trajectory detects events at sensor pairs (9, 10) and (7,8), it is necessary to find another unique location further south of these sensor so as to accept this sequence as a valid trajectory. Herein, the motivation is to include both temporal and spatial constraints within the trajectory estimation so as to ascertain the movements with greater confidence.

Finally, since movements in opposite directions can take place simultaneously and impact the same set of sensors, the analysis for N□S and S□N movements is carried out simultaneously.

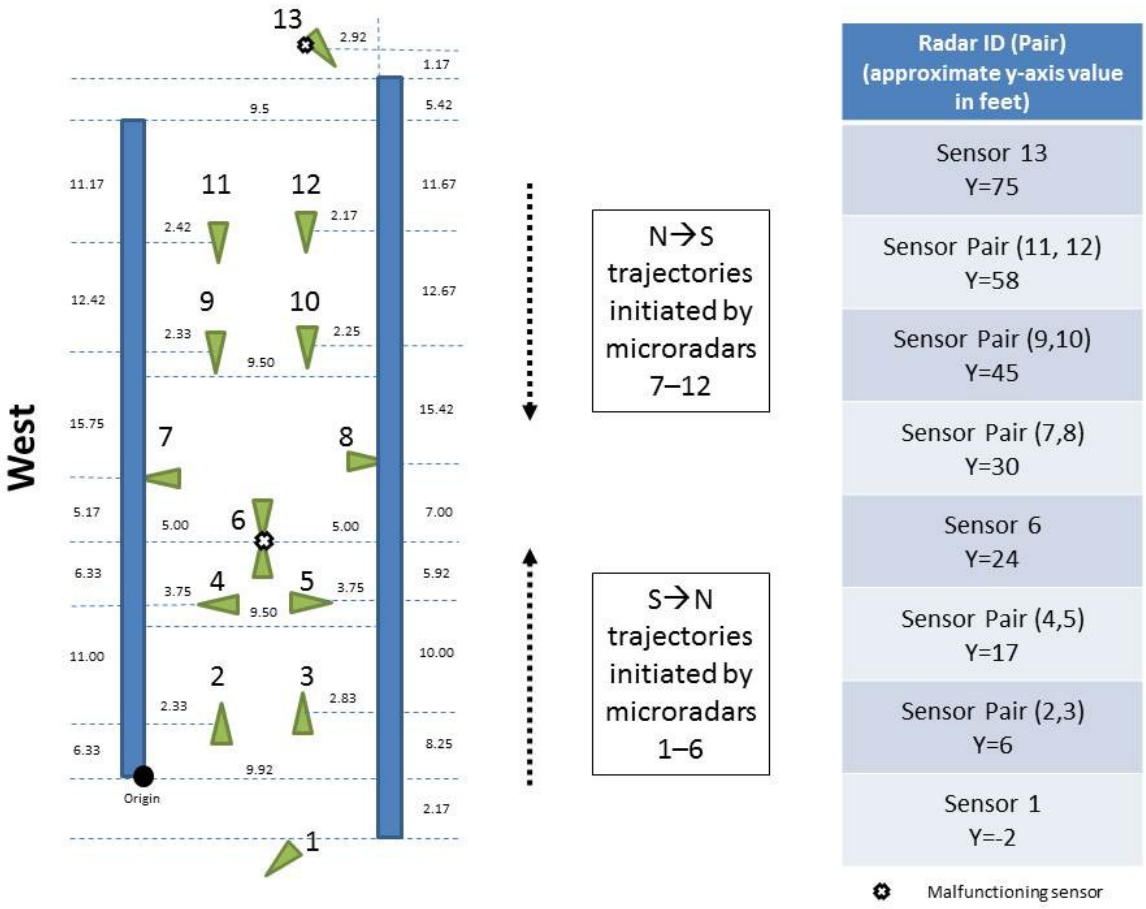

Figure 4.8 Scenarios indicating the crosswalk-related movements

The algorithm for crosswalk movements is summarized below:

- Input: Dataset of microradars and magsensors sorted by their de-activation times
  1. Starting from the beginning of the dataset, progressing chronologically:
     a. If the first unclassified microradar is in the top of the half of the crosswalk (sensors 7 to 12), initiate a N→S trajectory. Otherwise, initiate a S→N trajectory. *(start of the trajectory)*
     b. Find all unclassified microradar events that can be potentially triggered in the time taken to travel from the initial location of the trajectory to the other end of the crosswalk at a speed of 4 feet per second plus a buffer of 3 seconds:
        i. For each of these unclassified events, if the corresponding microradar can be potentially triggered along the trajectory's current direction of travel, include it to the trajectory, subject to the following conditions:
           1. If the microradar under consideration and the current location of the estimated trajectory belong to the same sensor pair, then their event durations must overlap.
           2. If the microradar under consideration is further along the direction of travel, then the time difference between the two events should be within the following range:
              a. Less than the time taken to traverse the distance between the two sensor locations at a speed of 4 feet per second, plus a buffer of 3 seconds.
              b. More than the time taken to traverse the distance between the two sensor locations at a speed of 20 feet per second (to account for runners and cyclists).
        ii. Once the estimated trajectory cannot progress any further along its designated direction of travel, the following condition must be met for the selected sequence of events to be classified as a valid trajectory:
           1. The trajectory should include at least three distinct sensor/sensor pair locations *(start of the trajectory)*
     c. Resume the classifier from the next available unclassified microradar event.

To illustrate the crosswalk trajectory classification, consider the sequence of events described in Table 4.1. Table 4.1 shows two complete trajectories (55 and 56), and a partial representation of a third trajectory (57). In addition to the classification results, the trajectory also shows the sensor labels which help validate the classifier results.

Table 4.1 An example of the trajectory estimation

Sensor ID	Time	Duration	Ped_S_N	Ped_N_S	Label
3	0	1.625	55	0	cycle(ride) (SN)
2	0.625	2.5	55	0	cycle(walk (SN)
12	1.063	1.125	0	56	cycle(ride)

					(NS)
4	1.375	1.125	55	0	cycle(ride) (SN)
9	2.313	1.375	0	56	1 ped (NS)
10	2.75	1	0	56	cycle(ride) (NS)
8	3.188	0.875	55	0	cycle(ride) (SN)
5	3.313	1.375	57	0	cycle(walk (SN)
10	5.875	1.625	55	0	cycle(ride) (SN)
9	5.938	1.125	55	0	cycle(ride) (SN)
8	6.938	3.125	0	56	cycle(ride) (NS)
3	7.75	0.75	0	0	cycle(ride) (NS)
11	8.125	1.375	55	0	cycle(ride) (SN)

In the case of trajectory 55, sensors 2 and 3, which appear to have been triggered around the same time by two separate road users, get grouped under the same trajectory. Thereafter, the trajectory seems to follow the cyclist who is riding the crosswalk from south to north. As part of this trajectory, another sensor pair (9 and 10) is also grouped together. However, in this instance, the sensors are labeled as a riding cyclist, which implies that the same user may be triggering both sensors.

Trajectory 56 begins with sensor 12, thus initiating an N□S trajectory, as validated by the associated label. Thereafter sensors 9 and 10 are grouped together, although the labels indicate that two different user types may have triggered these events. Thereafter, the trajectory is terminated at sensor 8.

Trajectory 57 is initiated at sensor 5, which corresponds to the walking cyclist whose previous position get grouped under trajectory 55. However, even in the absence of the earlier sensor event, it appears that there are a enough number of sensor events in this instance to classify this trajectory further upstream on the crosswalk.

Finally, there is an event associated with microradar 3 at 7.75 seconds which is not classified under any trajectory. In this particular instance, the video recording helps identify that the event is associated with the cyclist riding from N□S. However, the timeline of the events appears too close as the previous detection of this cyclist at sensor 8 could not get de-activated once the cyclist departed as another user entered its detection zone which extended the event even further. This dynamic is illustrated in Figure 4.9.

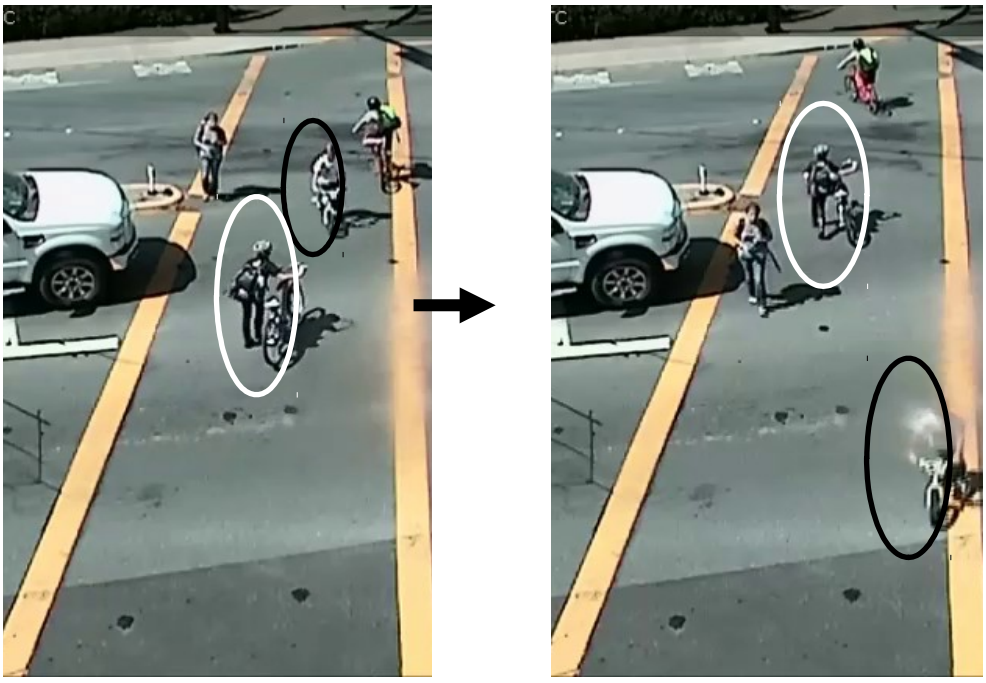

Figure 4.9 An example of a microradar getting triggered by one user and getting extended by another user

The images in Figure 4.9 also show various road users crossing on the edge of the crosswalk which also results in trajectories not getting completely captured by the sensor along the crosswalk. Hence, these sets of examples illustrate the challenges associated with tracking crosswalk movements.

4.4 Results: Training Data

The results of the trajectory classifier using labeled pedestrian phase data from April 22, 24 and October 12-14 are shown in Table 4.2.

Table 4.2 Results of trajectory-based classification using training data

Mode	Count	Right N□W	Right W□S	Straight E□W	Straight W□E	Crosswalk S□N	Crosswalk N□S	Unclassified
Motorized	1100	344	40	547	136	0	2	31
Non-Motorized	559	2	6	5	0	117	374	55
Grand Total	1659	346	46	552	136	117	376	86

An evaluation of the unclassified labeled data reveals that some of the Right (N□W) movements are not getting classified in scenarios where the right turn movements do not get detected at the exit lanes. Consequently, a modified right turn classifier is implemented at the end of the crosswalk algorithm which gets initiated at the crosswalk (microradar 11) as opposed to the exit lane. The benefit of implementing the right turn algorithm at the end of the analysis is that it can only identify right turn events using the remaining unclassified microradar events. The revised set of results are shown in Table 4.3. As can be seen from the Right (N□W) column, the additional pass of the right turn algorithm added 6 additional microradar events.

Table 4.3 Revised results of trajectory-based classification using training data

Mode	Count	Right N□W	Right W□S	Straight E□W	Straight W□E	Crosswalk S□N	Crosswalk N□S	Unclassified
Motorized	1100	350	40	547	136	0	2	25
Non-Motorized	559	2	6	5	0	117	374	55
Grand Total	1659	352	46	552	136	117	376	80

The results shown in Table 4.3 indicate that the accuracy of the classifier, defined as the sum of correctly classified motorized events and non-motorized events divided by the total number of labeled microradar events, is 94.5%. When excluding the unclassified microradar events from the analysis, the accuracy jumps to 99.1%. This implies that the misclassification error of the classifier within the training data is less than 1 %. The relatively poor quality of the right (W□S) classifier is primarily because of the absence of a functioning magsensor 8 to correctly establish the start of the trajectory.

Table 4.4 shows a more detailed evaluation of the classifiers by comparing their performance for different movement types. Herein, the results show that accuracy for classifying right turns, straight movements, N□S and S□N crosswalk movements are 93.7%, 97.2%, 87.2% and 85.4% respectively.

When excluding the unclassified information, the accuracy estimates increase to 96.3%, 99%, 95.7% and 97.4% respectively. The accuracy of the classified data is important in terms of understanding whether there are any biases within the classification, which affects the subsequent analysis of mode-specific and multi-modal safety critical dynamics.

Table 4.4 Movement-based evaluation of classifiers (training data)

Right Turns (Ground Truth)	**Right N→W**	**Right W→S**	**Straight E→W**	**Straight W→E**	**Crosswalk S→N**	**Crosswalk N→S**	**Unclassified**
411	345	40	15	0	0	0	11
Straight Movements (Ground Truth)	**Right N→W**	**Right W→S**	**Straight E→W**	**Straight W→E**	**Crosswalk S→N**	**Crosswalk N→S**	**Unclassified**
679	5	0	524	136	0	2	12
Crosswalk N→S (Ground Truth)	**Right N→W**	**Right W→S**	**Straight E→W**	**Straight W→E**	**Crosswalk S→N**	**Crosswalk N→S**	**Unclassified**
429	1	6	4	0	6	376	36
Crosswalk S→N (Ground Truth)	**Right N→W**	**Right W→S**	**Straight E→W**	**Straight W→E**	**Crosswalk S→N**	**Crosswalk N→S**	**Unclassified**
130	1	0	1	0	111	1	16

Table 4.4 also reveals that in spite of running two passes of the right (N→W) classifiers, about 5% of the microradar events get misclassified as straight moving vehicles. The primary cause for this misclassification is that sometimes a single magsensor event captures multiple vehicles. In this case, when vehicles are close to each other at the right turning lane (magsensor 31), a sensor event triggered by one vehicle is extended by another vehicle. As a result, the right turn classifier cannot find an accompanying magsensor event for the first vehicle, since the triggered sensor event may eventually end after the first vehicle traversing the crosswalk microradars.

Also, since the evaluation period includes some buffer period around the pedestrian phases, there are nine left turn movements which get included in the training data. These events are classified as straight (E→W) trajectories, since the stop bar lane sensors associated with the straight (E→W) movement are not used for the analysis.

4.5 Results: Test Data

While the trajectory classification algorithm wasn't completely trained on the classifier data, it was calibrated by iteratively improving the classification accuracy using the labeled training data. Consequently, it is important to evaluate the accuracy of the classifier using the two days of labeled microradar data were exclusively kept as test data.

Table 4.5 Results of trajectory-based classification using test data

Mode	Count	Right N→W	Right W→S	Straight E→W	Straight W→E	Crosswalk S→N	Crosswalk N→S	Unclassified
Motorized	401	164	20	136	50	2	2	27
Non-Motorized	210	0	4	3	0	32	143	28
Grand Total	611	164	24	139	50	34	145	55

Table 4.5 indicates that the accuracy of the classifier, when evaluating the test data, is 89.2%. When excluding the unclassified microradar events from the analysis, the accuracy increases to 98%. In comparison to the training data, the results are worse by five percent, which is largely driven by an increase in the unclassified events. In particular, the misclassification errors are associated with right (W→S) and straight (E→W) classifiers, both of which suffer from non-functioning magsensors. In the case of right (W→S) classification, it appears that successive right turn movements can lead to overlapping microradar 3 detections, which leads to a long sensor event capturing multiple vehicules. Consequently, a fully functional sensor setup can help improve accuracy for these vehicle movements by providing additional sensor events to infer the trajectories from.

The movement-based evaluation of the classifiers is shown in Table 4.6. The accuracy for classifying right turns, straight movements, N→S and S→N crosswalk movements are 85.4%, 95.6%, 82.6% and 76.3% respectively. When excluding the unclassified information, the accuracy estimates increase to 93.3%, 98.9%, 93.4 % and 96.7% respectively. These results reveal that the crosswalk movements have a higher percentage of unclassified movements. When only considering the misclassified events, the crosswalk (N→S) movement has the highest percentage of misclassifications.

Table 4.6 Movement-based evaluation of classifiers (test data)

Right Turns (Ground Truth)	Right N→W	Right W→S	Straight E→W	Straight W→E	Crosswalk S→N	Crosswalk N→S	Unclassified
213	162	20	10	0	1	2	18
Straight Movements (Ground Truth)	**Right N→W**	**Right W→S**	**Straight E→W**	**Straight W→E**	**Crosswalk S→N**	**Crosswalk N→S**	**Unclassified**
182	2	0	124	50	0	0	6
Crosswalk N→S (Ground Truth)	**Right N→W**	**Right W→S**	**Straight E→W**	**Straight W→E**	**Crosswalk S→N**	**Crosswalk N→S**	**Unclassified**

172	0	4	3	0	3	142	20
Crosswalk S□N (Ground Truth)	**Right N□W**	**Right W□S**	**Straight E□W**	**Straight W□E**	**Crosswalk S□N**	**Crosswalk N□S**	**Unclassified**
38	0	0	0	0	29	1	8

Similar to the training data, there are two left turn events in the test data, which are classified as straight (E□W) trajectories.

4.6 Comparisons with other mode classification techniques

With regards to the performance of the trajectory-based classifier vis-à-vis other mode classification efforts within the traffic safety literature, Zangenehpour et al. (2015) developed an image recognition and trajectory speed-based classification method to differentiate between pedestrians, cyclists and pedestrians, which had an accuracy between 86 and 93.3%. Kumar et al. (2005) developed a Bayesian network-based classifier for categorizing objects within a video as different vehicle categories. The classification accuracies of their algorithm for pedestrians, motorcycles, cars, trucks and heavy trucks was vehicles were 86.7%, 92.5%, 96.3%, 93.3%, and 93.6% respectively. Based on these comparisons, it can be said that the trajectory-based classifier performs similarly to some of the computer vision-based mode-classification techniques, although some of the classification errors with regards to the trajectory-based classification method can be minimized with a fully functioning sensor network. At the same time, it is acknowledged that the proposed method does not differentiate between cyclists and pedestrians as yet, which shall be investigated in the future.

4.7 Discussion

After evaluating the classification results of both the training and test data, here are some observations associated with the trajectory-based classification:

- Presence of fully functioning sensors along a vehicle's path is important for accurately estimating the trajectory (e.g., straight (W□E) classification)
- In the absence of complete trajectories, it is possible to use sensor-specific information and interactions between sensors to estimate events (e.g., straight (E□W) trajectories). However, it is important to ensure that the subset of the trajectory used to classify the events do not match with other types of unclassified movements.
- A major limitation of the proposed trajectory is that it limits the sensor events to be associated to only one trajectory. As evidenced in the case of right turn as well as the crosswalk movements, a single sensor event can comprise of multiple objects traveling in close proximity. Consequently, relaxing this assumption in future approaches can improve the accuracy significantly.

5 Extracting Variables for Right Turn Safety Analysis

At a signalized intersection, pedestrians encounter potential conflicts with vehicles under three circumstances: right turns on a green (RTOG), right turns on a red (RTOR), and permitted left turns on a green (LTOG) (Hubbard et al, 2009). RTOR and LTOG may be prohibited by signal timing, however, the conflicts resulting from RTOG are more difficult to address. Thus, the present study, focuses mainly on pedestrian-vehicle interactions under RTOG, to determine vehicle yielding behaviors, and to assess the safety level of right-turn and improve pedestrians' walking environment. The first step of the analysis involves extracting the necessary variables.

5.1 Overview of Raw Data

The locations of mag-sensors and micro-radars are shown in Figure 5.1, to help explain the following algorithms. The raw data is listed in Table 5.1. Because the focus is on right turns on a green (RTOG), the raw data include only the events that occurred during two phases (pedestrian green and vehicle green for North-South direction).

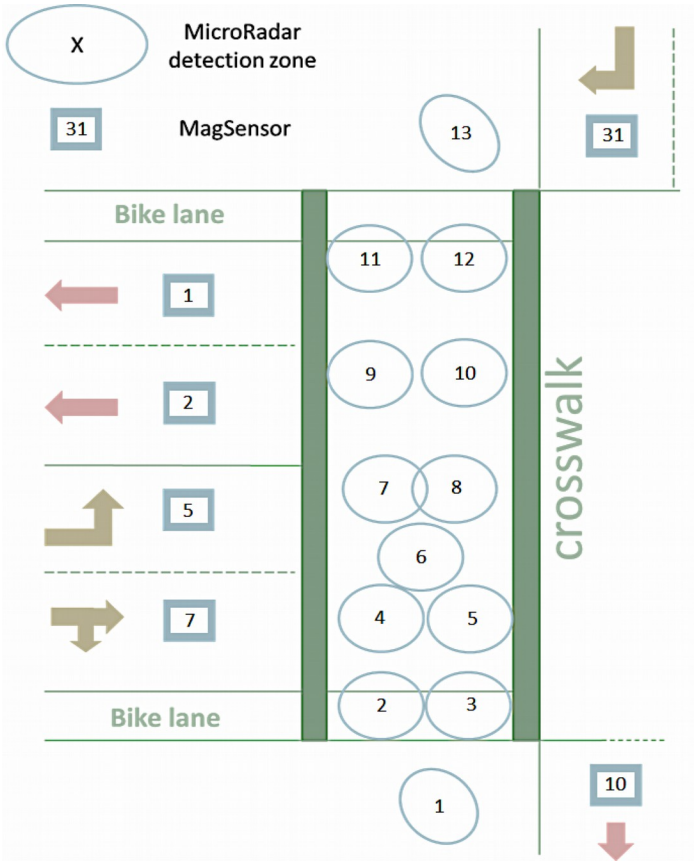

Figure 5.1 Configuration of sensors

Table 5.1 Raw data set

Event timestamp (hour, minute, second)
Event duration (of time)
Event Location (Mag-sensor or Micro-radar ID)
Event classification (ped or veh)
If ped event, the walking direction (NS or SN).
If veh event, whether car stops or not.
If veh event, whether a right-turn or through-driving vehicle

5.2 Variables

Table 5.2 Variable list

	Behavior	Variables
Pedestrian	(a) Go/No-go	(c) Age, gender, color of clothing
		(d) Group population
		(e) Walking direction
		(f) Walking speed
Vehicles	(b) Yield/Not-yield	(g) Right-turn traffic volume
		(h) Upstream speed
		(i) Position in a platoon
Intersection	---	(j) Time
		(k) Phase
		(l) Location
		(m) Geometry layout

The potential variables are listed in Table 5.2. Below is a brief description of variables and data accessibility.

(b): Yield/Not Yield: When confronting pedestrians, whether or not vehicles yield or continue forward. Many researchers use a binary output to simplify the modeling (Hubbard, 2009; Ling et al, 2012). The current study identifies three different types of behavior, categorized into three classes. This variable is obtained using the yielding algorithm described in the following sections.

(c)(d)(f): Age, gender, color of clothing, group population, and walking: These variables are obtained via video data or field investigation, which are not incorporated in the current study.

(e): Walking direction: from north to south, or south to north. This variable was identified in Chapter 4. Some researchers have found a behavioral difference between the far-side and near-side pedestrians as they perceive the same right-turn car moving toward them (Alhajyaseen, 2013).

(g): Right-turn traffic volume are obtained from the mag-sensors. Akin (2007) has shown its significant impact on yielding behavior.

(h): Upstream speed: Vehicles' operating speed at the upstream of the approach, which can be calculated based on the location of sensors and the time at which a vehicle passes them. Abdulsattar et al. (2013) observed that vehicle speed impacts drivers' decisions, but upstream speed is less of a factor.

(i): Position in a platoon: Whether the vehicle is in a leading or following position in the traffic flow. Since headway can be calculated by the mag-sensors, position of a platoon can also be obtained.

(k): Phase: Whether the interactions between vehicles and pedestrians occur at pedestrians green only (early phase), vehicle green only (end phase), or both (middle phase).

(l)(m): Location is related to land use, such as whether the intersection is in CBD. Geometry layout is related to the turning radius, width of crosswalks, and other characteristics. Although as found by Hubbard (2009), drivers in CBD are more likely to look for pedestrians and yield to them in the crosswalks. Since the study focuses on a single intersection, these data are not considered, but warrant further research in the future.

The following sections elaborate on the algorithms of each variable.

5.3 Yielding

Definition: For right-turn vehicles, the driver who yields has two choices: to wait at the stop line or to wait at the turning area. Thus, the yielding algorithm is divided into two parts.

For the first case, a yielding maneuver is defined as a vehicle which stops at the stop line and leaves after the pedestrian exits the conflict area. For the second case, yielding is defined as car which arrives at the intersection before the pedestrian, but exits the conflict area after the pedestrian.

Algorithm: The basic idea of the yielding algorithm is to determine the time difference between consecutive vehicle and pedestrian events under different conditions. A brief description of the algorithm is shown in Figure 5.2. The procedure is as follows:

i) Loop over the entire dataset chronologically.
ii) Select the vehicle event if “its sensor ID = 31” AND “a right-turning event,” then record the event’s timestamp and its right-turn id.
iii) Select the pedestrian event if “its sensor type is 1 (micro-radar)” AND “its sensor ID = 9, 10, 11, 12,” then record the event’s timestamp.
iv) Calculate the time difference between the recorded vehicle and pedestrian events.
v) Label the vehicle event as yielding (at the stop line) if “it’s a stopped vehicle” AND “time difference≤7s.”
vi) Label the vehicle event as yielding (at the turning area) if “time difference≤0s” AND “second time difference>0s,” where the second time difference is obtained by:

a) Using right-turn id, find the corresponding vehicle event in the same trajectory after passing the turning area. Record the timestamp.
b) Calculate the time difference between this new vehicle event and the pedestrian event.

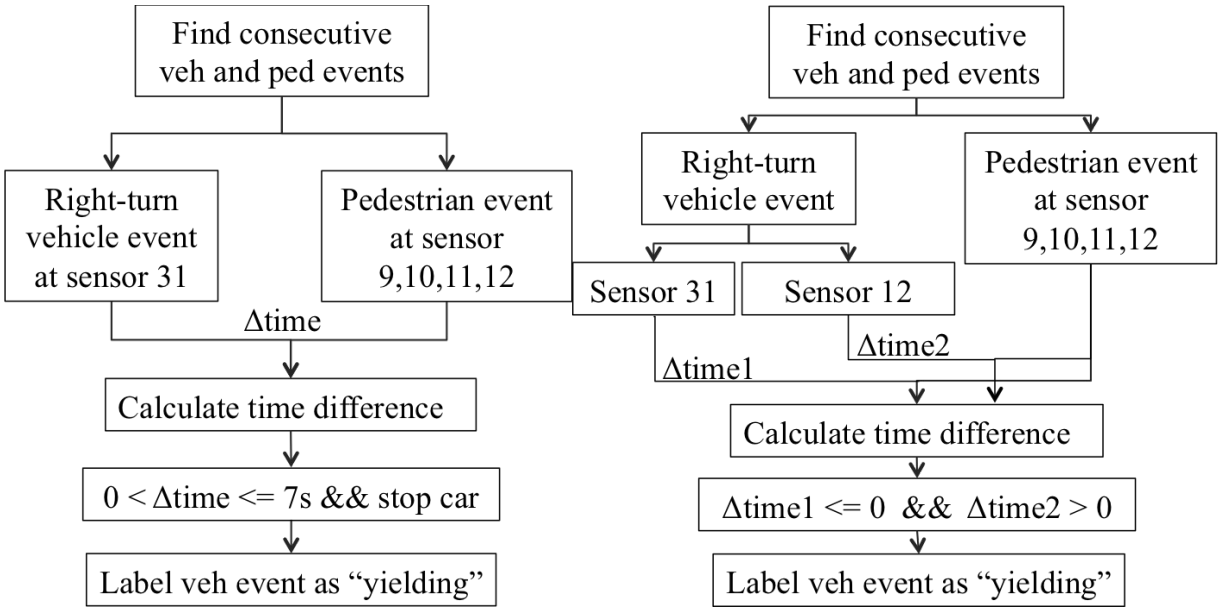

Figure 5.2 Algorithm: Yielding at the stop line (left) and yielding at the turning area (right)

A threshold of seven seconds is established as the maximum waiting time of vehicles after the last pedestrian leaves the conflict area. If the time difference is greater than seven seconds, it is determined that there was no interaction between vehicles and pedestrians. This threshold is determined by the experimental data collected from April 22nd to April 24th and Oct 12th to Oct 16th. Five to nine second periods are checked based on video data, and seven seconds offers the best accuracy. The accuracy analysis will be provided in the following section..

Example: Data collected on April 22, 2015 at 15:31:53 PDT is used as an example.

	A	B	C	D	E	F	G	H
1	SensorTyp	SensorID	Hours	Min	Sec	Right_N_V	PhaseNo	Veh_yield
4562	1	10	15	31	53	10000	37	-2
4563	1	9	15	31	53	10000	37	-2
4564	1	11	15	31	54	10000	37	-2
4566	2	31	15	31	55	124	37	1
4567	2	29	15	31	57	125	37	-2
4569	2	30	15	31	58	125	37	-2
4571	1	12	15	31	59	124	37	-2

Figure 5.3 Yielding example: data*

**Note: Right_N_W=10000 denotes that this is a pedestrian event; 0<Right_N_W<10000 denotes that this is a right-turn vehicle event, the number is ordered chronologically. Veh_yield=1 represents yielding; Veh_yield=-2 represents no interaction.*

Figure 5.4 Yielding example: screenshot of video.

5.4 Non-Yielding

Definition: A non-yielding maneuver is defined as a vehicle which passes the conflict area just a few seconds before a pedestrian passes.

Algorithm: Similar to the yielding algorithm, **the** time difference is a crucial index to classify non-yielding events. A brief description of the algorithm is shown in Figure 5.5. The procedure is as follows:

i) Loop over the entire dataset chronologically. Select events at the conflict area where “its sensor ID = 9, 10, 11, 12” AND “its sensor type is 1 (micro-radar).”

ii) If it is a vehicle event, mark it as a current vehicle event and restore the timestamp; if it is a pedestrian event, mark it as current pedestrian event and restore the timestamp.

iii) If the timestamp of the current vehicle event is three seconds less than the timestamp of the current pedestrian event, then label that vehicle event as non-yielding (0).

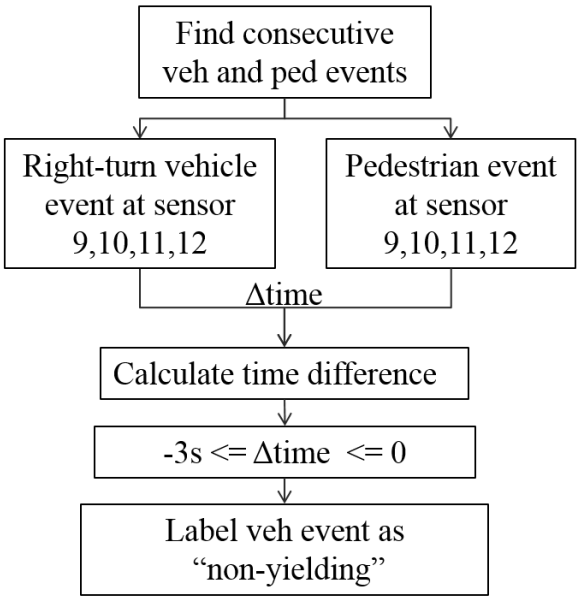

Figure 5.5 Algorithm: Non-yielding

Three seconds is a critical threshold for judging the situation of non-yielding. Time periods of 2s, 3s, 4s and 5s were used to determine whether different thresholds offer different results. By comparing the video data, the 3s time period captures the non-yielding feature more accurately.

Example:

A non-yielding case that occurred at on October 12, 2015 at 07:34:37 PDT is used as an example.

	A	B	C	D	E	F	G	H
1	SensorType	SensorID	Hours	Min	Sec	Right_N_W	PhaseNo	Veh_yield
18095	2	31	7	34	35	3	1	-2
18099	1	12	7	34	37	3	1	-2
18100	1	11	7	34	37	3	1	0
18104	1	9	7	34	39	10000	1	-2
18105	1	10	7	34	39	10000	1	-2
18106	1	12	7	34	40	10000	1	-2
18107	1	11	7	34	40	10000	1	-2

Figure 5.6 Non-yielding example: data*.

**Note: Veh_yield=0 represents non-yielding; Veh_yield=-2 represents no interaction.*

Figure 5.7 Non-yielding example: screenshot of video.

Error Analysis:

Error analysis shown in Table 5.3, using the 8-hour video data.

The results are as follows:

- Accuracy of identified interactions: 100%.
- Missing rate of actual interactions: 13.16%.

Table 5.3 Accuracy of yielding and non-yielding algorithm.

Error analysis		Ground Truth (8-hour video data)			
		No interaction	Yielding	Non-yielding	
Automated algorithm results	No interaction	---	5	0	
	Yielding	0	31	0	100%
	Non-yielding	0	0	2	
			13.16%		

Of the five missing interactions, four were caused by pedestrians (usually one of the crossing guards) who walked outside of the crosswalk area, and thus were unable to be detected by the micro-radar. This phenomenon results in the time difference between consecutive vehicles and pedestrians being greater than the actual value and is therefore not included in the yielding events category.

The last of the missing interactions is related to the threshold of seven seconds in the yielding algorithm. For this missing interaction, the time difference is eight seconds, one second longer than the current threshold. If the threshold is reset to eight seconds, the accuracy remains acceptable, however, seven seconds was established as the threshold for the present study.

In summary, the yielding/non-yielding algorithms present good accuracy and robustness.

Strengths and Weaknesses:

The yielding/non-yielding algorithms are established by sensor data and can automatically obtain yielding behavior for long periods of time, which offers convenience and feasibility for future yielding-related research. The high rate of accuracy (100% correctly identified interactions) makes it nearly as reliable as video data.

However, the thresholds in the algorithms may be intersection-specific. Researchers must calibrate them again for new intersections. In addition, all sensors must be operational, which is challenging since in California it is quite common for sensors to break down.

5.5 Speed

Detection Zone:

For the mag-sensors, sensor 31 and sensor 30 share a rectangular detection zone, shown in Figure 5.8. Initially, the following formula was used: speed = (detection zone distance + car length)/(time difference between two events + duration of Sensor 30) to accurately calculate the speed. However, recently Sensor 30 ceased working and yielded no data. An approximation was generated by dividing the detection zone in half and using the new detection distance to calculate the speed.

The detection zones of micro-radar are irregular (more like an ellipse), as shown in Figure 5.9, therefore the detection area is roughly identified as a rectangular region. Follow up field investigation to test the accuracy of the algorithm indicates that the speed is reasonable under such an assumption.

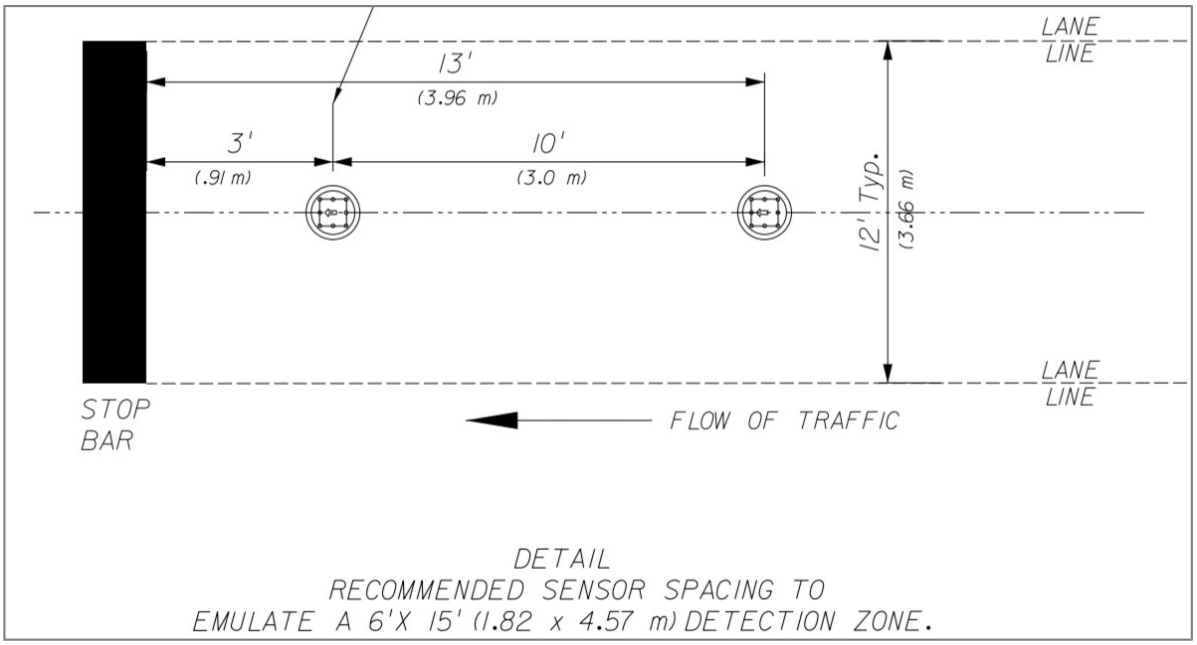

Figure 5.8 Detection zone of mag sensors (Source: Sensys Networks, Inc.)

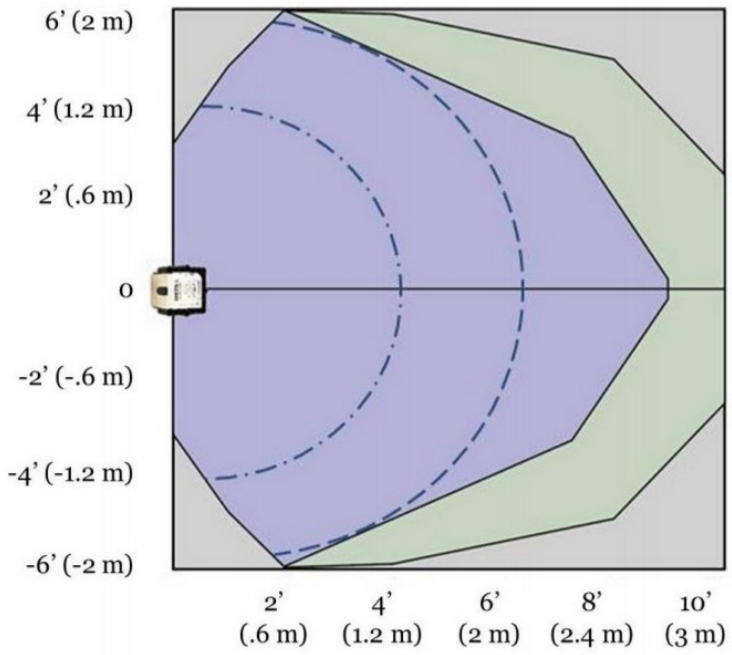

Figure 5.9 Detection area of micro-radars (Source: Sensys Networks, Inc.)

Algorithm:

i) For vehicle events at sensor ID = 9, 10, 11, 12, speed = (approximate detecting distance + car length) / duration of event = (4m + 4.4m) / duration of event.

ii) For pedestrian events at sensor ID = 9, 10, 11, 12, speed = (approximate detecting distance) / duration of event = 3m / duration of event.

iii) For vehicle events at sensor ID = 29, 30, 31, speed = (detecting distance + car length) / duration of event) = (2.285m + 4.4m) / duration of event.

iv) Convert the unit from meter/second to mile/hour.

Accuracy:

A field study was conducted at the intersection in Danville on Dec 2, 2015, including a test of the accuracy of the speed. A speed gun to was used to test the speed upstream of the approach (Figure 5.10), near the stop line and the speed of vehicles passing the crosswalk (Figure 5.11).

The results from the speed gun confirmed the expectations. The speed of vehicles passing the crosswalk was approximately 12 mph, the upstream speed was approximately 20 mph but shows variability. Figure 5.10 illustrates how the speed gun was used in the field study.

Figure 5.10 Detect speed using speed gun in field study.

5.6 Position in a Platoon

Definition: Research of yielding behavior did not include vehicles' positions in the platoon in which the interactions occurred, but should be noted before the driver makes a decision.

Algorithm:

i) Select events at sensor ID = 29.

ii) Store two consecutive vehicles' timestamp. If the time difference between the two timestamps is less than five seconds, then the second car is a following car, label the leading variable as 0; if not, the second car is a leading car, label the variable as 1.

iii) For each right-turn vehicle event, A, labeled as either yielding or non-yielding, using its right-turn ID find the corresponding vehicle event, B, at Sensor 29 in the same trajectory. Assign the value of position in a platoon for event B to event A (1 represents a leading vehicle while 0 represents a following vehicle).

5.7 Right-Turn Volume

Algorithm: Right-turn volume is calculated for each fifteen-minute period. Thus, the right-turn volume at 7:05 a.m. is determined as the volume from 7:00 a.m. to 7:15 a.m., which is generated based on how many vehicles passed Sensor 31 from 7:00 a.m. to 7:15 a.m.

Phase

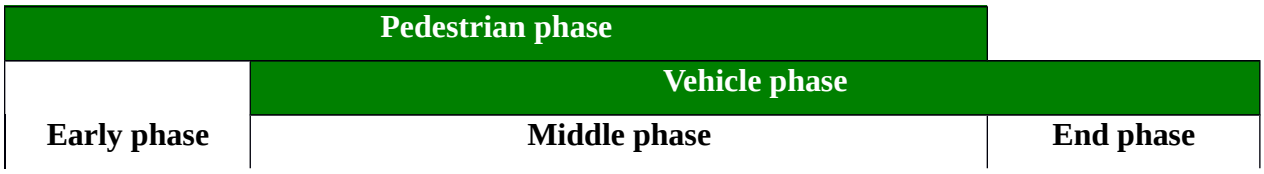

Figure 5.11 Definition of phase variable

Algorithm: Early phase, middle phase, and end phase are dummy variables. For an interaction, if the corresponding vehicle event occurs in the early phase, it should be labeled as 1, and the other two dummy variables as 0. Interactions that occur during the middle phase and the end phase are labeled similarly.

6 Assessment of Right-Turn Related Safety

This chapter provides surrogate measures to evaluate the safety of the intersection and offers additional quantitative analysis to identify factors to explain yielding/non-yielding behavior.

6.1 Surrogate Measures

The safety of intersections is typically evaluated using historical crash data. However, many intersections experience zero, or very few crashes, and therefore do not provide enough information about the countermeasures that are needed to improve safety. Monitoring safety-critical events, such as yielding and non-yielding interactions, can be used as surrogate safety measures that allow proactive assessment of safety hazards without the occurrence of a crash. Two indicators are used to assess right-turn related safety at the intersection.

6.2 Yielding Rate

The yielding-related statistics are summarized in Table 6.1. The dataset is from April 22nd to April 24th and from Oct 12th to Oct 16th; all weekdays.

Table 6.1 Statistics summary: yielding rate

# of total interactions		197	
# of yielding events	Waiting at stop line	179	156 (87.15%)
	Waiting at turning area		23 (12.84%)
# of non-yielding events		18	
Yielding rate		90.86%	
Non-yielding rate		9.14%	

The non-yielding rate is approximately 10%, which is at normal level. However, since the intersection in near a primary school, and considering the vulnerability of children, the aim is to eliminate the non-yielding cases as much as possible. Therefore, it is important to determine which factors can significantly affect vehicles' yielding behavior, as analyzed in the following chapter.

Another interesting finding is that up to 30% of yielding vehicles stop at the turning area. This phenomenon can be explained by two potential causes. One is that a group of drivers is accustomed to yielding by slowing approaching to the crosswalk instead of coming to a full stop. The other is that some drivers fail to see pedestrians until they turn right, leading to a sudden braking at the turning area. More attention to yielding at the turning area warrants future research.

6.3 Post-Encroachment Time (PET)

For cyclist safety, PET is defined as the time difference between the moment when a rear part of the vehicle leaves (or arrives at) the area of potential collision and the moment when a bicycle's front wheel arrives at (or the rear wheel departs from) this area (Kassim et al. 2014).

Similarly, for pedestrian safety, PET is defined as the time difference between the moment when a rear part of the vehicle leaves (or a pedestrian leaves) the area of potential collision and the moment when a pedestrian arrives at (or the rear wheel arrives at) this area. PET statistics are summarized in Table 6.2.

Table 6.2 Statistics summary: PET (s)

Date	Yielding A*	Yielding B*	Non-yielding
4/22/15	5.8816	1.2813	1.2917
4/23/15	4.6442	1.0625	---
4/24/15	5.2356	1.8333	1.7083
10/12/15	5.2188	1.1250	2.3750
10/13/15	5.3073	0.2500	---
10/14/15	5.6447	1.5417	1.1563
10/15/15	5.5486	2.1875	1.8125
10/16/15	4.7868	0.7500	0.2188
Weighted average*	**5.3109**	**1.3000**	**1.1389**

** Yielding A denotes yielding at the stop line.*

** Yielding B denotes yielding at the turning area.*

** Weighted average: The average of PET is weighted on the number of yielding or non-yielding events in each day.*

Great differences between PETs in yielding and non-yielding cases can be observed. Since PET data is easier to obtain than yielding data, it can alternatively be used as a reference of assessing safety.

6.4 Preliminary Analysis

6.4.1 Yielding Rate & Time

The yielding rate and the histogram of total number of interactions over time are plotted, as shown in Figure 6.1. The yielding rate is the average value of eight days' data; the number of interactions is the sum of eight days' data.

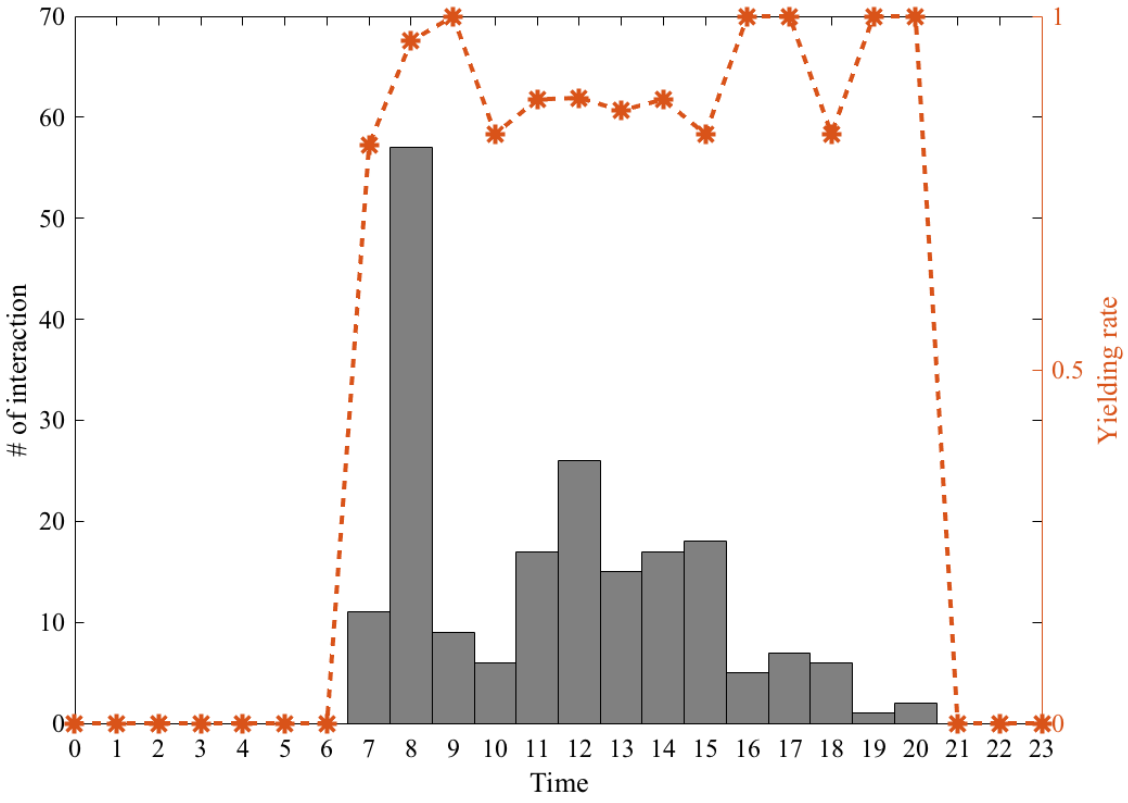

Figure 6.1 Yielding rate and total number of interactions over time

From 8-9 a.m., 4-5 p.m. and 7-8 p.m., the yielding rate gets to the highest point of the entire day while the yielding rate at other time slots maintains approximately 85%. Thus, time can be considered as an important factor that may impact yielding rate.

Furthermore, the yielding rate does not present a strong relationship with the number of interactions, which also imply that yielding rate might not be related to volume.

6.4.2 Yielding Rate & Crosswalk Guard

Combining the eight-hour videos and the field study, it appears that from 8-9 a.m., there was a crosswalk guard who raised a warning sign to the right-turn vehicles when the pedestrians walked on green. Thus, the 100% yielding rate from 8 to 9 a.m. might also be connected to the presence of guard.

6.4.3 Yielding & Position of a Platoon

For all interaction events, **92.9%** of them are leading vehicles.

For yielding cases, **93.3%** of them are leading cars.

For non-yielding case, **88.9%** of them are leading cars.

For the leading cars, **91.3%** of them yield.

For the following cars, **85.7%** of them yield.

These numbers imply that the following vehicles are more likely to make non-yielding choice while the leading vehicles are more inclined to make yielding choice. However, the relationship is not notable and needs further analysis.

6.4.4 Yielding & Pedestrian Direction

For all interaction events, **48.3%** of pedestrians are walking from north to south (N-S).

For non-yielding case, **61.1%** of them confront N-S pedestrians.

For yielding case, **46.8%** of them confront N-S pedestrians.

For N-S pedestrians, **86.9%** of vehicles they meet yield.

For S-N pedestrians, **92.2%** of vehicles they meet yield.

These numbers imply that vehicles are more likely to yield to S-N pedestrians than N-S ones. Still, the difference is not obvious enough and needs further analysis.

6.4.5 Yielding & Speed

Figure 6.2 plots the average speed change of right-turn trajectories under different scenarios. Sensor 29 is the upstream of the approach where appears a clear difference between non-yielding case and yielding (plus non-interaction) case. Thus it can be assumed that upstream speed can largely affect vehicles' yielding behavior. Quantitative analysis will be presented in following chapter.

In addition, a similar change pattern of speed is observed between non-yielding and non-interaction, suggesting that these non-yielding drivers behave as though they fail to see the pedestrians.

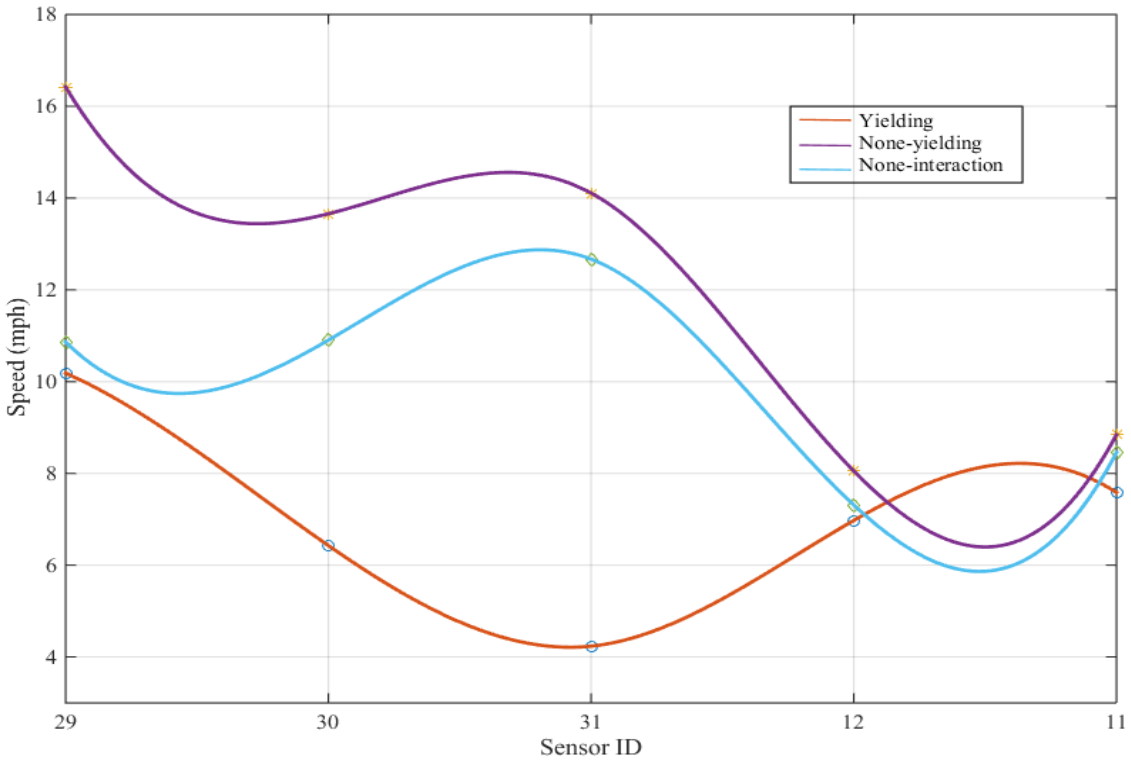

Figure 6.2 Change of speed under three scenarios

6.5 Discrete Choice Model

6.5.1 Limitations of Previous Literature

Previous studies (Abdulsattar et al., 1996; Leden, 2002; Akin and Sisiopiku, 2007; Alhajyaseen et al., 2013; Elmitiny et al, 2010; Hubbard et al., 2009; Ling et al, 2012) are mostly conducted based on video data, thus they contain a relatively wide range of choices of potential factors which cannot be obtained

from sensor data, such as the group population, the dressing color of the pedestrians. However, there exist some problems.

i) These studies are based on several hours' video data, which are restricted to the data size and might weaken the reliability of results.

ii) Some of the studies only conduct qualitative analysis from psychology perspective. More statistical tests should be addressed.

iii) For the studies that conducted quantitative analysis, to simplify the model, most used a binary output to denote yielding or non-yielding, ignoring the variations of vehicles' responses.

iv) Furthermore, additional characteristics have not been counted into consideration, such as the phase factor discussed in Chapter 5.

v) Some variables need further revised. For example, for the variables, speed and the vehicle's position in a platoon, these two attributes of the upstream events that occurred prior to the interactions should be considered.

Weaknesses in this study were addressed by the use of eight-day sensor data, carefully constructed variables, and use of logistic regression to quantitatively analyze vehicles' yielding behavior. Three discrete choice models, including Binary Logit model, Multinomial Logit model and Nested Logit model were used, to probe how the potential factors affect yielding behavior and the correlations between each kind of behavior, yielding at the stop line, yielding at the turning area and non-yielding.

6.5.2 Binary Logit Model

The two behaviors, yielding at the stop line and yielding at the turning area are considered as one. Thus in Binary Logit model, there are two alternatives (or outputs, choices), yielding and non-yielding. The deterministic utility of each alternative is as follows:

$$V_{Yielding} = \beta_2 \times volume_i + \beta_3 \times \text{¿}\ position_{\text{¿}}\ \beta_4 \times upstream_{speedi} + \beta_5 \times n2\,s_i + \beta_6 \times crosswalk_{guardi} + \beta_7 \times early_{phasei} + \beta_8 \times end_{phasei}$$

$$V_{Non-yielding} = \beta_1$$

The utility function of each alternative is:

$$U_{Yielding} = V_{Yielding} + \varepsilon_1$$

$$U_{Non-yielding} = V_{Non-yielding} + \varepsilon_2$$

$\varepsilon_1, \varepsilon_2$ are error terms which follows same extreme value distribution.

Estimate these ten parameters on R-studio, the results is shown in Table 6.3.

Table 6.3 Estimation of parameters for Binary Logit Model*

Name	Estimate	Std Error	P-value
Volume	-2.668e-03	7.518e-03	0.723
Position in platoon	1.547	1.362	0.256
Upstream speed	1.009e-01	1.078e-01	0.349
N_S	8.075e-01	1.060	0.446
Crosswalk guard	-1.706e+01	3.293e+03	0.996

Early phase	-4.077e+01	5.911e+03	0.994
End phase	4.798e-01	1.482	0.746

* *Note*: The total number of observations of the model is 165 based on our eight-day sensor data.

The p-values clearly show that these factors are all not significant. Thus, Binary Logit Model is not a good choice. One of the possible reason might be that yielding at the stop line and yielding at the turning area cannot be considered as a same kind of behavior, yielding behavior is treated as two and the Multinomial Logit Model is constructed.

6.5.3 Multinomial Logit Model

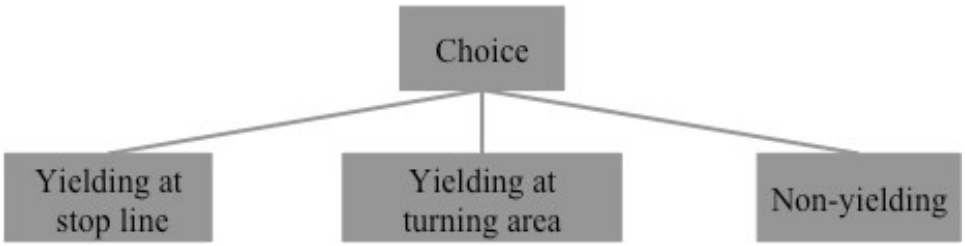

Figure 6.3 Structure of Multinomial Logit Model

The two behaviors; yielding at the stop line and yielding at the turning area are treated as independent from each other. Thus in a multinomial logit model, there are three alternatives, in which the error terms corresponding to utility functions are independent. The model structure is shown in Figure 6.3. The deterministic utility of each alternative is as follows:

$$V_{YieldingA} = \beta_2 \times volume_{platoon\ i} + \beta_3 \times position_{platoon\ i} + \beta_4 \times upstream_{speed\,platoon\ i} + \beta_5 \times n2\,s_{platoon\ i} + \beta_6 \times crosswalk_{guard\,platoon\ i} + \beta_7 \times middle_{phase\,platoon\ i} + \beta_8 \times end_{phase\,platoon\ i}$$

$$V_{YieldingB} = \beta_2 \times volume_{platoon\ i} + \beta_{11} \times position_{platoon\ i} + \beta_{12} \times upstream_{speed\,platoon\ i} + \beta_{13} \times n2\,s_{platoon\ i} + \beta_{14} \times crosswalk_{guard\,platoon\ i} + \beta_7 \times middle_{phase\,platoon\ i} + \beta_8 \times end_{phase\,platoon\ i} + \beta_{15}$$

$$V_{Non-yielding} = \beta_1$$

The utility function of each alternative is:

$$U_{YieldingA} = V_{YieldingA} + \varepsilon_1$$

$$U_{YieldingB} = V_{YieldingB} + \varepsilon_2$$

$$U_{Non-yielding} = V_{Non-yielding} + \varepsilon_3$$

$\varepsilon_1, \varepsilon_2, \varepsilon_3$ are error terms which follows same extreme value distribution.

The estimation results are shown in Table 6.4.

Two types of variables are significant. One is phase; the other is upstream speed. And the Rho-square shows a good fit of the model. However, the signs of the coefficients are out of our a-prior expectation since we expected that the higher the upstream speed, the less likely the vehicles will yield to non-motorized modes.

Table 6.4 Estimation of parameters for Multinomial Logit Model

Name	Estimate	Std Error	t-test	P-value
Constant (NonYielding)	10.0	1.18e-07	8.49e+09	0.00
Constant (Yielding A)	2.98	1.11	2.69	0.01
End phase dummy	**8.63**	**2.18**	**3.96**	**0.00**
Middle phase dummy	**8.84**	**2.22**	**3.99**	**0.00**
Position in platoon A	1.40	1.27	1.10	0.27
Position in platoon B	1.79	1.56	1.15	0.25
Presence of crosswalk guard A	0.713	1.23	0.58	0.56
Presence of crosswalk guard B	-0.307	1.39	-0.22	0.83
Upstream speed A (mph)	0.122	0.0710	1.72	0.09
Upstream speed B (mph)	0.151	0.0725	2.08	0.04
Volume (veh/min)	-0.100	0.317	-0.32	0.75
Walking direction A (1:north to south)	0.0591	1.06	0.06	0.96
Walking direction B (1:north to south)	1.13	1.16	0.98	0.33
Final log likelihood: -72.670		**Rho-square-bar 0.527**		

6.5.4 Nested Logit Model

Next a nested structure was considered to capture the heterogeneity of scenarios of yielding at stop line and yielding at turning area while at the same time they have some correlation since they both include "yielding." The structure of this model is shown as Figure 6.4. And this model is estimated in *Pythonbiogeme*.

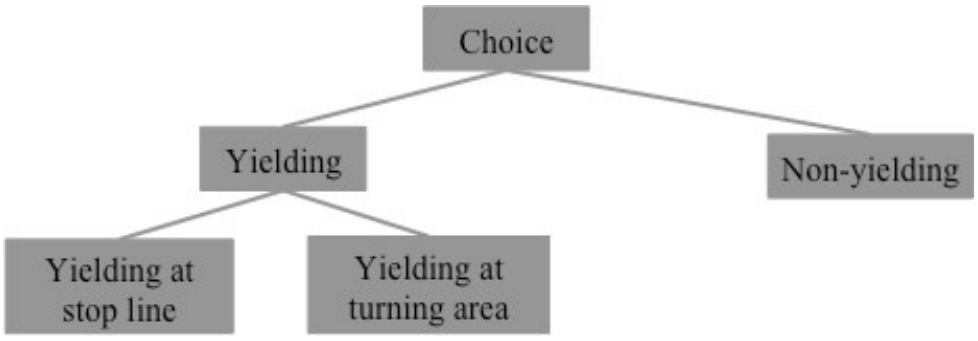

Figure 6.4 Structure of Nested Logit Model

The parameters estimation is shown as Table 6.5.

Table 6.5 Estimation of parameters for Nested Logit Model

Name	Estimate	Std Error	t-test	P-value
Constant (NonYielding)	8.78	3.23	2.72	0.01
Constant (Yielding A)	0.173	0.0443	3.91	0
End phase dummy	**10**	**0.000692**	**14456.47**	**0**
MU1	*17.1*	*15.1*	*1.14*	*0.26*
Middle phase dummy	**10.2**	**2.01**	**5.06**	**0**
Position in platoon A	1.52	1.79	0.85	0.4
Position in platoon B	1.54	1.79	0.86	0.39
Presence of crosswalk guard A	0.606	1.81	0.33	0.74
Presence of crosswalk guard B	0.546	1.81	0.3	0.76
Upstream speed A (mph)	0.135	0.183	0.74	0.46
Upstream speed B (mph)	0.137	0.183	0.75	0.45
Volume (veh/min)	-0.0725	0.47	-0.15	0.88
Walking direction A (1:north to south)	0.198	1.5	0.13	0.9
Walking direction B (1:north to south)	0.261	1.5	0.17	0.86
Constant (NonYielding)	8.78	3.23	2.72	0.01
Final log likelihood: -72.610		**Rho-square-bar 0.563**		

Do T-test to justify if it is a reasonable model.

H0: MU1=1

H1: MU1≠1

t-statistics = (17.1-1)/15.1=1.067 < 1.65 < 1.96

The null hypothesis at 95% confidence level cannot be rejected, which also implies that the multinomial model should be applied and that the two types yielding behavior should be considered independently.

6.6 Discussion

The comparison of the multinomial logit model and nested logit model reveals that two types of yielding should be treated independently from each other. In addition, the phase time and upstream speed show high statistical significance. However, according to the signs of the coefficients, vehicles arriving during the middle and end phases are more inclined to yield to pedestrians/bicycles than those arriving in the early phase (leading pedestrian interval). Similarly, the coefficient associated with the upstream speed indicates that the higher the upstream speed, the more likely the vehicles will yield to pedestrians. These observations do not match with the a-priori expectations since the leading phase aims to provide an independent and safe environment for pedestrians/cyclists crossing the road, and a higher upstream speed usually represents lower yielding rate.

Some of the biases associated with these results might come from:

1. The accuracy of extracting each variable using sensor data;

2. Errors propagating from the trajectory-based analysis;
3. The model specifications;
4. The size of the dataset is small (due to low levels of non-motorized activity at the intersection).

Thus, to further research on the yielding analysis, the following steps can be undertaken in the future:

1. Enlarge our dataset to check if the new results are consistent with our previous ones.
2. Revise the model specification, such as try nonlinear formula of utility function.
3. Increasing the accuracy of the algorithms by probing other methodology instead of using time difference.
4. Improve the accuracy of the mode classification algorithms.

7 Analysis of Mode-Specific Safety-Critical Behavior

The trajectory-based classification developed in chapter 4 facilitates the inference of vehicle and crosswalk movements. The trajectories in effect provide an estimate of the number of modes traveling across different parts of the intersection. Chapter 5 and 6 reveal the application of the trajectories for inferring multi-modal safety-critical dynamics such as right-turn yielding. In this chapter, a couple of other applications of the trajectories shall be explored to identify mode-specific safety-critical events. In particular, this chapter will focus on red light running and crosswalk movement in the absence of a pedestrian phase.

7.1 Crosswalk Movement in the Absence of a Pedestrian Phase

The analyses in the previous chapters have focused on events surrounding the pedestrian phase, which is activated by a push-button at the edges of the crosswalk. However, it has been observed in urban surroundings that pedestrians may choose to cross the street when there is a green signal for the accompanying straight movement, but the road user is unable to activate the pedestrian phase in time. The safety concern in this setting is that in the absence of a dedicated pedestrian phase, the road user may not get sufficient time to cross.

The analysis presented in this section focuses exclusively on finding vehicle green phases associated with the N–S movement, and which do not have any overlapping lead pedestrian phase. The search for such instances in both the training and test data revealed a total of 4925 phases (~615 phases per day). In comparison, the number of N–S movement phases with a lead pedestrian phase averaged 55/day. The difference in the number of pedestrian-activated and non-pedestrian-activated phases is indicative of the relatively low levels of non-motorized traffic at this crosswalk location.

The results of the trajectory-based analysis using the training and test data are shown in Table 7.1. The accuracy of the classifier vis-à-vis differentiating motorized and non-motorized modes was 98.4%. However, about 4% of the right (N–W) movements were misclassified as straight (E–W) movements, for reasons described earlier.

Table 7.1 Results of trajectory-based classification during non-pedestrian N–S movement phase

Mode	Count	Right N–W	Right W–S	Straight E–W	Straight W–E	Crosswalk S–N	Crosswalk N–S	Unclassified
Motorized	1126	920	82	98	8	0	0	18
Grand Total	1126	920	82	98	8	0	0	18

The results reveal that there were no non-motorized modes crossing the crosswalk during the time periods that video recordings were available. In fact, for the eight days of sensor data available, there were only two crosswalk trajectories estimated for the N–S vehicle phases without a pedestrian-actuated signal. Both the crosswalk trajectories corresponded to the same vehicle phase, which took place during 5:32 and 5:33 PM on March 22, 2015. While there was no video evidence for this time period, the time-space diagram plotted within the data visualization tool shows the trend to correspond to a N–S movement (Figure 7.1).

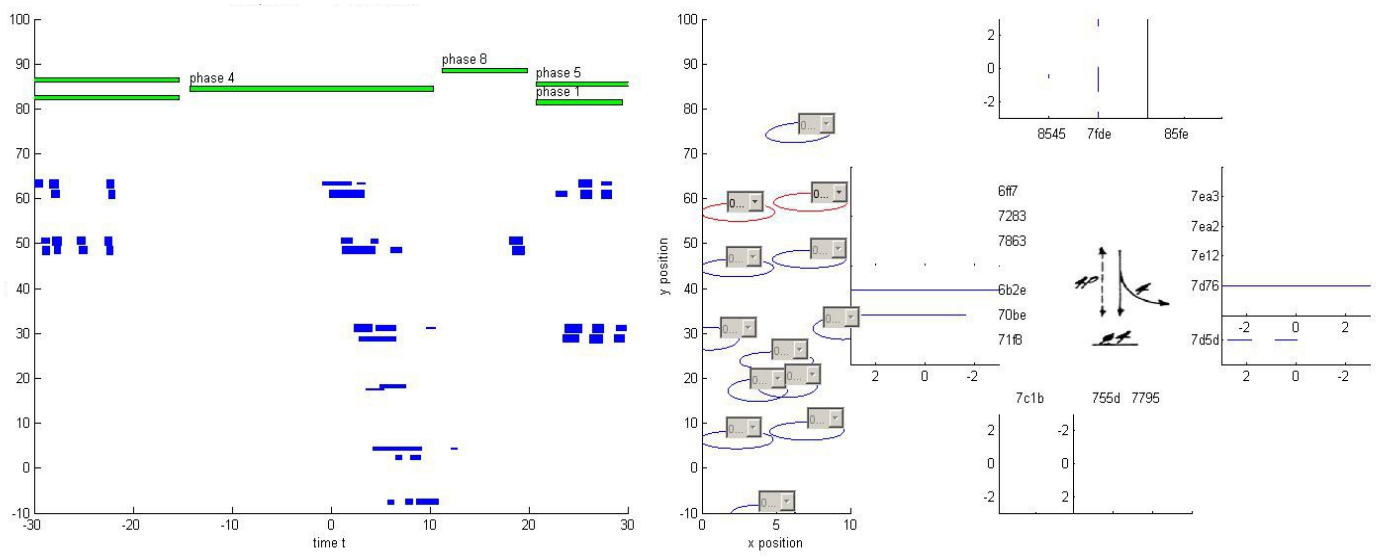

Figure 7.1 Crosswalk movement detected during non-pedestrian phase

Using Figure 7.1, it can be inferred that the N–S vehicle movement phase is active, and much of the traffic is moving from N–E as part of a dedicated left turn movement. In comparison, the exit lanes in the western leg of the crosswalk are inactive, indicating an absence of any evidence of right (N–W) movements. Given the evidence, the most likely scenario is follows:

> In the absence of a pedestrian actuation upfront (probably because there were no pedestrian available on site at first), only the vehicle phase was activated. Subsequently, it appears that two (or more) pedestrians arrive at the intersection. Even though the pedestrian phase was not active, they decide to cross 12-14 seconds into the vehicle phase. The undertaken crossing was completed by the time the vehicle phase ended.

Under the given circumstances, the crossing seems to have been navigated safely, and the surrounding traffic conditions do not appear to pose any threat to the road users crossing the intersection. However, in the absence of a dedicated pedestrian signal, there may not always be sufficient time for pedestrians and cyclists to cross the intersection, and thus such a manoeuver can be safety-critical for non-motorized modes.

The detection of such a low probability event shows the advantages of round-the-clock routine monitoring—a peak period analysis may not capture such a dynamic. In fact, at other locations where the non-motorized traffic is more in number and spread across in time, the probability of a pedestrian arriving during a vehicle phase maybe not be as low. Considering that different people have different risk-taking preferences, it lead may lead to vehicle-pedestrian interactions, which can be captured by this automated framework.

7.2 Vehicles Running Red Lights

Figure 7.1 shows some E–W and W–E movements taking place during the N–S (and N–E) green phase, which is typically not to be expected. A deeper look at the data reveals that these events correspond to spillovers from the end of the previous phase. It is possible that some of those trajectories may have been initiated prior to the end of the previous green, but their arrival at the crosswalk at the start of another phase can be a cause for concern.

To capture the red light violations, it is possible to classify trajectories within a short time window which begins at the end of the phase corresponding to E–W and W–E movements (phases 2 and 6) and ends three seconds later (capturing the loss time). More specifically, the trajectory classification was conducted using the following approach:

- Find the ends of all phases which correspond to E–W and W–E movements. For each such time, t :
  - Find the magsensor events as follows:
    - Find all events associated with magsensors 4, 5, 19, and 21 which took place in the time period $(t, t+3)$. These sensors are the stop bar magsensors associated with the E–W and W–E movements, and the time period under consideration ensures that the motor vehicles leave the stop bar locations after the signal has turned red.
    - For all other magsensors, find events which took place between $(t-10, t+10)$, so as to capture both exit lane events as well as any other trajectories which may be getting triggered during the study period.
  - Find all microradar events getting de-activated between $(t+1, t+4)$.

The cross-validation of the results associated with this classification against the labeled training and test data, is shown in Table 7.2.

Table 7.1 Results of trajectory-based classification during the loss time following E–W and W–E movements

Mode	Count	Right N–W	Right W–S	Straight E–W	Straight W–E	Crosswalk S–N	Crosswalk N–S	Unclassified
Motorized	213	93	10	93	8	0	0	17
Grand Total	213	93	10	93	8	0	0	17

The accuracy of the trajectory-based classifier vis-à-vis classifying motorized and non-motorized modes is 93% with all the errors associated with unclassified events. The accuracy for classifying the straight vehicle movements and right turning movements are 96% and 90.3%, respectively. The errors associated with the right turn movements are some right (N–W) movements which got misclassified as straight (E–W) movements, and some right (W–S) movements which remained unclassified.

The results of the analysis reveal that red light violations can be identified using trajectory-based classification, the accuracy of which would also improve with all the magsensors functioning properly. A snapshot from the video recordings of one of the classified events is shown in Figure 7.2 wherein a pickup truck is shown to be crossing the crosswalk while a couple of vehicle on the top-right corner of the image are getting ready to move.

Figure 7.2 An example of a vehicle violating the red light

Overall, across the eight days of observations, there were 485 red-light violation trajectories (76 W□E and 409 E□W trajectories) which were estimated to have taken place at the end of 5166 E□W/W□E phases. Assuming a 96% accuracy, the probability of seeing such red light violations is 9.02% during a straight movement phase.

The distribution of all red light violations by time of day is shown in Figure 7.3. The distribution reveals that there are two spikes between 8 to 9 AM, and 3 to 4 PM.

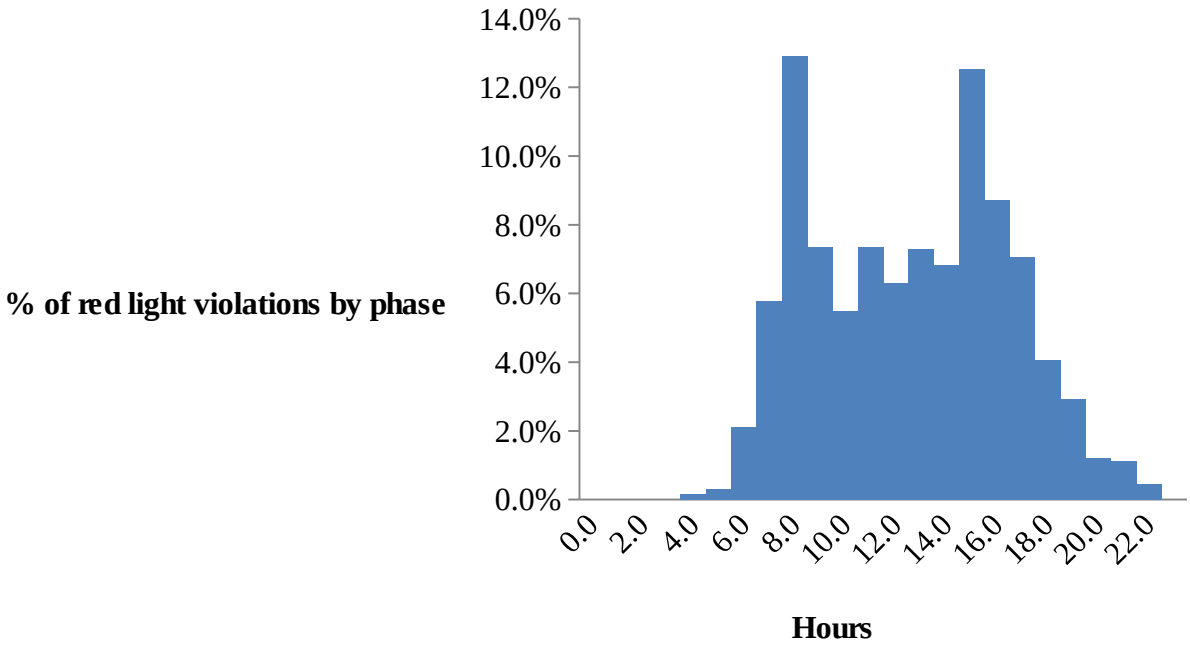

Figure 7.3 Distribution of red light violation by time of day

8 Sensor-Based Classification of Motorized/Non-Motorized Modes

In Chapter 4, a trajectory-based classification method was proposed to distinguish the microradar events by movement type. Since the movements themselves can also be differentiated by whether they are oriented along the crosswalk or not, the trajectory-based classification method also implicitly classifies the microradar events by whether they were triggered by a motorized or a non-motorized mode. However, as the results indicated, a majority of the classification errors using the trajectory-based approach were linked to unclassified events.

In this chapter, the labeled microradar events shall be used to train a binary logit model to differentiate between motorized and non-motorized events. In contrast to the trajectory-based classification, this model shall evaluate individual microradar events, which imposes fewer restrictions on the classifier. The explanatory variables used to develop the model include microradar event information such as event duration, bulk values, sub-channel statuses, etc. In addition, information such as overlapping sensor events, time difference between other sensor events, can also be utilized.

In the following sections, the binary logit models developed for microradar sensors 2 to 12 will be described. For each of these models, the deterministic utility function for the motorized modes will be assumed to be 0, and the explanatory variables described will be associated with the utility function defined for non-motorized modes. As a result, the utility functions can be written as follows:

$$U_{Non-Motorized} = \beta X + \varepsilon_1$$

$$U_{Motorized} = \varepsilon_2$$

Once the binary logit models are trained, the in-sample and out-of-sample predictions are done by comparing the value of the utility functions for a given sensor event.

The data used to train and test the sensor-specific models are the labelled data described in chapter 4. The binary logit model was estimated in MATLAB as a generalized linear model.

8.1 Microradar 12

The explanatory variables associated with the deterministic utility function for non-motorized modes at microradar 12 are show in Table 8.1. The p-values indicating a statistical significance of more than 99% are shown in **bold**.

Table 8.1 Binary logit model for microradar 12

Microradar 12 (Accuracy: 287/290)		
X	β	*p*
Constant	-0.11935	0.939
Bulkchanges	-0.86464	**0.061**
Log(mrad_11_aft)	0.658816	**0.079**
Log(min(mrad_10_bef, mrad_10_aft))	-1.67191	**0.013**
Log(min(mrad_7/8_bef, mrad_7/8_aft))	-1.66184	**0.044**

Log(min(mag_1_aft, mag_2_aft))	3.131508	**0.001**

The results of the classification using the model developed in Table 8.1 leads to an accuracy of 98.9% for the microradar 12 events in the training data. The description and the interpretation of the explanatory variables are provided below:

- *Bulkchanges*: This variable represents the number of times the bulk value changes during a single event. The negative sign of this variable matches the a-priori expectation, which is that a motorized vehicle has a more variation in the single strength, thus leading to more bulk changes than an event associated with non-motorized mode.
- *Log(mrad_11_aft)*: *mrad_11_aft* represents the time difference between the sensor 12 deactivation and the earliest sensor 11 de-activation after that. Since motor vehicle movements across microradar 12 are also likely to cross microradar 11 in quick succession, the positive sign associated with this variable implies that longer the time difference between successive events at these two microradar locations, the more likely that the associated sensor 12 event is a non-motorized mode.
- *Log(min(mrad_10_bef, mrad_10_aft))*: This variable seeks to capture the closest microradar 10 event either before and after the microradar 12 event under consideration. Since microradar 10 is just downstream of microradar 10, the detection of an event at this location maybe an indication that a non-motorized mode may have left from or is approaching microradar 12. Hence, a longer time interval between successive microradar 10 and 12 events would correspond to a higher probability of the sensor being triggered by a motorized mode due to the corresponding coefficient's negative sign.
- *Log(min(mrad_7/8_bef, mrad_7/8_aft))*: This variable captures the time difference between closest microradar 7 or 8 event, with the rationale that detecting other events along the crosswalk can be indicative of crosswalk movement. As a result, a large value of this variable would be more likely to be associated with motorized modes.
- *Log(min(mag_1_aft, mag_2_aft))*: Similar to the time comparisons with other microradars on the crosswalk, this variable looks at the time lag between events on microradar 12 and the magsensors in the exit lanes. Since vehicles traversing the crosswalk at microradar 12 are likely to trigger an event in the exit lane, a smaller time gap between these two types of sensor events is more likely to be indicative of a motor vehicle event.

8.2 Microradar 11

The explanatory variables associated with microradar 11 are shown in Table 8.2. The results show a p-value of 1, which was primarily because the estimation process could not be completed once the underlying algorithm achieved a 100% accuracy.

Table 8.2 Binary logit model for microradar 11

Microadar 11 (Accuracy: 362/362)		
X	*β*	***p***
Constant	*10.85481*	*1.000*
Duration	*19.15198*	*1.000*
*BulkMax + BulkMax*Channel*	*-0.65941*	*1.000*
Log(min(mrad_7/8_bef, mrad_7/8_aft))	*-68.106*	*1.000*
Log((mrad_12_bef))	*13.10707*	*1.000*
Log(min(mag_1_aft, mag_2_aft))	*103.5633*	*1.000*
Log(mag_19_bef)	*5.598572*	*1.000*

The variables associated with the deterministic utility model for non-motorized modes are described in further detail below:

- *Duration*: The duration of a microradar event is typically longer for non-motorized modes which travel across the length of the crosswalk, as opposed to motorized vehicles which travel across the width of the crosswalk. Hence, a positive sign indicates that longer the duration of a microradar event, the more likely that it is a non-motorized event.
- *BulkMax + BulkMax*Channel*: This variable combines the signal strength of the event along with the presence of a sub-channel status of (1,1). The negative sign is consistent with the a-priori hypothesis that motorized events are more likely to have higher bulk values as well as trigger the sub-channel status of (1,1).
- *Log(min(mrad_7/8_bef, mrad_7/8_aft))*: The negative sign associated with this variable is consistent with the a-priori expectations, which is to detect the presence of activity along the crosswalk.
- *Log(mrad_12_bef)*: The positive sign indicates that the longer the time separation between events at microradars 12 and 11, the more likely that the event at microradar 11 is triggered by a non-motorized mode.
- *Log(min(mag_1_aft, mag_2_aft))*: The positive sign of the coefficient indicates that the longer the time separation between events on the crosswalk and the exit lane, the more likely that the event is triggered by a non-motorized mode.
- *Log(mag_19_bef)*: Similar to the previous variable, a longer time separation between events associated at the crosswalk and the approach lane at the other end of the intersection leads to a higher probability that the event is a non-motorized mode.

8.3 Microradar 10

The explanatory variables associated with microradar 10 are shown in Table 8.3. Once again, the p-value of 1 is a result of the estimation process getting interrupted once the underlying algorithm achieved 100% accuracy.

Table 8.3 Binary logit model for microradar 10

Microradar 10 (Accuracy: 231/231		
X	*β*	***p***
Constant	1662.416	*1.000*
Duration	143.7259	*1.000*
BulkMax	-12.3136	*1.000*
BulkMax + BulkMax*Channel	-0.48317	*1.000*
Log(min(mrad_9_bef, mrad_9_aft))	7.056118	*1.000*
Log(min(mrad_7/8_bef, mrad_7/8_aft))	-86.5482	*1.000*
Log(magbef_19)	23.83776	*1.000*
Log(magaft_2)	2.660745	*1.000*

The variables described in Table 8.3 can be divided into sensor-specific information (duration, bulkmax, channel), sensor events that can be part of vehicle trajectories (microradar 9, magsensors 2 and 19), and sensor events that can be part of crosswalk movements (microradars 7 and 8). The signs of the coefficients match the a-priori expectations.

8.4 Microradar 9

The explanatory variables associated with microradar 9 are shown in Table 8.4. This classifier also has an accuracy of 100%.

Table 8.4 Binary logit model for microradar 9

Microradar 9 (Accuracy: 248/248)		
X	*β*	***p***
Constant	-83.7352	*1.000*
Duration	272.3876	*1.000*
BulkMax + BulkMax*Channel	-1.347	*1.000*

Log(min(mrad_7/8_bef, mrad_7/8_aft))	-275.973	*1.000*
Log(magaft_2)	160.2486	*1.000*

The variables described in Table 8.4 match the a-priori expectations.

8.5 Microradar 8

As the results in Table 8.5 show, the binary logit model for microradar 8 has an accuracy of 100%. However, since the data looks at events around the pedestrian phase, it turns out that all the microradar events in the training data correspond to non-motorized events. Consequently, the coefficient estimates of all variables are close to zero, while the constant sign dominates the classification (the positive sign of the constant term means that all events will be assigned to be non-motorized modes).

Table 8.5 Binary logit model for microradar 8

Microradar 8 (Accuracy: 71/71)		
X	*β*	***p***
Constant	102.5661	*1.000*
Duration	-3.14E-13	*1.000*
BulkMax	-1.82E-13	*1.000*
BulkMax + BulkMax*Channel	1.25E-14	*1.000*
Log(min(mrad_10_bef, mrad_10_aft))	-8.56E-14	*1.000*
Log(min(mrad_7_bef, mrad_7_aft))	-6.20E-14	*1.000*
Log(magbef_5)	4.29E-12	*1.000*

8.6 Microradar 7

Similar to microrda r 8, all but one of the 67 events in the training data corresponds to non-motorized modes. In addition, the one motorized event in the training data corresponds to a vehicle which stops beyond the stop bar location, thus triggering the microradar for a long period of time (~30 seconds), but with a low bulk strength (130). As a result, the classifier seeks to distinguish that single motorized event from the rest, which is reflected in the negative sign associated with the duration of the event.

Table 8.6 Binary logit model for microradar 7

Microradar 7 (Accuracy: 64/64)

X	*β*	***p***
Constant	-106.368	*1.000*
Duration	-6.47E+00	*1.000*
BulkMax	1.60E+00	*1.000*
BulkMax + BulkMax*Channel	-3.03E-02	*1.000*
Log(min(mrad_9_bef, mrad_9_aft))	-2.06E+00	*1.000*
Log(min(mrad_8_bef, mrad_8_aft))	-1.60E+00	*1.000*
Log(magbef_5)	2.93E+00	*1.000*

8.7 Microradar 5

For the binary logit model associated with microradar 5, in addition to the sensor-specific information, the other explanatory variables include microradar events occurring at its neighrboring sensor (microradar 4), as well as the magsensors which lie along the straight W□E movement (magsensors 7 and 16). The accuracy of the classifier is 100% and signs of the coefficients are consistent with the a-priori expectations.

Table 8.7 Binary logit model for microradar 5

Microradar 5 (Accuracy: 126/126)		
X	*β*	***p***
Constant	2302.435	*1.000*
Duration	11.98371	*1.000*
BulkMax	-17.3867	*1.000*
Log(min(mrad_4_bef, mrad_4_aft))	-3.4733	*1.000*
Log(magbef_7+magaft_16)	40.77626	*1.000*

8.8 Microradar 4

The binary logit model associated with microradar 4 is described in Table 8.8. The accuracy of the classifier is 100% and signs of the coefficients are consistent with the a-priori expectations.

Table 8.8 Binary logit model for microradar 4

Microradar 4 (Accuracy: 113/113)		
X	*β*	***p***
Constant	747.8174	*1.000*
Duration	53.79612	*1.000*
BulkMax + BulkMax*Channel	-6.47204	*1.000*
Log(min(mrad_3_bef, mrad_3_aft))	-17.9803	*1.000*
Log(magbef_7+magaft_16)	60.31058	*1.000*

8.9 Microradar 3

The binary logit model associated with microradar 3 is described in Table 8.9. In this case, the best fit model utilized only the bulk and sub-channel status, as well as using the information that sensors 7 and 8 events are almost always likely to indicate the presence of non-motorized modes. The accuracy of the classifier is 96.6% and the signs of the coefficients are consistent with the a-priori expectations.

Table 8.9 Binary logit model for microradar 3

Microradar 3 (Accuracy: 84/87)		
X	β	***p***
Constant	11.2401 7	0.0 0
BulkMax + BulkMax*Channel	-0.02441	**0.0 2**
Log(min(mrad_7/8_bef, mrad_7/8_aft))	-3.42847	**0.0 0**

8.10 Microradar 2

The binary logit model associated with microradar 2 is described in Table 8.10. The accuracy of the classifier is 100% and the signs of the coefficients are consistent with the a-priori expectations even though the p-values could not be appropriately estimated within MATLAB.

Table 10 Binary logit model for microradar 2

Microradar 2 (Accuracy: 67/67)		
X	β	***p***
Constant	488.886 9	*1.0 0*
BulkMax + BulkMax*Channel	-1.22736	*1.0 0*
Log(min(mrad_7/8_bef, mrad_7/8_aft))	-127.847	*1.0 0*
Log(magaft_9)	53.7889 3	*1.0 0*

8.11 Analysis of Test Data

The results of the sensor-specific classification shown in the previous section reflect a high level of accuracy of the binary logit models. However, it is possible that the models developed using the training data may have been overfitted. Consequently, it is important to test the validity of the models against the test data. These results are shown in Table 8.11. The overall accuracy of 96.9% when labeling the test data is significantly higher than the trajectory-based classification accuracy of 89.2%.

Table 8.11 Accuracy of the binary logit models on the test data

Test Data: Oct 15-16 (incomplete)			
Sensor ID	**Matched**	**Total**	**Accuracy**
12	117	118	99.2%
11	151	154	98.1%
10	60	63	95.2%
9	63	68	92.6%
8	24	24	100.0%
7	22	25	88.0%
5	42	42	100.0%
4	41	41	100.0%
3	37	39	94.9%
2	35	37	94.6%
Total	592	611	96.9%

The worst performance corresponded to sensor 7, which was due to the misclassification of three events which were triggered by vehicles stopping in front of the stop bar location, but for short time intervals. Since such events were not observed in the training data, the binary logit model could not classify such events accurately.

When compared to the performance of video-base mode classifiers, the prediction accuracy of the sensor-based classification system might be superior. However, the future work should look into incorporating additional modes such as cyclists, buses, and trucks, into the classifier using additional labeled data.

Based on the results of the sensor-based classification, some of the major difference between the trajectory-based and the sensor-specific classification can be summarized as follows:

- Trajectory-based classification is primarily a rule-based approach, while the sensor-specific classification is a more data-driven approach. Consequently, while the latter can let the data identify the appropriate features that best classify the events, it also relies on a large enough sample of events to cover all possible scenarios. In comparison, the trajectory-based classification can still be developed with limited data based on the spatio-temporal aspects of the trajectories.
- Trajectory-based classification simultaneously classifies multiple sensor events at once, or none at all. This leads to unclassified events when the requisite conditions are not met. In comparison, the sensor-specific analysis provides the flexibility of classifying individual sensors.
- Trajectory-based classification can facilitate counts by movements and modes, whereas the proposed sensor-specific classification is thus far limited to mode differentiation.

9 Additional Algorithms for Inferring Non-motorized Trajectories

In the mode classification frameworks presented thus far, a major challenge has been differentiating the number of non-motorized modes using the crosswalk. In the case of the trajectory-based approach, the limiting factor was the assumption that a microradar event can be uniquely associated with only one trajectory. In the sensor-based classification, it might be possible to extend the binary logit classification to a multinomial/mixed logit specification which can accommodate a wide variety of modes. However, since these models are implemented on individual sensors, the mode trajectories do not get directly inferred from such a framework.

As part of this research effort, some trajectory estimation algorithms have been approached which can utilize classified non-motorized mode events as inputs. The objective of these approaches is to utilize the duration of the microradar events to ascertain if one or more trajectories may be crossing the crosswalk. The proposed frameworks are exploratory in nature and are thus not evaluated as exhaustively using the labeled events.

9.1 Hough Transform

The Hough transform is a technique originally used in image analysis for edge detection. It seeks to identify line segments which can be formed from individual points in an image. The approach works as follows:

For each point, for all lines going through this point, there exists a unique distance-angle relationship that can be used to characterize the lines. For each point, it is possible to plot in a distance-angle diagram all possible lines going through, which is represented as a sine curve. In an ideal setting, a perfect overlap of all curves at a unique point results in the identification of a straight line that passes through all the points of interest. An example of this approach is shown in Figure 9.1.

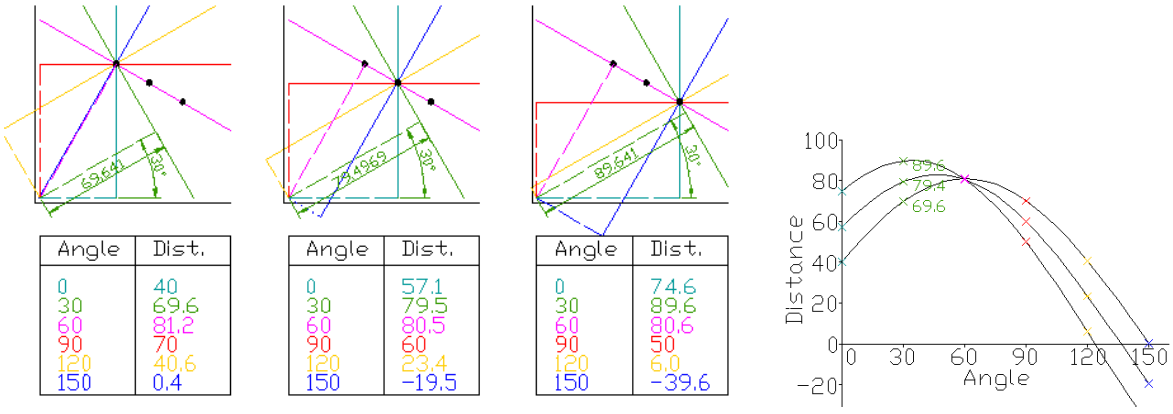

Figure 9.1 Implementation of Hough Transform (Source: Wikipedia)

In the context of this study, a potential application of this technique is to plot the Hough transform of all microradar events in the time-space diagram and then apply the clustering method to combine disjointed lines. Figure 9.2 illustrates an implementation of the Hough transform using the microradar data.

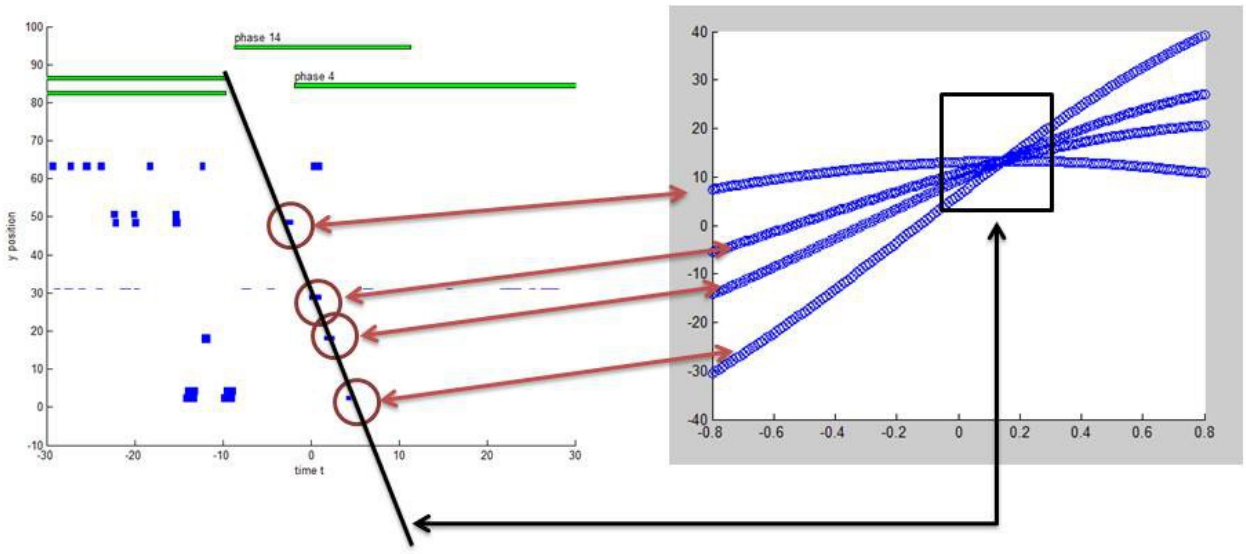

Figure 9.2 Implementation of Hough Transform using microradar data

The steps required to implement the Hough Transform shall be outlined in the following sections.

9.1.1 Data Preparation

For each pedestrian phase, the labeled data from the binary logit models can be used to identify potential non-motorized mode events. For each of those events, the event duration is discretized using a sampling rate of 8 Hz. The y-axis values of each microradar are used to represent the sensor location. As a result, a collection of points, referred to by their (t,y) co-ordinates, is available as an input for Hough Transform.

9.1.2 Hough Transform Algorithm

Using the (t,y) pairs associated with each non-motorized mode, it is possible to implement the Hough Transform algorithm within each pedestrian phase. Herein, for each point, an array of potential straight lines passing through it are identified. These lines are parameterized using an (r,θ) pair, as illustrated in Figure 9.3.

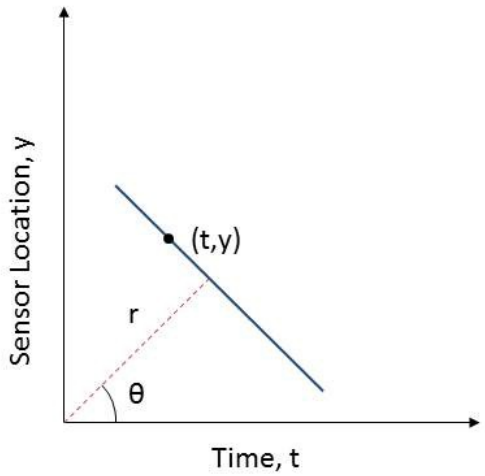

Figure 9.3 Representing a line as an (r,θ) pair

However, since each sensor event is discretized into multiple points (1 second duraction = 8 discrete points), the Hough Transform can identify multiple similar-looking straight lines which can pass through all sensor events. In order to infer unique trajectory events from the distribution of (r,θ) values, Kernel Density Estimation is used.

The role of Kernel Density Estimation is to produce a smoothened distribution of (r,θ) by summing up the values associated with independent and identically distributed kernels centered at each observation. The size of the kernels is determined by a bandwidth parameter, and the output of KDE can be visualized as a heatmap, as shown in Figure 9.4.

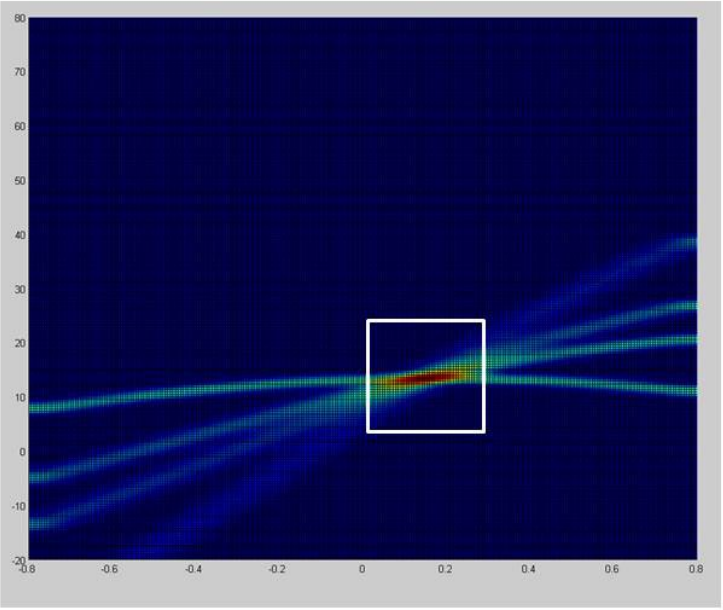

Figure 9.4 A heatmap representing the distribution obtained using KDE

The heatmap can help identify different locations within the (r,θ) plot with the highest density, by finding modes with the highest density. At this juncture, bounds can also be imposed on the range of θ's and/or r's, so as to ensure meaningful trajectories. In addition, since there can be many modes within the density distribution, some metric needs to be identified to limit the number of trajectories that can be identified, such as by creating a threshold for the density distribution or evaluating the decay of the highest values within the density distribution.

The results associated with the Hough Transform are still preliminary but some initial attempts look promising. Figure 9.5 illustrates an example where the heatmap reveals two distinct modes, which in turn reflect in two separate trajectories being inferred.

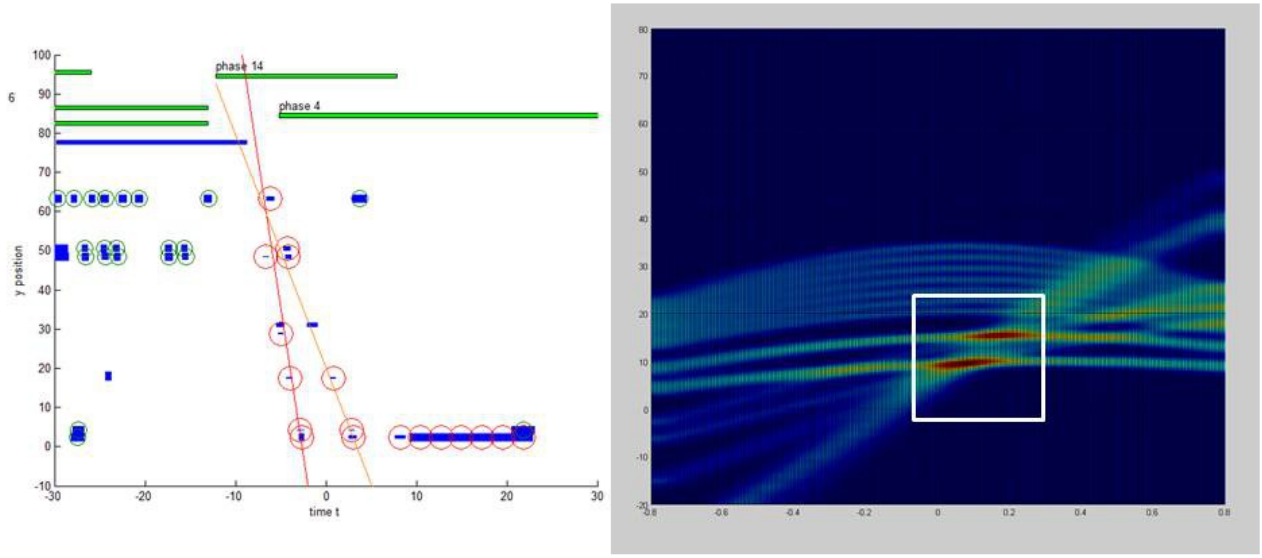

Figure 9.5 An example of the Hough Transform capturing multiple trajectories

In order to refine the Hough Transform, future work must look into identifying a method to determine the threshold for identifying trajectories using the labeled non-motorized data. While the straight line representation of trajectories can accommodate some variation in the speed of the underlying modes, the inherent can be restrictive under conditions where the modes change their speeds drastically midway through the trajectory.

9.2 Particle Filtering

Particle filtering is an example of a state estimation problem, wherein the challenge is to accurately track the true states of the targets given noisy observations and also follow their through time. The tracking of the target maybe done through a *motion model*, and the state estimation is conducted through a *measurement model*. In order to account for the noisy observations, the underlying, unobserved state of an object can be modeled as part of a hidden Markov model which depends on the observed sensor state (Figure 9.6).

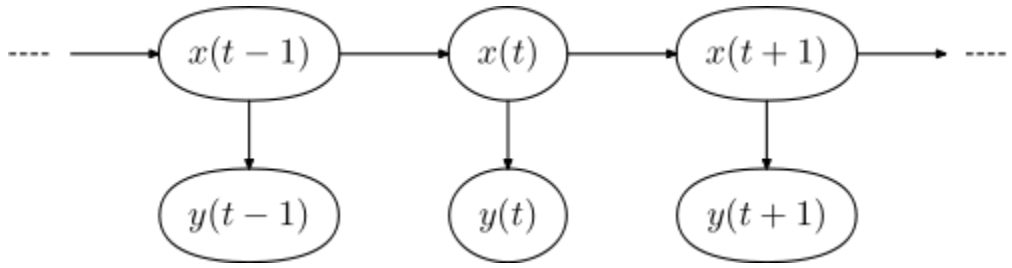

Figure 9.6 Representation of a Hidden Markov Model

The main idea of particle filtering is to simulate all possible trajectories with a sample of "particles" using Monte Carlo methods. The advantage of a simulation-based framework is that it is possible to create a large sample of trajectories with varying speeds which can potentially trigger the observed sensor events.

A preliminary implementation of a particle filtering algorithm using a Markov Chain Monte Carlo (MCMC) simulation technique is explained below:

9.3 Definitions

- *Unallocated point (false negative)*: when a microradar is triggered in the ground truth but there is no trajectory estimated to go through the detection zone.
- *Non-existent point (false positive)*: when a trajectory goes through a detection zone but the radar does not actually light up
- Hidden Markov model:
    - Assume we know position and speed at time **t**
    - Between **t** and **t+dt**, speed is modified according to a Gaussian noise with mean zero in both directions **x** and **y**.
    - We can compute now position at time **t+dt**
- *Trajectory Likelihood:* the likelihood that a pedestrian had such a trajectory given the Markov model. It is the product of the likelihoods of all the Gaussian noises from each step **dt** in the Hidden Markov model.

9.4 Algorithm

1. **Define** the physics of the model
    a. Microradars
        i. Positions
        ii. Detection zone dimensions and shapes (approximate)
    b. Hidden Markov model
        i. Variance of noise in speed
        ii. Probabilities of false positive and false negative
    c. Data parameters
        i. Time sampling interval **dt**
2. Initialization
    a. Load pedestrian phase data
    b. All points are considered as *unallocated* (or 'false negative')
3. **For each** time **t** in the phase
    a. **For each** *unallocated point* **p** at time **t**
        i. **Assume** speed $\mathbf{v_t}$ at time **t** is
            1. Negative if **p** is in the 'upper part' of the crosswalk
            2. Positive otherwise
        ii. **Assume** position of pedestrian is $\mathbf{y_t}$, the position of the radar **p**
        iii. Trajectory Sampling:
            1. **Samples N** random trajectories such that at time **t,** position is $\mathbf{y_t}$**,** and speed is $\mathbf{v_t}$
            2. **For each** trajectory, computes the *added likelihood*:
                a. Trajectory Likelihood (see definitions)
                b. Add likelihood of *inexistent points* added by trajectory (see definitions)
                c. Substract likelihood of *unallocated* points removed by trajectory (thus called *allocated* points)
            3. **Returns** trajectory with *maximum added likelihood*
        iv. **If** added likelihood > *threshold*
            1. **Add** the trajectory as a new pedestrian
            2. **Remove** newly allocated points from the set of unallocated points

While the implementation of the algorithm still needs to be refined further, it can be seen that particle filtering can provide a lot of flexibility in estimating different types of movement trajectories. For instance, Figure 9.7 shows an example of the trajectories identified using particle filtering for a sample pedestrian phase. Herein, the simulated movements are captured along the time-space diagram, as well as a top-down representation of the crosswalk. The ellipses are represented as approximate detection zones for the microradars. In this case, the particle filter is able to classify the two emerging S□N trajectories efficiently. However, the trajectory in green is estimated to be a pedestrian reversing his/her direction. While such a pedestrian movement is feasible, if the sensor classification as non-motorized/motorized modes is either unavailable/inaccurate, the particle filter can overfit the data.

Once again, as part of the future work, the particle filtering algorithm needs to be improved to optimize the trajectory identification, as well as identify appropriate thresholds to terminate the process so as to not overfit the model.

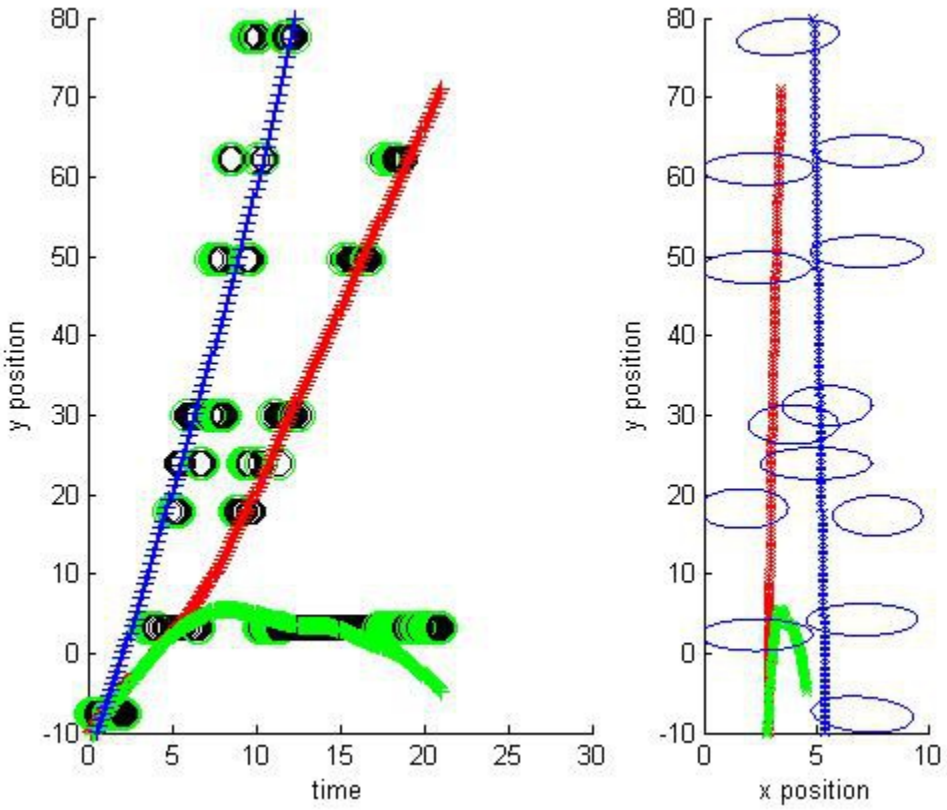

Figure 9.7 An example of a particle filtering simulation

9.5 Discussion

In summary, the trajectory estimation approaches discussed above represent potential approaches to utilize classified non-motorized data. While the particle filtering framework provides a lot of flexibility in identifying a wide variety of trajectories, its current implementation is computationally inefficient. In comparison, the Hough Transform provides a computationally efficient technique to infer movements across the crosswalk. Since these frameworks use labeled microradar events as inputs, the future work shall look into distinguishing events triggered by 2+ pedestrians/cyclists, so as to better isolate overlapping trajectories.

10 Computer Vision-based Tracking of Modes

The focus of the chapters presented thus far has been on developing algorithms to infer movements and interactions between different transportation modes using in-pavements sensors. The in-pavement sensors summarize all the transportation activity taking place in their vicinities as individual, disaggregated events, which enables long-term data collection. However, the quality of information is determined by the number of sensors involved as well as their placement with respect to the several traffic movements. In addition, the sensing architecture cannot be shared by multiple locations to conduct short-term studies. In comparison, a mobile sensing platform, such as video cameras, is more flexible in nature, and can be easily deployed for both short-term and long-term studies. However, historically, a major limitation of video analysis has been the capability to automatically infer modes and their trajectories. In recent times, there have been some research efforts to harness computer vision techniques to automate traffic safety analysis using video data, and this chapter will briefly explore their suitability for the study location.

This chapter utilizes an open-source computer vision code repository called *Traffic Intelligence* which implements a feature-based tracking algorithm that infers movements of objects by grouping trajectories of distinguishable features that move in similar fashion. The details of the algorithms are provided in Saunier and Sayed (2006). In order to customize the tool for the study location, the following steps are required to be undertaken:

1. Compute a homography matrix to calibrate the camera for the study location.
2. Develop a mask for the video analysis which determines the parts of the video are available for identifying features and objects.
3. Calibrate the parameters of the feature-based tracking algorithm to identify the modes accurately.

10.1 Computing Homography Matrix

The homography matrix provides the ability to translate distances within the video frames (represented in pixels) into the real world setting. It can be computed for a given location by comparing the images seen from the video with an aerial view. The advantage of using aerial imagery is that distances between different parts of the intersection can be inferred using the distance scale associated with the aerial image.

The images used to develop the homography matrix for the study location are shown in Figure 10.1. In order to compute the homography matrix, points referring to different parts of the intersection are first established from within the image captured by the camera. Thereafter, the corresponding intersection locations are identified within the aerial image. Using the paired points from the two images, along with information about the distance scale of the aerial image, the homography matrix can be computed using a pre-written code provided by *Traffic Intelligence*. Further details associated with the camera calibration procedure are available at Ismail et al (2013).

(a) View from the camera (b) Aerial view

Figure 10.1 Images used to compute the homography matrix

10.2 Preparing Mask for Video Analysis

The mask is a black-and-white image with the same dimensions as the video frame. The primary purpose of the mask is to limit the scope of the video analysis to locations of interest. For instance, in the videos under consideration, the top part of the videos contains a timestamp. Since the changes in the timestamp are not relevant for the purposes of feature extraction, it can be omitted from the analysis using a mask. Alternatively, a mask can also be prepared which focuses the analysis solely on the crosswalk. These mask representations are provided in Figure 10.2.

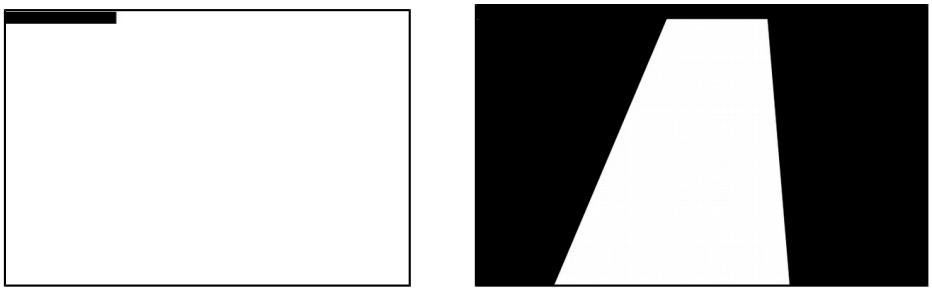

(a) Excluding the timestamp (b) Including only the crosswalk region

Figure 10.2 Examples of masks

10.3 Feature-Based Tracking & Grouping

Once the camera calibration and mask preparation is complete, the final step involves the parameters associated with tracking and grouping features. The term “features” refers to any distinguishable points/lines within an image which can be tracked across frames. Since a moving object can have multiple features associated with it, a subsequent procedure groups features which move in a similar fashion across several frames within the video. Both feature-tracking and feature-grouping are a function of several different parameters which need to be calibrated to be able to infer the different objects observed within the video.

Some of the parameters associated with feature-tracking include *maximum number of features added at each frame, minimum distance between features (in pixels), minimum displacement to keep features (in pixels), maximum feature deviation*, etc. Changing these parameter estimates influences both the quality and the quantity of features that would be tracked by the algorithm.

Once the features are tracked and stored, the feature-grouping component of the algorithm evaluates each feature with respect to other features to ascertain the ones that are in close proximity along both space and time. For instance, *maximum distance between features for grouping* would identify the maximum separation between two trajectories over time and group them into a single object if their relative separation was below the chosen threshold. Another similarly functioning parameter is the *segmentation distance*, which is defined as the upper limit for the difference in the maximum and minimum relative distance between two features. In other words, the segmentation distance limits how much relative separation is allowed between two features. *Connection distance* is used to evaluate whether a new feature added at any given time, *t*, can be grouped with an existing feature—this parameter helps combine features which may potentially represent the same object, but are initiated as trajectories at different points in time. Other parameters may also put constraints on whether a group of trajectories can be considered to be a valid vehicle hypothesis or not. These parameters include *minimum average number of features per frame*, *minimum length of feature*, *minimum cosine of the angle between the velocity vectors*, etc.

But more generally, the principal trade-off that is required to be made as part of feature-tracking algorithm is to maintain a balance between erring towards over-segmentation versus over-grouping. Over-segmentation refers to a single mode being inferred as two or more object trajectories, while over-grouping refers to two or more modes being grouped as single object.

Once the parameters are chosen, the feature-tracking and feature-grouping elements of the algorithm can be computed in succession. Thereafter these trajectories/objects can be overlaid on top of the video frames to visualize how the chosen parameters influence the tracking process. It is important to recognize here that while the code repository comes with a set of default values, the calibration process may lead to some different values based on the orientation of the camera, the angle of view, the quality of the video, and the types of modes being tracked.

10.4 Initial Findings

While an exhaustive comparison of video analysis and in-pavement sensor-based detection could not be completed as part of this effort, some preliminary observations associated with calibrating *Traffic Intelligence* can be reported using some illustrative case studies.

Consider the images shown in Figures 10.3 that correspond to events taking place on April 24, 2015. These images show different types of traffic movements. While Figure 10.3 (a) shows turning maneuvers by automobiles, Figure 10.3 (b) shows light non-motorized traffic on the crosswalk (a pedestrian, a crossing guard, and a cyclist) along with an automobile traveling from north to south. Finally, Figure 10.3 (c) shows a large group of cyclists crossing the intersection that can be used as an example of heavy non-motorized traffic at the intersection. Using these scenarios, the performance of Traffic Intelligence is evaluated for three types of settings:

(a) Using parameters calibrated to favour motorized traffic
(b) Using parameters calibrated to favour non-motorized traffic, and
(c) Using parameters calibrated for non-motorized traffic using a mask for crosswalk.

These settings help understand how feature-tracking and feature-grouping parameters influence the output, especially in terms of the issues of over-segmentation and over-grouping. In addition, role of the mask as a tool to restrict the tracking to a part of the intersection is also be explored.

(a) Automobile movements

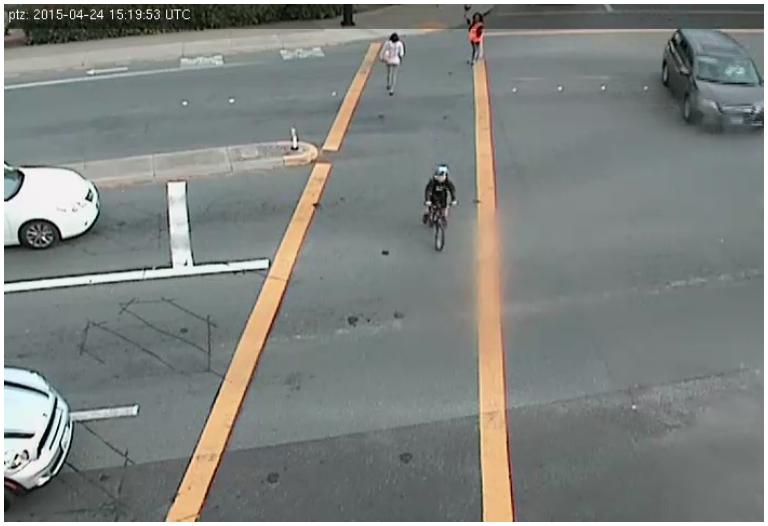

(b) Light non-motorized traffic

(c) Heavy non-motorized traffic

Figure 10.3 Different types of traffic movements

10.4.1 Motorized Mode-Based Calibration

The results associated with calibrating feature-tracking and feature-grouping to favour motorized modes are shown in Figure 10.4. Herein, the features and the objects identified for the three types of traffic movements are shown in the left and right panes of each subfigure respectively. Since automobiles are bigger objects than non-motorized modes, it can be seen that their presence within a video frame leads to a large number of features. Hence, in order to ensure that the inferred objects do not get over-segmented, high segmentation and connection distances are used to facilitate grouping of features. As a result, the various motor vehicles are able to be represented by unique object trajectories. However, an unintended consequence of grouping features in close proximity is that features associated with different non-motorized modes can also get grouped together, as seen in Figures 10.4 (b) and (c). This also adversely affects the motion of the inferred object, which is determined as the mean of the individual features within the group.

(a) Automobile movements (left:features, right:objects)

(b) Light non-motorized traffic (left:features, right:objects)

(c) Heavy non-motorized traffic (left: features, right: objects)

Figure 10.4 Results associated with motorized mode-based calibration

10.4.2 Non-Motorized Mode-Based Calibration

Based on the results of the motorized mode-based calibration, it can be inferred that in order to distinguish non-motorized modes better, lowering the segmentation and connection distances may be helpful. The impact of the adjustments made to the feature-tracking and grouping parameters so as to favour non-motorized modes are reflected in Figure 10.5. In choosing a lower segmentation distance, the

motor vehicle trajectories end up with an over-segmented representation, as shown in Figure 10.5(a). In contrast, a large number of unique non-motorized object trajectories can now be observed within a heavy non-motorized traffic setting (Figure 10.5 (c)). The non-motorized object trajectories inferred in Figure 10.5 (c) also show the advantage of video analysis over in-pavement sensors, as the former is able to capture trajectories which emanate from beyond the crosswalk. Unfortunately, in the case of the light non-motorized traffic setting (Figure 10.5 (b)), feature-grouping is only able to provide an over-segmented representation of the pedestrian crossing the crosswalk while not suggesting any object trajectory for the other modes.

(a) Automobile movements (left:features, right:objects)

(b) Light non-motorized traffic (left:features, right:objects)

(c) Heavy non-motorized traffic (left: features, right: objects)

Figure 10.5 Results associated with non-motorized mode-based calibration

10.4.3 Non-Motorized Modes-Based Calibration Using a Crosswalk Mask

While the results using the parameters favouring non-motorized modes were somewhat encouraging, in the quest for identifying individual trajectories for non-motorized modes, over-segmentation becomes a concern for automobiles. A potential solution in this regard is to apply a more restrictive mask to explore the possibility of analyzing only a part of the intersection. Figure 10.2 (b) shows an example of a mask,

which restricts the analysis to the crosswalk and a buffer region surrounding it. By super-imposing this mask on to the original video, it is ensured that the feature trajectories start and end within the region of interest. The results associated with this analysis are shown in Figure 10.6.

The feature trajectories observed for the various traffic movements in Figure 10.6 (all left panes) reveal that the feature tracking is now restricted only to the region surrounding the crosswalk, which limits inference of motor vehicle-based trajectories. In comparison, it appears that there are more non-motorized mode features getting tracked, as inferred from a thicker set of lines associated with them in Figures 10.6 (b) and (c). Consequently, in the case of Figure 10.6 (b), the presence of more features might be leading to the identification of both the cyclist as well as the pedestrian crossing the street. Also, in the case of the heavy non-motorized traffic shown in Figure 10.6 (c), the feature-grouping is still able to differentiate a large number of trajectories.

(a) Automobile movements (left:features, right:objects)

(b) Light non-motorized traffic (left:features, right:objects)

(c) Heavy non-motorized traffic (left: features, right: objects)

Figure 10.6 Results using a mask for crosswalk

The results associated with the crosswalk-related mask are promising in terms of isolating non-motorized modes from the motorized modes. Hence, customizing the parameters and masks for different modes may help mitigate the issue of over-segmentation/over-grouping. However, more work is required to integrate these parameters to jointly estimate the motorized and non-motorized modes and test it against the ground truth.

Finally, it is acknowledged that the trajectory of the crossing guard could not get captured using the parameters described above, probably because of they can remain stationary for prolonged periods of time.

10.5 Discussion

In this chapter, a feature-based tracking algorithm called *Traffic Intelligence* was explored as an alternative to tracking modes using in-pavement sensors. The preliminary findings based on the calibration process reveal that identifying a unique set of parameters to accurately track both motorized and non-motorized modes is a concern. However, developing masks to isolate the non-motorized modes from the motor vehicle activity may be helpful for developing customized parameters for non-motorized and motorized modes separately. Based on a qualitative analysis of the accuracy of the feature-grouping analysis, the results shown in Figure 10.3 (for motorized modes) and Figure 10.5 (for non-motorized modes) look promising.

While more work is required to compare the performance of the video-based sensing framework with the in-pavement sensing framework, based on the case studies, it can be said that video analysis can provide a cost-effective alternative to analyze locations of interest without the significant investment of installing sensing infrastructure. Unlike the in-pavement sensors, the accuracy of the computer-vision based algorithms appears to be relatively less dependent on the placement of the video camera itself, although a more top-down perspective is recommended to be more effective for feature-tracking. Consequently, the approach relies on identifying the right set of parameters for tracking and grouping features to infer modes, and that requires a more comprehensive understanding of the underlying algorithms. To facilitate this calibration process, additional post-processing techniques must also be looked into for customizing a general purpose code to meet the needs of the study location.

In comparison, an in-pavement sensing platform, while being limited in its information over space, provides precise markers of activity which are easier to store and process over long periods of time. It is possible that combining the relative merits of video processing and in-pavement sensing can help develop a superior mode detection/tracking framework.

11 Conclusions and Future Work

The work presented as part of this research project focuses on developing an automated framework for analyzing and monitoring mode-specific and multi-modal safety-critical interactions using in-pavement sensors at a study intersection in Danville, CA. The sensing platform comprises of: (i) magnetometer sensors (magsensors) deployed at intersection stop bars and departure lanes, (ii) microradar sensors deployed along different parts of one crosswalk, (iii) signal conflict monitor card providing signal phase information. Together, these sensors provide round-the-clock time-synchronized event information which in turn is processed using various algorithms to infer motorized and non-motorized vehicle movements which are necessary to analyze mode-specific and multi-modal safety-critical interactions. The performance of the algorithms and classifiers in tracking and distinguishing movement through the intersections are described below.

11.1 Research Findings

Sensor and video data were obtained for the study location for April 22 and 24, 2015, and October 12-16, 2015, with the data associated with October 15 and 16 being reserved exclusively for testing the algorithms developed as part of this effort.

11.1.1 Classifying movements across modes

The results associated with tracking non-motorized and motorized trajectories provide an accuracy of 94.5% when using the training data and 89.2% in the test data. When evaluating the results of the different turning movements, the accuracy for classifying right turns, straight movements, N□S and S□N crosswalk movements is 93.7%, 97.2%, 87.2% and 85.4% respectively in the training data, and 85.4%, 95.6%, 82.6% and 76.3% respectively, in the test data. In addition, when classifying individual microradar sensor events as motorized/non-motorized modes, the accuracy of the sensor-specific classifiers is 99.6% for the training data and 96.9% for the test data.

11.1.2 Driver yielding behavior

The analysis of the multi-modal safety-critical analysis focuses on motor vehicles' yielding behavior, the key methodology of which is to use the time difference between consecutive vehicle and pedestrian events under different conditions. The results indicate that there are two types of yielding behavior of right-turning vehicles during a green phase: (i) drivers who wait behind the crosswalk while allowing pedestrians to cross; and (ii) drivers who yield, but after encroaching into the intersection. This distinction in the types of yielding behavior (passive versus aggressive yielding) is typically difficult to capture, and quantify, in traditional observational studies.

11.1.3 Signal violation by drivers and non-motorized modes

The analysis of driver red-light violations revealed that the probability of witnessing such a violation at the end of a straight movement phase is 9.02%, with about 25% of the daily red-light violations take place between 8 to 9 AM, and 3 to 4 PM. The results associated with identifying non-motorized modes crossing the street without pedestrian signal actuation revealed only two such trajectories over a period of eight complete days of observation.

Finally, the implementation of an automated video analysis methodology, while incomplete, provided insights into classifying automobile and non-motorized movements. In particular, the analysis reveals a flexible, cost-effective approach to conducting short-term traffic safety studies. However, implementing such analysis over multiple days of video data may be computationally prohibitive.

11.2 Contributions

To the best knowledge of the researchers, no study prior to this has been undertaken that evaluates multi-modal safety-critical behavior at an intersection for extended periods of time. The performance of the trajectory-based algorithms in classifying motorized and non-motorized modes is, given the absence of some critical of magsensors, comparable to the video-based mode classification frameworks. The performance of the sensor-based classification method is superior to the video-based classification techniques, and thus can be incorporated into the trajectory-based classification method to improve its accuracy.

The development of the classification algorithms in conjunction with the signal phase information helps provide valuable insights for both mode-specific as well as multi-modal safety-critical dynamics. For instance, the insights gained about the different types of yielding behavior can have important implications for other intersections as well (both signalized and non-signalized), where aggressive yielding behavior may be more common in reality (but not as well documented). Similarly, even in instances where ground truth was not available, the trajectory-based classifier was able to identify events which can be intuitively visualized using the data visualization tool.

In summary, this study demonstrates the feasibility of using a sensor-based classification framework to automatically monitor safety-critical interactions at intersections.

11.3 Future Work

11.3.1 Improving the classification framework

One of the major shortcomings of the trajectory-based classification framework was the significant number of unclassified events on the crosswalk. In addition, the identification of non-motorized trajectories has been inferior in comparison to motorized modes, which is also a common shortcoming of computer vision-based approaches. While there are a number of ways to improve the algorithms, some of which have been documented elsewhere in the manuscript, it is important to recognize that the classification errors also have implications on subsequent analyses, in particular when evaluating multi-modal interactions. Consequently, future work shall prioritize improving the accuracy of the underlying mode-classification algorithms further. Finally, the automated video analysis methodology will also be refined so as to undertaken a comprehensive comparison between the two automated safety evaluation frameworks.

11.3.2 Vision for a Smart Intersection

With the advent of emerging technologies which can assist cities to develop “smart” and/or “intelligent” transportation infrastructure systems, urban intersections are being increasingly equipped with various types of video and in-pavement sensor architectures to facilitate round-the-clock monitoring and optimization of multi-modal flows. In comparison, the assessment of the safety performance of these facilities continues to be largely based on either crash history or citizen grievances. Using collision data

as the only metric for traffic safety represents a reactive approach, and it may take a long time for a recurring safety-concern to reveal itself.

In comparison, the use of surrogate measures of traffic safety can help analyze large number of traffic conflicts and document any emerging traffic safety concerns prior to an occurrence of a crash. While there has been a push in recent times to develop automated algorithms to compute such surrogate measures using video data, the work presented as part of this research effort shows that the scope for proactively (and non-intrusively) monitoring multi-modal interactions can be significantly expanded when including in-pavement sensors. To support this vision future work should also study the association between various surrogate measures and different types of crashes. Establishing the link between crashes and surrogates safety measures will provide valuable opportunities to fully harness technology to enhance existing safety management practices.

REFERENCES

Abdulsattar, H., Tarawneh, M., McCoy, P., & Kachman, S. (1996). Effect on Vehicle-Pedestrian Conflicts of" Turning Traffic Must Yield to Pedestrians" Sign. *Transportation Research Record: Journal of the Transportation Research Board*, (1553), 38-45.

Alhajyaseen, W. K., Asano, M., & Nakamura, H. (2013). Left-turn gap acceptance models considering pedestrian movement characteristics.*Accident Analysis & Prevention*, *50*, 175-185.

Akin, D., & Sisiopiku, V. P. (2007). Modeling Interactions Between Pedestrians and Turning Vehicles at Signalized Crosswalks Operating Under Combined Pedestrian-Vehicle Interval. In *Transportation Research Board 86th Annual Meeting* (No. 07-2710).

Bandera, A., Pérez-Lorenzo, J. M., Bandera, J. P., & Sandoval, F. (2006). Mean shift based clustering of Hough domain for fast line segment detection. *Pattern Recognition Letters*, *27*(6), 578-586.

Bonneson, J., Brewer, M., & Zimmerman, K. (2001). Review and evaluation of factors that affect the frequency of red-light-running (No. FHWA/TX-02/4027-1).

Brosseau, M., Zangenehpour, S., Saunier, N., & Miranda-Moreno, L. (2013). The impact of waiting time and other factors on dangerous pedestrian crossings and violations at signalized intersections: A case study in Montreal. *Transportation Research Part F*, 21, 159-172.

Buch, N., Velastin, S. A., & Orwell, J. (2011). A review of computer vision techniques for the analysis of urban traffic. *Intelligent Transportation Systems, IEEE Transactions on*, 12(3), 920-939.

California Department of Transportation. (2012). Active Transportation and Livable Communities Advisory Group Meeting (URL: http://www.dot.ca.gov/hq/tpp/offices/ocp/ATLC/documents/Nov2012/ATLC_11-15-12_Notes.pdf)

California Department of Transportation. (2013). 2010-12 California Household Travel Survey Final Report. (URL: http://dot.ca.gov/hq/tsip/otfa/tab/documents/chts_finalreport/FinalReport.pdf)

California Department of Transportation. (2014). State Smart Transportation Initiative (URL: http://www.calsta.ca.gov/res/docs/pdfs/2013/SSTI_Independent%20Caltrans%20Review%201.28.14.pdf)

Djuric, P. M., Kotecha, J. H., Zhang, J., Huang, Y., Ghirmai, T., Bugallo, M. F., & Miguez, J. (2003). Particle filtering. *Signal Processing Magazine, IEEE*, *20*(5), 19-38.

Elmitiny, N., Yan, X., Radwan, E., Russo, C., & Nashar, D. (2010). Classification analysis of driver's stop/go decision and red-light running violation. *Accident Analysis & Prevention*, *42*(1), 101-111.

Gettman, D., & Head, L. (2003). Surrogate safety measures from traffic simulation models. *Transportation Research Record: Journal of the Transportation Research Board*, 1840(1), 104-115.

Grembek, O., Li, Y. I., Zhang, W. B., & Zhou, K. (2007). Analysis of cycle-based data and development of enhanced signal timing models to reduce red light running. In *Transportation Research Board 86th Annual Meeting* (No. 07-0774).

Huang, H., Zegeer, C., Nassi, R., and Fairfax, B. (2000) The Effects of Innovative Pedestrian Signs at Unsignalized Locations: A Tale of Three Treatments, Report No. FHWA-RD-00-098.

Hubbard, S. M., Bullock, D. M., & Mannering, F. L. (2009). Right turns on green and pedestrian level of service: Statistical assessment. Journal of Transportation Engineering, 135(4), 153-159.

Ismail, K., Sayed, T., Saunier, N., & Lim, C. (2009). Automated analysis of pedestrian-vehicle conflicts using video data. *Transportation Research Record: Journal of the Transportation Research Board*, (2140), 44-54.

Jackson, S., Miranda-Moreno, L. F., St-Aubin, P., & Saunier, N. (2013). Flexible, Mobile Video Camera System and Open Source Video Analysis Software for Road Safety and Behavioral Analysis. *Transportation Research Record: Journal of the Transportation Research Board*, 2365(1), 90-98.

Jason, L. A., & Liotta, R. (1982). Pedestrian jaywalking under facilitating and non-facilitating conditions. *Journal of Applied Behavior Analysis*, 15(3), 469-473.

Kassim, A. (2014). *Innovative techniques for analyzing cyclist behaviour and predicting cyclist safety* (Doctoral dissertation, Carleton University Ottawa).

Khan, Z., Balch, T., & Dellaert, F. (2005). MCMC-based particle filtering for tracking a variable number of interacting targets. *Pattern Analysis and Machine Intelligence, IEEE Transactions on*, *27*(11), 1805-1819.

King, M. J., Soole, D., & Ghafourian, A. (2009). Illegal pedestrian crossing at signalized intersections: incidence and relative risk. *Accident Analysis & Prevention*, 41(3), 485-490.

Kumar, P., Ranganath, S., Weimin, H., & Sengupta, K. (2005). Framework for real-time behavior interpretation from traffic video. *Intelligent Transportation Systems, IEEE Transactions on*, *6*(1), 43-53.

Laureshyn, A., Svensson, Å., & Hydén, C. (2010). Evaluation of traffic safety, based on micro-level behavioural data: Theoretical framework and first implementation. *Accident Analysis & Prevention*, 42(6), 1637-1646.

Leden, L. (2002). Pedestrian risk decrease with pedestrian flow. A case study based on data from signalized intersections in Hamilton, Ontario.*Accident Analysis & Prevention*, *34*(4), 457-464.

Ling, Z., Ni, Y., & Li, K. (2014). Modeling Interactions between Pedestrians and Right-Turn Vehicles at Signalized Intersections. *Bridges*, *10*, 9780784412442-211.

Marisamynathan, S., & Vedagiri, P. (2013). Modeling pedestrian delay at signalized intersection crosswalks under mixed traffic condition. *Procedia-Social and Behavioral Sciences*, *104*, 708-717.

Metropolitan Transportation Commission. Plan Bay Area. (URL: http://files.mtc.ca.gov/pdf/Plan_Bay_Area_FINAL/Plan_Bay_Area.pdf)

Milazzo, J. S., Rouphail, N. M., Hummer, J. E., & Allen, D. P. (1998). Effect of pedestrians on capacity of signalized intersections. *Transportation Research Record: Journal of the Transportation Research Board*, *1646*(1), 37-46.

Mohamed, M. G., Saunier, N., Miranda-Moreno, L. F., & Ukkusuri, S. V. (2013). A clustering regression approach: A comprehensive injury severity analysis of pedestrian–vehicle crashes in New York, US and Montreal, Canada. *Safety science*, *54*, 27-37.

Muralidharan, A., Flores, C., & Varaiya, P. (2014). Pedestrian Detection and Real-Time Performance Measures at Intersections. *In Transportation Research Board 93rd Annual Meeting* (No. 14-4230).

Pucher, J., Buehler, R., Merom, D., & Bauman, A. (2011). Walking and Cycling in the United States, 2001–2009: Evidence from the National Household Travel Surveys. *American Journal of Public Health*. 101 (S1), pp. S310-S317.

Retting, R. A., Ulmer, R. G., & Williams, A. F. (1999). Prevalence and characteristics of red light running crashes in the United States. *Accident Analysis & Prevention*, *31*(6), 687-694.

Saunier, N., & Sayed, T. (2006). A feature-based tracking algorithm for vehicles in intersections. In *Computer and Robot Vision, 2006. The 3rd Canadian Conference on* (pp. 59-59). IEEE.

Saunier, N., & Sayed, T. (2007). Automated analysis of road safety with video data. Transportation Research Record: Journal of the Transportation Research Board, 2019(1), 57-64.

St-Aubin, P., Miranda-Moreno, L., & Saunier, N. (2013). An automated surrogate safety analysis at protected highway ramps using cross-sectional and before–after video data. *Transportation Research Part C: Emerging Technologies*, 36, 284-295.

Tarko, A., Davis, G., Saunier, N., Sayed, T., & Washington, S. (2009). Surrogate measures of safety. White paper, *Subcommittee on Surrogate Measures of Safety*, *Transportation Research Board*

Tiwari, G., Bangdiwala, S., Saraswat, A., & Gaurav, S. (2007). Survival analysis: Pedestrian risk exposure at signalized intersections. *Transportation research part F: traffic psychology and behaviour, 10*(2), 77-89.

Yagil, D. (2000). Beliefs, motives and situational factors related to pedestrians' self-reported behavior at signal-controlled crossings. *Transportation Research Part F: Traffic Psychology and Behaviour, 3*(1), 1-13.

Yu, J., Li, X., & Zhao, Y. (2011). Jaywalker Detection Based on Motion Path Analysis. In *Third International Conference on Transportation Engineering (ICTE)*.

Zangenehpour, S., Miranda-Moreno, L. F., & Saunier, N. (2015). Automated classification based on video data at intersections with heavy pedestrian and bicycle traffic: Methodology and application. *Transportation Research Part C: Emerging Technologies*, *56*, 161-176.

Zhang, L., Zhou, K., Zhang, W. B., & Misener, J. A. (2009). Prediction of red light running based on statistics of discrete point sensors. *Transportation Research Record: Journal of the Transportation Research Board*, *2128*(1), 132-142.